WSRC-TR-200140520, Revision 0

Keywords: waste glass, crystallization, statistical process control, process model

RELATING LIQUIDUS TEMPERATURE TO COMPOSITION FOR DEFENSE WASTE PROCESSING FACILITY (DWPF) PROCESS CONTROL (U)

K. G. BROWN and C. M. JANTZEN
Westinghouse Savannah River Co.
Savannah River Site
Aiken, SC 29808

AND

G. RITZHAUPT
Oral Roberts University
Department of Chemistry
Tulsa, OK 74171

Approved by

E.W. Holtzscheiter, Research Manager
Immobilization Technology Section

Publication Date: October 25, 2001

Westinghouse Savannah River Co.
Savannah River Site
Aiken, SC 29808

PREPARED FOR THE U.S. DEPARTMENT OF ENERGY UNDER CONTRACT DE-AC09-96SR18500

This document was prepared in conjunction with work accomplished under Contract No. DE-AC09-96SR18500 with the U.S. Department of Energy.

WSRC-TR-2001-00520, Revision 0
Distribution Category: Unlimited

Keywords: **waste glass, crystallization, statistical process control, process model**

Retention: **Permanent**

RELATING LIQUIDUS TEMPERATURE TO COMPOSITION FOR DEFENSE WASTE PROCESSING FACILITY (DWPF) PROCESS CONTROL (U)

K. G. Brown, C. M. Jantzen, and G. Ritzhaupt

Publication Date: October 25, 2001

Westinghouse Savannah River Company
Savannah River Site
Aiken, SC 29808

PREPARED FOR THE U.S. DEPARTMENT OF ENERGY UNDER CONTRACT NO. **DE-AC09-96SR18500**

Approvals

K. G. Brown, Author — Date: 11/1/2001

C. M. Jantzen, Author — Date: 11/6/2001

D. K. Peeler, Technical Reviewer — Date: 11/5/01

A. D. Cozzi, Technical Reviewer — Date: 11/5/01

T. B. Edwards, Technical Reviewer — Date: 11/7/01

S. L. Marra, Level 4 Manager,
Glass Formulation and Process Development -- DWPF
Immobilization Technology Section — Date: 11/2/01

E. W. Holtzscheiter, Level 3 Manager,
Immobilization Technology Section — Date: 11-7-01

EXECUTIVE SUMMARY

At the Savannah River Site (SRS), waste from 35 years of defense material production is stored on-site in large underground tanks. Vitrification of the waste began in 1996 in the Defense Waste Processing Facility (DWPF) and over 2000 tons of glass have been produced to date. The DWPF product is controlled using a statistical process control system, the Product Composition Control System (PCCS), to ensure that the glass is both durable and processable. This is accomplished by PCCS through the use of a collection of models. One such model is the DWPF liquidus model, LIQCOMP™, which is being revised to enlarge the DWPF processing window. Enlarging said window allows higher waste loadings to be achieved without compromising processing which, in turn, allows more waste to be processed per canister, producing fewer canisters for ultimate storage in a geologic repository. The production of fewer canisters translates into lower, overall disposal costs.

The liquidus temperature (T_L) for a glass is the *maximum* temperature at which the molten glass and primary crystalline phase (e.g., spinel for DWPF) are at equilibrium. The constraint on liquidus temperature in the DWPF melter prevents melt pool crystallization, i.e., volume crystallization from nucleation sites, during routine operation. This type of crystallization can involve almost simultaneous nucleation of the entire melt pool volume. Furthermore, once formed in the DWPF melter, spinel crystals are refractory and cannot be redissolved into the melt pool. When a significant amount of volume crystallization has occurred and the material has settled to the floor of the melter, the pour spout may become partially or completely blocked. In addition, the melt pool may no longer be able to sustain Joule heating which would cause the melt pool to solidify. Finally, minimizing volume crystallization simultaneously minimizes subsequent devitrification of the glass once it is poured into a canister. Thus prevention of volume crystallization is of primary concern for DWPF process control.

Glasses produced in DWPF must have liquidus temperatures below 1050°C; this limit was defined to be safely below the nominal DWPF melter operating temperature of 1150°C. However, the liquidus temperature of a glass cannot be measured in situ. Savannah River Technology Center (SRTC) personnel have thus modeled liquidus temperature as a function of composition (which can be measured and controlled) using mechanistic information including the solution to a freezing point depression problem. That is, the form of the relationship between liquidus temperature and composition is based upon thermodynamics. However, since necessary properties (e.g., fusion enthalpy or $\Delta\overline{H}_{fus}$, melt temperature or T_S^*, etc.) of the melt phase complexes assumed to control crystallization are unavailable, the necessary properties were estimated from the least-squares results obtained from qualified, experimental data representative of expected DWPF compositions (including sludge-only). This approach provided a parsimonious model (i.e., few independent variables) with small prediction uncertainties (including bias) which, in turn, will increase the available processing window (and allow higher waste loading) for DWPF.

Because spinel is the primary liquidus phase expected in most DWPF glasses (and, for a given DWPF glass composition, the bias in the predicted liquidus temperature for other likely phases was shown not to be practically significant), modeling efforts were concentrated on predicting spinel formation in DWPF glasses. The model developed in this study to predict spinel liquidus temperature, T_L, from composition is defined as:

$$T_L(^oC) = \{a\ln(M_2) + b\ln(M_1) + c\ln(M_T) + d\}^{-1} - 273$$

where

$$\Sigma_{MT} \equiv \phi_{T,SiO_2} z_{SiO_2} + \phi_{T,Al_2O_3} z_{Al_2O_3} + \phi_{T,Fe_2O_3} z_{Fe_2O_3}$$

$$\Sigma_{M1} \equiv \phi_{M1,Al_2O_3} z_{Al_2O_3} + \phi_{M1,Fe_2O_3} z_{Fe_2O_3} + \phi_{M1,TiO_2} z_{TiO_2} + \phi_{M1,Cr_2O_3} z_{Cr_2O_3} + \phi_{M1,ZrO_2} z_{ZrO_2} + \phi_{M1,NiO} z_{NiO} + \phi_{M1,MgO} z_{MgO} + \phi_{M1,MnO} z_{MnO}$$

$$\Sigma_{M2} \equiv \phi_{M2,NiO} z_{NiO} + \phi_{M2,MgO} z_{MgO} + \phi_{M2,MnO} z_{MnO} + \phi_{M2,CaO} z_{CaO} + \phi_{M2,K_2O} z_{K_2O} + \phi_{M2,Li_2O} z_{Li_2O} + \phi_{M2,Na_2O} z_{Na_2O}$$

$$\Sigma_{T1} \equiv \phi_{T1,SiO_2} z_{SiO_2} + \phi_{T1,Al_2O_3} z_{Al_2O_3} + \phi_{T1,Fe_2O_3} z_{Fe_2O_3} + \phi_{T1,TiO_2} z_{TiO_2}$$

$$\Sigma_{N1} \equiv \phi_{N1,K_2O} z_{K_2O} + \phi_{N1,Li_2O} z_{Li_2O} + \phi_{N1,Na_2O} z_{Na_2O}$$

and

$$M_2 \equiv \frac{\Sigma_{M2}}{\Sigma}, M_1 \equiv \frac{\Sigma_{M1}}{\Sigma}, M_T \equiv \frac{\Sigma_{MT}}{\Sigma}, \text{ and } \Sigma \equiv \Sigma_{M2} + \Sigma_{M1} + \Sigma_{MT} + \Sigma_{T1} + \Sigma_{N1}.$$

Assuming that pyroxene-like melt phase complexes or precursors control crystallization in expected DWPF glasses, the ϕ coefficients representing the distribution of the various species in the pyroxene-like precursors are provided in the body of the report. The least-squares results for the $(1/T_L)$ versus the above expression for 105 model data representing DWPF compositions were used to estimate the parameters in the above model; these were a = –0.000260, b = –0.000566, c = –0.000153, and d = –0.00144 for the model data. The summary statistics for the least-squares fit obtained were $R^2 = 0.891$ and $s_r = 2.28 \times 10^{-5} K^{-1}$ and the results indicated no significant lack-of-fit. Note that because the model is semi-empirical, its predictions are only guaranteed for compositions and pyroxene-like terms within the ranges from which the model was developed (as shown in the body of the report). However, relevant West Valley Nuclear Services (WVNS) and Pacific Northwest National Laboratory (PNNL) data confirm that prediction biases are tolerably small under conditions expected in DWPF, and the model adequately predicts liquidus temperatures for DWPF glasses within the spinel primary phase field for many glasses falling outside the model data composition range. Thus this model appears significantly better (i.e., more accurate) than the current model used in DWPF for process control.

Modeling volume crystallization in the melt will ensure that gross crystallization will not affect operation of the DWPF melter. An examination was made of waste loading as it applies to the first two sludge batches (SB1a and SB1b) processed through DWPF and the next three sludge-only batches (SB2 through SB4). The T_L predictions for the first two sludge batches processed through DWPF appear to have been very conservative. Also waste loading is generally higher when the proposed model is used; glasses representing SB2 through SB4 would have higher waste loadings of between 0.9 and 7.3 kg of sludge per 100 kg of glass produced (or by between 3.0 and 24.1% higher than those based upon the current T_L model).

There is a case (SB2 or the next sludge-only batch for DWPF and Frit 200) where use of the current T_L model may allow higher waste loading than the proposed, more accurate model. However, because the proposed model is more accurate than the current one and such parameters as the T_L limit (of 1050°C) and the confidence level used correspond to the risk DWPF is willing to assume, their impacts should be noted. For example, the melter T_L limit was shown to have a more profound impact on waste loading (and thus the operating window) than the required confidence level. Furthermore, because the proposed T_L model is more accurate than that currently used in DWPF, the fact that it may require a lower sludge loading should not be discounted; however, this sludge loading would be allowed if the T_L limit was raised to approximately 1075°C for processing of the SB2 material. Therefore, because the T_L constraint is process and not product related (and corresponds to the risk DWPF is willing to take while processing), such an adjustment to the T_L limit should be considered for future DWPF operation or, at least, justification for using the current model if the proposed T_L model is not implemented in DWPF before processing of SB2 material with Frit 200.

Thus the proposed liquidus temperature model is both more accurate and less restrictive (in terms of waste loading as defined in this report) than the current DWPF model. It is illustrated in this report that this will result in increased DWPF operating windows as the other process and product properties are not problematic even at these higher waste loadings. Implementation of this new liquidus temperature model should allow DWPF to increase waste loading significantly and thus minimize the number of canisters produced; these results indicate that the original projected cost reductions of between $100 million and $533 million over the lifetime of the DWPF are very conservative.

TABLE OF CONTENTS

LIST OF ILLUSTRATIONS

LIST OF TABLES

This page intentionally left blank.

RELATING LIQUIDUS TEMPERATURE TO COMPOSITION FOR DEFENSE WASTE PROCESSING FACILITY (DWPF) PROCESS CONTROL (U)

K.G. Brown, C. M. Jantzen, and G. L. Ritzhaupt[†]

Westinghouse Savannah River Company
Savannah River Site
Aiken, South Carolina 29808

1. INTRODUCTION

In its 35 years of production of defense materials, the Savannah River Site (SRS) has generated about one million cubic meters of radioactive waste by-products. This waste is stored in large, underground tanks on the plant site. Processing of the waste into glass began in 1996 in the Defense Waste Processing Facility (DWPF). The DWPF uses a statistical process control system, the Product Composition Control System (PCCS), to ensure that the glass is both durable and processable [1]. The PCCS incorporates various property models[††] to ensure that the glass is durable, homogeneous, and pourable, and will not crystallize in the melter. The last criterion is related to the DWPF liquidus temperature model, LIQCOMP™, which is being revised to enlarge the available DWPF processing window which will allow higher waste loading to be achieved. Higher waste loading will allow more waste to be immobilized per pound of glass produced resulting in fewer canisters for storage in a geologic repository. Fewer canisters for storage translate into both lower disposal and operational costs.

The development of a liquidus temperature model for the DWPF melter is needed to prevent melt pool or volume crystallization during operation. Volume crystallization needs to be avoided because it can involve almost simultaneous nucleation of the entire melt pool as volume crystallization often occurs very rapidly. Furthermore, once spinel crystals are formed in the DWPF melter, these crystals are refractory and cannot be redissolved into the melt pool. The presence of such crystals may cause the melt viscosity and resisitivity to increase [2,3] which may cause difficulty in discharging glass from the melter as well as difficulty in melting via Joule heating [3]. Once a significant amount of volume crystallization has occurred and the resulting crystalline material has settled to the melter floor, melting may be inhibited and the pour spout may become partially or completely blocked making pouring difficult. This was observed in several pilot scale vitrification tests between 1977 and 1981 [2,4,5,6]. Minimizing volume crystallization also has the benefit of minimizing subsequent devitrification of the glass once it is poured into canisters.

In fact, liquidus temperature concerns have historically been focused on volume rather than other types of crystallization (e.g., surface, wall, etc.) because of the greatest potential impact of volume crystallization on glass processing. The DWPF melt volume is much larger than either the exposed melt surface area [7] or the area exposed to the refractory walls and floor. Furthermore, spinel precursors such as $NaFe_2O_4$ rather than insoluble spinels such as $NiFe_2O_4$ (trevorite) have been found to form in the cold cap [2], and the melt appears to form a protective layer along the refractory walls which minimizes spinel formation from the refractory surfaces [8].

Because spinel is the primary liquidus phase expected in most DWPF glasses (and for a given composition the predicted spinel liquidus temperature will be higher than that for the other phases), modeling efforts have been concentrated on predicting spinel formation in DWPF glasses. Modeling the tendency of DWPF glass to undergo volume crystallization has been pursued using a mechanistic approach where possible, that is, the model derived adheres as closely to accepted fundamental laws governing the behavior of matter and energy as possible. Since certain necessary parameters (e.g., enthalpy of fusion, melt temperature, etc.) were unavailable for DWPF spinel, it was necessary to estimate these from experimental information. However, this approach allowed parsimony in the number of necessary model parameters which decreased the corresponding prediction errors which directly affect both the available operating window and waste loading. Modeling volume

---

[†] Oral Roberts University, Department of Chemistry, Tulsa, OK 74171.

[††] The durability and homogeneity model is THERMO™ (Thermodynamic Hydration Energy MOdel) U.S. Patent #5,846,278, the viscosity model is VISCOMP™ U.S. Patent #5,102,439, and the crystallization or liquidus temperature model is LIQCOMP™ (patent in preparation).

crystallization in this manner ensures that gross crystallization will not affect facility operation while also allowing DWPF to increase waste loading and reduce the number of canisters produced. The results in this report indicate that the original projected cost reductions[†] of $100 million to $533 million over the lifetime of the facility are very conservative.

2. SRTC APPROACH TO MODELING LIQUIDUS TEMPERATURE

The fundamental approach that SRTC has undertaken in modeling the critical properties (e.g., durability, liquidus temperature, melt viscosity, etc.) for DWPF process and product control has been to relate these properties to rational functions of composition representing the appropriate mechanistic information. As described in Section 4.2, the current DWPF liquidus temperature model is based upon a pseudo-equilibrium constant describing the gross formation of trevorite in a spinel-nepheline-amorphous silica system. However, this simple model was based upon a set of 22 liquidus temperature measurements and it was believed that additional data would provide an improved model and, thus, waste loading in DWPF. This report describes the development of an improved mechanistic model for DWPF liquidus temperature prediction.

2.1. The Composition Basis for DWPF Liquidus Temperature Prediction

As described in Section 4.2, the current DWPF liquidus temperature model is based upon a pseudo-equilibrium constant describing the formation of trevorite spinel, or $NiFe_2O_4$, in a spinel-nepheline-amorphous silica system. In the current model, only the concentrations of Fe_2O_3, Al_2O_3, and SiO_2 (representing spinel, nepheline, and amorphous silica, respectively) are needed[††] to describe the simple relationship between liquidus temperature and composition for the 22 qualified liquidus temperature measurements available at the time of model development. These glasses all exhibited spinel (composed primarily of trevorite) at the liquidus temperature. However, it was believed that additional data would provide a more robust and descriptive model for DWPF process control and likely provide increased waste loading (because the constraint on liquidus temperature primarily restricts waste loading for DWPF).

As will be discussed in Section 3.1, there were two main sources of additional model data for model improvement. The first source was a set of additional liquidus temperature measurements made by Corning Engineering Laboratory Services (CELS) on the original DWPF glasses (from which the aforementioned 22 model data were generated) using a gradient furnace method. These glasses were not statistically designed, instead they were intended to cover the extremes of processing in DWPF based upon macrobatch (i.e., blended) sludge type (e.g., HM, PUREX, etc.), waste loading, and REDuction/OXidation conditions (REDOX) in the DWPF melter. The results for these glasses were very similar to the original 22 measurements including the fact that all the glasses exhibited spinel (mainly trevorite) as the primary crystalline phase at their corresponding liquidus temperatures.

The second source of new data was a set of liquidus temperature measurements [9] made by the Pacific Northwest National Laboratory (PNNL) using an isothermal method on an additional 53 glasses designed by the Savannah River Technology Center (SRTC) [10] to cover the expected DWPF coupled composition range while not imposing the aforementioned correlation introduced via sludge type. However, there were major differences between both the compositions of the glasses tested by PNNL and the preparation and liquidus temperature measurement methods used between the original model data (and the additional data generated by CELS) and the PNNL data.

[†] DRAFT Cost Analysis by Tony Robinson, BDM International. Attachment to Tanks Focus Area Technical Response 98059, 1997.

[††] The liquidus temperature relationship in Section 4.2 employs the *normalized* molar Fe_2O_3, Al_2O_3, and SiO_2 concentrations. However, because this relationship uses the ratio of normalized molar Fe_2O_3 concentration to the (weighted) difference of the normalized SiO_2 and Al_2O_3 concentrations and the molar sum used as the divisor for the molar oxide concentrations is the same, the normalized molar oxide concentrations can be replaced by their (unnormalized) molar counterparts. Thus the current DWPF liquidus temperature model is a function of only the mass concentrations of Fe_2O_3, Al_2O_3, and SiO_2 (which are directly proportional to their corresponding molar oxide concentrations).

Because the macrobatch (or blended) composition basis was not imposed on the SRTC design, the individual concentrations of the designed glass compositions varied much more than in the original glasses. An example was the NiO concentrations in the glasses produced for PNNL measurement. In the original model glasses, the NiO concentrations were greater than approximately 0.5% by weight since the sludge batches without NiO always happened to be blended with batches with relatively high concentrations of NiO; therefore, all the original glasses had significant concentrations of NiO. However, the SRTC design glasses had a minimum NiO concentration of 0.05% by weight since no macrobatch information was introduced.[†] It was likely that such differences led to primary phases (e.g., clinopyroxene) other than spinel being observed in the glasses tested by PNNL [9]. Thus it was decided that the simplified system employed for the current DWPF model was not sufficiently general for the overall DWPF composition range.

A better starting place to define a more general composition basis for DWPF liquidus temperature prediction is the natural acmite-nepheline-diopside system [11] illustrated in Figure 1. This system indicates the primary phase fields exhibited when acmite (or $Na_2O•Fe_2O_3•4SiO_2$), nepheline (or $Na_2O•Al_2O_3•2SiO_2$), and diopside (or $CaO•MgO•2SiO_2$) are combined, made into glass, and heat-treated appropriately. It is interesting to note that a simplification of this diagram can be said to represent the composition basis (i.e., spinel-nepheline-amorphous silica) for the current DWPF model when it is postulated that the hematite formed in this system will instead be trevorite when sufficient NiO is available. Furthermore, it is critical to note that Figure 1 indicates that pyroxenes (and, thus, clinopyroxenes) will be formed under the appropriate conditions. Therefore, because expected DWPF glasses will not be comprised of the strict proportions found in acmite, nepheline, and diopside (and there are components available that will substitute for components in these end-members), the natural analog system illustrated in Figure 1 is a particular case for the more general DWPF situation.

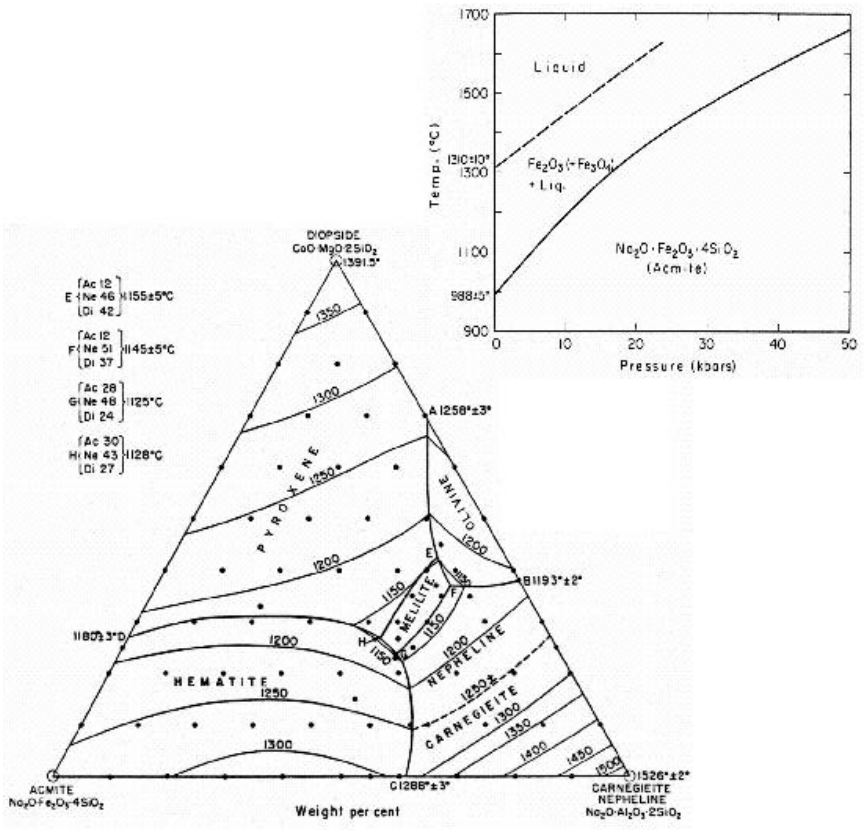

Figure 1. Preliminary liquidus diagram for the join acmite-nepheline-diopside at 1 atm (after Yagi [11]). Carnegieite in the nepheline corner of the diagram is the high temperature phase of nepheline. Inset shows the incongruent melting of acmite to Fe_2O_3 and liquid at atmospheric pressure (from [12]).

[†] This almost came to pass in DWPF because, at one time, only Tank 40, which contains little or no NiO, was considered for processing.

Another critical observation made for the system illustrated in Figure 1 is that, as shown in the inset, the hematite observed as the primary phase in acmite-rich (and thus iron-rich) compositions is formed via the incongruent melting of pyroxene [12]. This indicates that pyroxene is formed, but that the hematite (or its spinel analog) and other melt phase(s) represent a lower free energy state at the liquidus temperature for these glasses. Furthermore, this indicates that it is modeling the formation of pyroxene (which subsequently must melt to form the hematite or spinel discovered) that is critical to liquidus temperature prediction for DWPF glasses and not simply the formation of the hematite (or spinel analog) as has been the case historically.

Because the system in Figure 1 appears to describe generally the crystallization observed in DWPF glasses, it remains to define a reasonable (and more general) version of this system that will then adequately describe the compositions and crystallization of expected DWPF glasses. Such a system is proposed in Figure 2. In this system, the acmite, nepheline, and diopside of Figure 1 are replaced by substituted versions of acmite (which will be referred to as the more general pyroxene class) and substituted nepheline (since such substitutions have been observed in glasses) and the more general metasilicate (than the specific diopside referred to in Figure 1). Note, for example, that lithium metasilicate has been observed in both DWPF and Hanford type glasses. Also notice that the pyroxenes are represented on the figure are not the same. The new system hypothesized in Figure 2 can then be used to describe the more general compositions and crystallization expected in DWPF glasses. The primary phase fields also become necessarily uncertain, as indicated by the broadness of the boundaries in the figure, because the DWPF system has not been fully studied. Finally, without any information to the contrary, it is assumed that the two compounds at the ends of the horizontal line on Figure 2 exist.

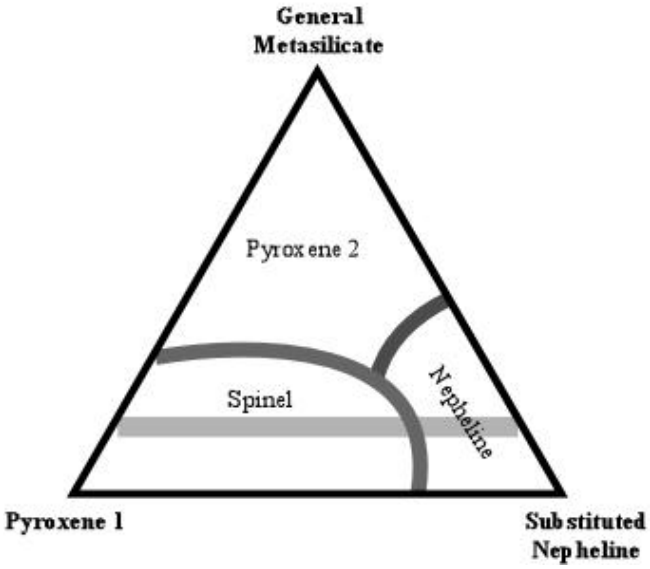

Figure 2. A generalized system to describe crystallization in DWPF glasses consistent with the system according to Yagi as illustrated in Figure 1. The light gray band at a constant "General Metasilicate" contribution represents an approximate Pyroxene-Substituted Nepheline pseudobinary region.

2.2. A Pseudobinary System for Describing DWPF Crystallization

If a horizontal (or constant general metasilicate contribution) slice is taken through the diagram illustrated in Figure 2 at a position where only spinel (from pyroxene) and nepheline are expected as primary phases, then a pseudobinary pyroxene-substituted nepheline region is obtained that can be used to describe crystallization in DWPF glasses. When temperature is introduced, then Figure 3 can be used to describe the general effects of composition and temperature on primary phase formation and, thus, liquidus temperature. This figure has been greatly simplified because the only concern is the formation of pyroxene which melts to form spinel—this melting step has been omitted from the diagram since it will have little impact on liquidus temperature prediction.

The addition of solute (i.e., substituted nepheline) to a solvent P (which, in this case, represents pyroxene) lowers the freezing point, which is equivalent to changing the solubility [13]. To understand this phenomenon, consider the situation described by the liquid-solid phase diagram in Figure 3. Consider the case represented by point C where pure liquid P is in equilibrium with pure solid P at the normal melt temperature, T_P^*. At this point, the chemical potentials of solid P and liquid P are equal [13]. The addition of the solute as indicated by point R (at concentration x_P') in Figure 3 changes the chemical potential of P in the liquid (but not solid) phase. Restoration of the equivalence of chemical potentials requires lowering the temperature (i.e., moving from point R to F). Point F describes the liquidus temperature of the solution at concentration x_P'. Therefore, modeling liquidus temperature as a function of composition based upon this approach (i.e., freezing point depression or solubility) requires that a crystalline phase[†] dominates the onset of crystallization for the range of composition considered (i.e., up to the eutectic point E in Figure 3). For crystallization in DWPF glasses, Figure 3 is most certainly a gross simplification of the complete, multi-component phase diagram. However, the supposition that a series of fairly similar pyroxenes dominating the onset of crystallization in DWPF glasses appears to be a reasonable starting place for modeling the liquidus temperature phenomenon as a function of composition.

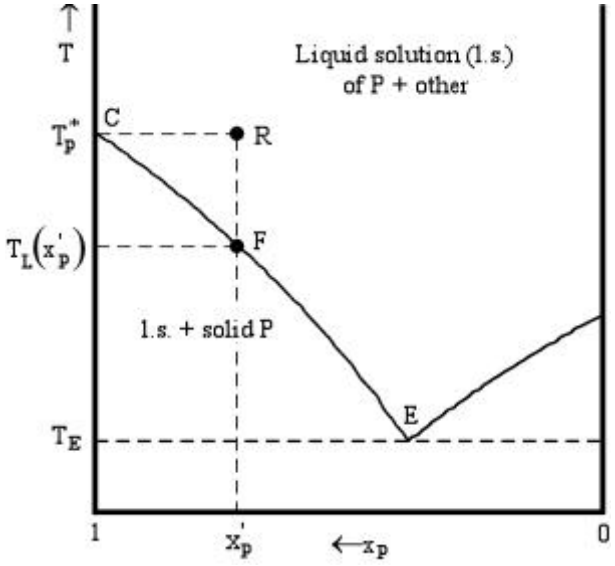

Figure 3. Solid-liquid phase diagram for complete liquid miscibility and solid immiscibility and ideal behavior. Only line CE is of interest as it describes the equilibrium between liquid (or melt) and crystallization of the primary phase (P or pyroxene) and, thus, the liquidus temperature as a function of composition (i.e., addition of the solute or substituted nepheline). The other characteristics of the phase diagram are immaterial for this discussion.

2.3. Thermodynamic Basis for Liquidus Temperature Prediction

As illustrated in Figure 3, the liquidus temperature represents the equilibrium between liquid and the primary phase, P, controlling the onset of crystallization as described by point F [14]. This condition implies that the chemical potentials, μ_P, of the pure crystalline (or solid) phase, P, and of P in the liquid (or melt) must be equal. At a given, constant pressure and liquidus temperature, T_L, this means that the potentials are related by [13]:

Equation 1
$$\mu^*_{P(s)}(T_L) = \mu^*_{P(l)}(T_L) + RT_L \ln\{a(P_{(l)})\}$$

[†] The crystalline phase controlling the DWPF liquidus temperature is assumed to be a series of pyroxenes with fairly similar thermodynamic properties; any differences will be "averaged over" during modeling.

where μ is the appropriate chemical potential, $a(P_{(l)})$ represents the activity of P in the liquid (or melt) phase, *R* is the appropriate gas constant, and the asterisk (*) indicates a pure substance. Rearranging this expression provides:

Equation 2 $$\mu^*_{P(l)}(T_L) - \mu^*_{P(s)}(T_L) = -RT_L \ln\{a(P_{(l)})\}.$$

As indicated in the appendix in Section 13, this can be used to provide a relationship between the activity of P in the liquid (or melt) phase and the reciprocal of the liquidus temperature:

Equation 3 $$-R \ln\{a(P_{(l)})\} \approx \Delta\overline{H}_{fus,P}(T^*_P)\left(\frac{1}{T_L} - \frac{1}{T^*_P}\right).$$

A relationship very similar to Equation 3 can be used to estimate the curve CE on phase diagrams such as that found in Figure 3 describing the relationship between liquidus temperature and composition [13]. For these ideal, binary systems, the molar concentration of P is substituted for the activity of P in Equation 3.

2.4. The Formation of Pyroxene as the Basis for DWPF Liquidus Temperature Prediction

However, there remains an unknown in Equation 3: the activity of P (or pyroxene) in the melt phase for DWPF glasses, which are not simple, binary systems. The pyroxene formula unit is:†

Equation 4 $$(M2)_1(M1)_1(MT)_2O_6$$

where M2 designates a distorted 6 to 8 coordination site and M1 and MT designate regular octahedral and tetrahedral coordination sites, respectively. The ideal cation site occupancy for pyroxene is presented in Table I where five cations can occupy multiple coordination sites.

Table I. Ideal-Site Occupancy of Pyroxene Cations (per Formula Unit $(M2)(M1)(MT)_2O_6$)*

MT (Scations = 2) (IV coordination)	M1 (Scations = 1) (VI coordination)	M2 (Scations = 1) (VI-VIII coordination)
Si^{4+}		
Al^{3+}	Al^{3+}	
Fe^{3+}	Fe^{3+}	
	Ti^{4+}	
	Cr^{3+}	
	Zr^{4+}	
	Zn^{2+}	
	Mg^{2+}	Mg^{2+}
	Fe^{2+}	Fe^{2+}
	Mn^{2+}	Mn^{2+}
		Li^{+}
		Ca^{2+}
		Na^{+}

* Rockware, Inc ® website: www.rockware.com.

Thus the unit formula for pyroxene can be represented by:

† Rockware, Inc ® website: www.rockware.com.

Equation 5 $$\left(M2^{(VI-VIII)}\right)\left(M1^{(VI)}\right)\left(MT^{(IV)}\right)_2O_6$$

or

Equation 6 $$\left(M2^{(VI-VIII)}\right)_2O\bullet\left(M1^{(VI)}\right)_2O_3\bullet 4\left(MT^{(IV)}\right)O_2$$

where the cation coordination numbers are provided in superscripts and Equation 6 is on the same basis as acmite (or, in other words, twice that of Equation 5). Thus for the system represented in Figure 2, the equilibrium activity of pyroxene (P) in the liquid phase (based upon Equation 6) would be proportional to the liquid phase oxide activities raised to their respective stoichiometric coefficients, or:

Equation 7 $$a\left(P_{(l)}\right)\propto a\left\{(M2)_2O_{(l)}\right\}a\left\{(M1)_2O_{3(l)}\right\}a\left\{(MT)O_{2(l)}\right\}^4$$

where the constant of proportionality is represented by the equilibrium constant, K_P, for pyroxene. The liquid phase activity for a component (e.g., a{A}) can then be expressed as the product of its activity coefficient (e.g., γ{A}) and molar concentration (e.g., [A]), or

Equation 8 $$a\left(P_{(l)}\right)=K_P\left\{\gamma\left\{(M2)_2O_{(l)}\right\}\left[(M2)_2O_{(l)}\right]\right\}\left\{\gamma\left\{(M1)_2O_{3(l)}\right\}\left[(M1)_2O_{3(l)}\right]\right\}\left\{\gamma\left\{(MT)O_{2(l)}\right\}\left[(MT)O_{2(l)}\right]\right\}^4$$

A number of assumptions and resulting simplifications will be made to Equation 8 to provide as simple a composition basis as possible that remains mechanistically reasonable. The initial assumption is that the liquid phase reaction producing pyroxene as described by Equation 8 behaves ideally, that is, all γ's equal unity[†]. This results in the following approximate relationship for the liquid phase pyroxene activity:

Equation 9 $$a\left(P_{(l)}\right)\approx K_P\left[(M2)_2O_{(l)}\right]\left[(M1)_2O_{3(l)}\right]\left[(MT)O_{2(l)}\right]^4$$

Another assumption is that, because many pyroxenes contain voids, the stoichiometric ratios of the M2:M1:MT sites in the liquid pyroxene phase are not necessarily in the ratios of 1:1:4. Thus the pyroxene liquid phase activity will be represented by:

Equation 10 $$a\left(P_{(l)}\right)\approx K_P\left[(M2)_2^{(VI)}O_{(l)}\right]^a\left[(M1)_2O_{3(l)}\right]^b\left[(MT)O_{2(l)}\right]^c$$

It remains to define the appropriate molar concentrations to allow liquidus temperature to be predicted from the melt composition.

Table I indicates that various cations (e.g., Fe^{3+}, Al^{3+}, Mg^{2+}, etc.) may occupy multiple sites in pyroxene and it is assumed to be the case in the hypothesized corresponding melt phase complex or precursor. However, the definition of a reasonable composition basis for liquidus temperature prediction is complicated by the fact that many of these same cations are present in the substituted nepheline precursor and/or metasilicate melt phase complex. It is further assumed that this will be the case in the hypothesized melt phase complexes or precursors representing (substituted) nepheline and general metasilicate. This is not to say that the melt phase complexes or precursors have exactly the same structure as their corresponding crystalline analogs (as they likely will not) nor that the cations in the melt phase precursors have the same coordination numbers as in the corresponding crystalline structures; this is merely one way to represent the complicated melt phase complexes. The resulting assumed cation distribution information (corresponding to the site occupancy information in Table I) is provided in Table II.

[†] Alternatively, one could assume that the activity coefficients are constant over the given temperature range. This would be akin to defining a new constant, $K'_P = K_P\gamma_1\gamma_2\gamma_3^4$, and proceeding as described. However, for the sake of simplicity, ideal behavior (i.e., unitary activity coefficients) will be assumed.

Table II. Proposed Cation Distribution for DWPF Melt Phase Complexes*

Pyroxene-like Precursor			Nepheline-like Precursor		General Metasilicate	
MT	**M1**	**M21**	**T2**	**N1**	**T3**	**N2**
Si^{4+}			Si^{4+}		Si^{4+}	
Al^{3+}	Al^{3+}		Al^{3+}			Al^{3+}
Fe^{3+}	Fe^{3+}		Fe^{3+}			Fe^{3+}
	Ti^{4+}		Ti^{4+}			Ti^{4+}
	Cr^{3+}					Cr^{3+}
	Zr^{4+}					Zr^{4+}
	Ni^{2+}	Ni^{2+}				Ni^{2+}
	Mg^{2+}	Mg^{2+}				Mg^{2+}
	Mn^{2+}	Mn^{2+}				Mn^{2+}
		Ca^{2+}				Ca^{2+}
		K^{+}		K^{+}		K^{+}
		Li^{+}		Li^{+}		Li^{+}
		Na^{+}		Na^{+}		

* Ni^{2+} is included as it has been found in DWPF spinels. Zn^{2+} is not included because it is not found in significant concentrations in DWPF glasses (nor in any of the modeling or validation glasses). Fe^{2+} was removed as its impact on liquidus temperature (T_L) is normally indistinguishable from the routine T_L measurement error. Lacking any other information, K^{+} was included in the sites containing the other alkali cations (i.e., Li^{+} and Na^{+}).

There is growing evidence that the cations that form crystalline material in DWPF glasses are not likely found in the melt as independent cations (e.g., Ni^{2+}, Fe^{2+}, Fe^{3+}, etc.) or in oxides (e.g., NiO, FeO, Fe_2O_3, etc.); these cations may even be in the form of nano- or quasicrystalline structures (e.g., $NiAl_2O_4$, $FeNi_2O_4$, $NaFeO_2$, etc.) that are analogous to the crystalline structures that ultimately form in the glass [15]. Thus, at equilibrium and at a temperature just above the liquidus temperature, it is assumed that if a cation is associated with a site in one melt phase complex or precursor, it will not be available to another complex or precursor. However, this does not mean that there is not some degree of interchange of cations as crystalline material begins to form at the liquidus temperature (i.e., the system establishes a new equilibrium at the given temperature). In fact, DWPF glasses are rich in modifier cation-tetrahedral groups [16] which suggests that the various cations are free to exchange sites with each other depending on the favored energetics.

The availability of cations to the various melt phase complexes or precursors can be accounted for by defining the following molar site distributions based on the information in Table II:

Pyroxene-like Complex or Precursor:[†]

$$\Sigma_{MT} \equiv \phi_{T,SiO_2} z_{SiO_2} + \phi_{T,Al_2O_3} z_{Al_2O_3} + \phi_{T,Fe_2O_3} z_{Fe_2O_3}$$

$$\Sigma_{M1} \equiv \phi_{M1,Al_2O_3} z_{Al_2O_3} + \phi_{M1,Fe_2O_3} z_{Fe_2O_3} + \phi_{M1,TiO_2} z_{TiO_2} + \phi_{M1,Cr_2O_3} z_{Cr_2O_3} + \phi_{M1,ZrO_2} z_{ZrO_2} + \phi_{M1,NiO} z_{NiO} + \phi_{M1,MgO} z_{MgO} + \phi_{M1,MnO} z_{MnO}$$

$$\Sigma_{M2} \equiv \phi_{M2,NiO} z_{NiO} + \phi_{M2,MgO} z_{MgO} + \phi_{M2,MnO} z_{MnO} + \phi_{M2,CaO} z_{CaO} + \phi_{M2,K_2O} z_{K_2O} + \phi_{M2,Li_2O} z_{Li_2O} + \phi_{M2,Na_2O} z_{Na_2O}$$

Nepheline-like Complex or Precursor:

$$\Sigma_{T1} \equiv \phi_{T1,SiO_2} z_{SiO_2} + \phi_{T1,Al_2O_3} z_{Al_2O_3} + \phi_{T1,Fe_2O_3} z_{Fe_2O_3} + \phi_{T1,TiO_2} z_{TiO_2}$$

$$\Sigma_{N1} \equiv \phi_{N1,K_2O} z_{K_2O} + \phi_{N1,Li_2O} z_{Li_2O} + \phi_{N1,Na_2O} z_{Na_2O}$$

[†] A term representing the ZnO concentration must be added to Σ_{M2} when the liquidus temperatures of glasses containing significant concentrations of this oxide are to be predicted.

where $\phi_{i,j}$ is the fraction of the moles of j associated with the i^{th} site and z_j represents the total moles of j per 100 grams of glass. The manner in which said fractions are defined will be examined in Section 4.3.1.

Thus the appropriate mole fractions to use in Equation 10 to represent the liquid phase activities for the components comprising the proposed melt phase complexes or precursors are:[†]

$$M_2 = \left[(M2)_2O_{(l)}\right] \equiv \frac{\Sigma_{M2}}{\Sigma}, \quad M_1 = \left[(M1)_2O_{3(l)}\right] \equiv \frac{\Sigma_{M1}}{\Sigma}, \text{and} \quad M_T = \left[(MT)O_{2(l)}\right] \equiv \frac{\Sigma_{MT}}{\Sigma}$$

where

$$\Sigma \equiv \Sigma_{M2} + \Sigma_{M1} + \Sigma_{MT} + \Sigma_{T1} + \Sigma_{N1}$$

because only the pyroxene-nepheline pseudobinary is of concern as indicated in Figure 3. The pyroxene melt phase precursor liquid phase activity can then be approximated by:

Equation 11
$$a\left(P_{(l)}\right) \approx K_P \left(M_2\right)^a \left(M_1\right)^b \left(M_T\right)^c$$

and Equation 3 then, upon substitution, becomes:

Equation 12
$$-R \ln\left\{K_P \left(M_2\right)^a \left(M_1\right)^b \left(M_T\right)^c\right\} \approx \Delta\overline{H}_{fus,P}\left(T_P^*\right)\left(\frac{1}{T_L} - \frac{1}{T_P^*}\right).$$

Equation 12 provides a relationship between melt concentrations and the liquidus temperature, T_L. Rearranging the above relationship provides a way to estimate the (reciprocal) liquidus temperature as a function of the molar melt constituent concentrations:

Equation 13
$$\left(\frac{1}{T_L}\right) \approx -\frac{R}{\Delta\overline{H}_{fus,P}\left(T_P^*\right)} \ln\left\{{M_2}^a {M_1}^b {M_T}^c\right\} + \left\{\left(\frac{1}{T_P^*}\right) - \frac{R \ln\left(K_P\right)}{\Delta\overline{H}_{fus,P}\left(T_P^*\right)}\right\}.$$

Equation 13 provides a parsimonious basis for predicting liquidus temperature for DWPF glasses assuming the presence of a pyroxene intermediate that then melts incongruently to spinel. Thus to a priori predict the liquidus temperatures for a given set of DWPF compositions, the enthalpy of fusion, melt temperature, distribution of cations among melt phase complexes or precursors, and equilibrium constant and stoichiometry of the pertinent equilibrium reaction must be known. In the case of DWPF glasses, such information is not available; therefore, this information will be estimated from available data.

[†] This appears consistent with the concept of site fractions (i.e., the number of atoms in a particular structural site divided by the total number of sites of that type available) that is normally applied to the chemistry of imperfect crystals. For more information, please refer to: F.A. Kroger, **The Chemistry of Imperfect Crystals**, North-Holland Pub. Co., Amsterdam, The Netherlands, 1039 pp. (1964).

3. EXPERIMENTAL AND ANALYTICAL

Many glasses have been fabricated that have had both the liquidus temperature and composition measurements made that are needed to be used in defining a new model for DWPF process control. Because the liquidus temperature-composition relationship is likely complicated and also non-linear, only those data that are pertinent to DWPF composition and melt conditions will be selected. This selection will provide the best possible opportunity for developing a mechanistic model for liquidus temperature prediction from composition. Melt and quenching conditions as well as compositions outside those expected for DWPF may result in variations that cannot likely be adequately described using any reasonable relationship derived from mechanistic information. Thus the intent of this report—to develop a better model than that currently employed by DWPF—requires a careful examination of the available experimental results.

3.1. Glass Fabrication, Melting, and Analysis

3.1.1. SRTC Glasses Melted at 1150°C

Approximately 50 glasses of varying, expected extreme DWPF compositions were fabricated between 1984 and 1996. During this time, liquidus temperature (T_L) measurements and replicate chemical analyses were performed on these glasses. The T_L measurements for the initial set of glasses, which were 1) melted by either SRTC or CELS at 1150°C (i.e., the nominal DWPF melt temperature), 2) air quenched, and 3) measured by either CELS or Sharpe-Shurtz in a gradient furnace using ASTM Procedure C829-81 or by Pacific Northwest National Laboratory (PNNL) using a uniform temperature method developed by PNNL, are provided in Table XXI in the appendix in Section 14. (The measurement techniques will be discussed below.) The corresponding composition information for these glasses is provided in Table XXII.

Of the 70 T_L measurements provided in Table XXI, only a subset of 22 was originally available to define the spinel liquidus temperature model currently used by DWPF for process control [1]; the sample identifiers for these glasses are italicized in Table XXI. At the time the existing DWPF model was developed, measured chemical compositions were not available for these glasses (i.e., as-batched compositions were used); however, chemical analyses for these glasses have since been obtained and that information is included in Table XXII.

Ten of the 70 T_L measurements listed in Table XXI were not used in development of the revised DWPF liquidus temperature model; the information for these ten glasses is shaded in the table. Two of the crucibles (i.e., those in which AH 131AL-1988 and AH 131AV-1988 were prepared) broke upon cooling so there was not sufficient spatial control in these samples to measure T_L, and thus these two glasses were excluded from model consideration. Another glass (i.e., AH 131FE-RED-1988) was found to be inhomogeneous by X-ray diffraction (XRD) upon fabrication and thus could not be included in the model data. Two glasses were excluded because the primary phases discovered were not spinel (and a spinel liquidus temperature model is being developed based upon a pyroxene intermediary for DWPF process control). The primary phase for white Frit 165 was cristobalite—not spinel—so this glass was excluded. Similarly, the T_L measurement for glass AH 168AL-1992 was also excluded from model consideration because the primary phase was not spinel.[†]

The CELS T_L measurement (i.e., 778°C) for glass AH-9-1985# was considered an outlier when compared to a Sharp-Shurtz gradient furnace T_L measurement (i.e., 1000°C) for the same glass. This appeared to be confirmed by the difference (i.e., 1080 – 778 = 302°C) between the air and internal T_L measurements which was twice that of any glass in Table XXI. The T_L measurement (i.e., 920°C) for glass AH 165FE-RED-1988 was considered an outlier when compared to measurements (i.e., 1102°C and 1085°C) made on the same glasses in 1985 and 1993, respectively. Two of the three values agree and the difference of at least 165°C between the third and the other two far exceeds any reasonable liquidus temperature measurement error[††].

[†] As will be subsequently shown in Exhibit 6, exclusion of this glass because of the phase that formed at the liquidus temperature will not be a problem as it is reasonably well-predicted by the proposed liquidus model and its liquidus is far below that which would be considered of practical importance.

[††] ASTM C829-81 states that a precision of ±10°C is achievable for T_L measurement with clear glasses tested in the same furnace. No precision is given for glasses tested in different furnaces or for opaque glasses. CELS provided estimates of ±25°C in CELS-009 for the opaque DWPF glasses that were tested.

The six T_L measurements performed in 1996 and reported in CELS report CELS-076 were considered suspect when compared to other CELS and PNNL T_L measurements. The T_L measurements for these glasses were subcontracted. Only the measurements that could be confirmed via both other CELS and PNNL measurements were included in Model Data. Thus the T_L measurement reported in CELS-076 for glass AH 168FE-RED-1992 appears to disagree significantly (i.e., by more than 120°C) with that performed by CELS in 1992 and 1993 and was thus removed from consideration. The remaining five T_L measurements were included in model data.

In an attempt to explore REDOX effects on liquidus temperature or its measurement, different amounts of coal were added to a number of DWPF glasses containing high total iron concentrations. However, since liquidus measurements were not carried out in a controlled atmosphere (and the resulting T_L samples were not measured for $Fe^{2+}/\Sigma Fe$), it is difficult to project what the REDOX ratios of the glasses were at the measured liquidus temperatures. One of the glasses from this study (i.e., glass AH 131FE-OX) appears to have been batched improperly as its measured composition (as shown in Table XXII) does not resemble any of the other AH 131FE (or DWPF) glasses, especially in its NiO and B_2O_3 concentrations. Thus its omission should not be problematic for DWPF liquidus temperature prediction.

A summary of the available liquidus measurements for the five high-iron glasses (i.e., AH 131FE, AH 165FE, AH 168FE, AH 200FE, and AH 202FE) studied for REDOX effects is provided in Table III. Two things can be noticed from this table: there appears to be no large bias between the CELS and PNNL T_L measurements for these glasses and there appears to be no consistent REDOX effect on measured T_L. Also the approximately 200°C change in T_L measurements for the AH 200FE glasses appears unreasonable due to either REDOX or normal measurement variations. Thus it was suspected that the single CELS T_L measurement for AH 200FE-OX was likely in error. To verify the T_L measurement for glass AH 200FE-OX, SRTC refabricated this glass and conducted a series of 24 hour isothermal crucible melts at temperatures of 900, 950, 1000, and 1050°C. The resulting glasses were examined via x-ray and were found to all possess spinel crystals in the bulk of the glass; therefore, the CELS T_L measurement of 895°C in Table XXI (and Table III) was likely erroneous. Thus the T_L measurement (i.e., 895°C) for AH 200FE-OX-1996 was excluded from further modeling considerations.

Table III. Summary of Liquidus Temperature Measurements[§] made to Examine Effects of REDOX

	Liquidus Temperature Measurements (°C)						
Glass	Reduced CELS	CELS Average	Reduced PNNL	PNNL Average	Reduced Average	Oxidized CELS	Diff.
AH 131FE	~~996~~, 1035, 1075	1055	1109, 1107	1108	1082	~~1035~~	n/a
AH 165FE	1102, ~~920~~, 1085, 1015, 1135	1084	1086, 1113	1100	1092	n/a	n/a
AH 168FE	1022, 1085, ~~900~~	1054	--	--[§§]	1054	1130	+76
AH 200FE	1126, 1065, 1070	1087	1113, 1062	1087	1087	~~895~~	n/a
AH 202FE	1123, 1110, 1160	1131	1118, 1127	1122	1127	1100	-27

§ The CELS T_L measurements that are struck through are ignored for modeling as described above.
§§ The repeated PNNL measurements were made on AH 168AV and not AH 168FE.

As illustrated in Table III, the range of differences in the repeated CELS data (which were measured over more than a four year span) is much greater than that in the repeated PNNL measurements for the same glasses. Such differences in short versus long-term liquidus temperature measurement errors have been exhibited in other data (i.e., those from the SG1 Study described in Section 3.1.2). Because the long-term errors appear to be much larger than those over much shorter times (and it is assumed that such long-term effects inflict both gradient and uniform temperature measurement methods), it has been decided to average the short term repeated data to represent better the liquidus temperature measurement errors. Thus the repeated PNNL T_L measurements for glasses AH 131FE, AH 165FE, AH 168AV, AH 200FE, and AH 202FE were averaged to provide a total of five T_L measurements, one for each glass. The examinations described resulted in 55 CELS or Sharpe-Shurtz liquidus temperatures and corresponding compositions for glasses melted at 1150°C that cover the extremes of the anticipated, DWPF composition range.

The compositions for the SRTC glasses whose liquidus temperature measurements are provided in Table XXI were primarily analyzed by CELS; the compositions for these glasses are provided in Table XXII and the ranges summarized in Table IV. CELS analyzed the AH glasses in quadruplicate[†] so that any effects of short term instrument bias on the whole element chemistry would be observable. CELS analyzed the various frits six times. All CELS composition analyses are traceable to the NBS777 standard glass. These data indicate little random or systematic variation for these analyses (especially when compared to the uncertainties in liquidus temperature measurement).

Table IV. The SRTC Model Data Composition Region

	Al_2O_3	B_2O_3	CaO	Cr_2O_3	FeO	Fe_2O_3	$(\Sigma Fe)_2O_3$	K_2O	Li_2O
Maximum	14.162	12.652	1.580	0.096	6.901	16.977	17.60	3.470	5.1100
Minimum	0.99	6.410	0.380	0	0.0161	3.427	3.452	0	2.4901
	MgO	MnO	Na_2O	NiO	SiO_2	TiO_2	U_3O_8	ZrO2	
Maximum	1.425	3.25	14.901	3.045	55.300	1.8549	0	0.97	
Minimum	0.490	0.7392	6.54	0.530	42.500	0	0	0.005	

The compositions for the AH 168AL-1988 and AH 168FE-RED-1988 glasses were analyzed by the Analytical Development Section (ADS) of SRTC. These samples were prepared using dissolution by either Na_2O_2 with an HCl uptake or HCl/HF/microwave followed by analysis by Inductively Coupled Plasma (ICP) Spectroscopy and Atomic Absorption (AA). REDOX-related analyses [17] were performed on selected glasses by the SRTC Mobile Laboratory (SRTC-ML) and used to compute the FeO values reported in Table XXII and summarized in Table IV. For those glasses without REDOX determinations (which were fabricated in such a way as to be oxidized), the $Fe^{2+}/\Sigma Fe$ values were assumed to be one-half the detection limit [18] for this measurement, or ½(0.03) = 0.015; these (and the available measured) values were used to partition the measured total iron between FeO and Fe_2O_3.

3.1.2. DWPF Design , or "SG" and "SG1" Study Glasses

In 1996, a set of 51 compositions was designed by SRTC to cover the range of expected DWPF compositions [10]. PNNL fabricated these glasses, designated the "SG" glasses, including two (i.e., SG05 and SG18) in duplicate and measured liquidus temperatures using a uniform temperature method developed by PNNL [9]. (This was the same technique employed to measure the liquidus temperatures for five SRTC glasses in Table XXI.) The primary phase discovered for most of these glasses was spinel; however, several glasses did show clinopyroxene (or clinopyroxene in combination with RuO_2 needles and/or spinel) as the primary liquidus phase. To make these glasses, batch chemicals were combined and then melted for one hour in a Pt-Rh crucible; the melt temperature for each glass was selected to give a predicted melt viscosity of 5 Pa•s (or 50 Poise) as predicted by an empirical PNNL composition to melt viscosity correlation. The glasses were quenched, ground, remelted, quenched again, and finally reground. Samples of the glasses were measured for T_L using a uniform temperature method. Other samples were measured by the SRTC-ML for composition. The liquidus temperature measurements and compositions for the SG glasses are provided in Table XXIII.

Of primary concern is the relationship between liquidus temperature and composition for glasses that were prepared under conditions representative of DWPF. One such condition is the melt temperature (which is nominally 1150°C in the DWPF melter). However, many of the SG glasses fabricated by PNNL were melted at temperatures (i.e., from 1107°C for glass SG01 to 1384°C for glass SG12) that were much different than the DWPF melt temperature. It has been shown that melt temperature may have a significant impact on the enthalpy of fusion (ΔH_f) for aluminosilicates, titanates, and oxides of network-forming types [19]. Another potential effect related to temperature concerns the manner in which (or rate at which) the glasses were quenched after melting. As indicated in Table XXIII, nine of the SG glasses were water quenched—the rest were quenched in air (i.e., at a slower rate) like the aforementioned SRTC glasses. The rate of cooling has been shown, for some glass systems, to impact key intensive parameters such as the fictive or glass transition temperature [20] and thus

[†] That is, two dissolutions were performed—one on each day—with each dissolution analyzed in duplicate.

the absolute enthalpy [21]. Again such effects on glass enthalpy may unnecessarily limit the ability of a mechanistic model (such as that in Equation 13) to describe the liquidus temperature phenomenon.

Since it was unknown whether or not melt temperature and cooling effects had significant impacts on the SG Study liquidus temperatures, it was decided to design a study (denoted the SG1 Study) to examine such potential effects. Because it was hypothesized that melt temperature would have the greatest potential impact on T_L (and only a single SG Study glass, SG35, was both quenched in water and melted within 50ºC of the DWPF melt temperature of 1150ºC), the melt temperature impact was studied in detail.

Four of the original SG Study glasses (i.e., SG06, SG12, SG13, and SG45) with large differences between PNNL and the nominal DWPF melt temperature (of 1150ºC) were selected as the basis of the SG1 Study. The SG1 Study consisted of 20 liquidus temperature measurements on either the original four SG Study glasses or replicate measurements on glasses fabricated to have the same target compositions as the original glasses, but using different fabrication techniques and temperatures. For each of the four target compositions, carbonates and oxides were batched, mixed, riffled, and collected into four batches which should have had approximately the same compositions. Then two of each of the resulting batches were melted according to the PNNL method used during the SG Study (i.e., two melts with temperatures of between 1317 and 1400ºC or each well above the nominal DWPF melt temperature of 1150ºC). The other two batches for each were then melted at the nominal DWPF melt temperature of 1150ºC for four hours. The resulting 16 glass samples and the four samples from the original SG Study glasses were sent to PNNL along with two samples of the PNNL SP-1 glass[†] for liquidus temperature measurement using the PNNL uniform temperature method [9]. The compositions of these glasses were measured by the SRTC Mobile Laboratory (SRTC-ML) and the average results are provided in Table XXIV in the appendix.

The measured liquidus temperature results for the 16 new (SG1) glasses are presented in Table V. These glasses were produced to exhibit any effects of melt temperature or other possible effects on liquidus temperature. Note that the samples for each glass type were heated in the same furnace so there should be no furnace to furnace effects in this particular set of data. The differences between repeated glasses for the SRTC protocol were: 3ºC for SG06, 7ºC for SG12, 48ºC for SG13, and 0ºC for SG45. For the PNNL protocol glasses, the differences were: 14ºC for SG06, 0ºC for SG12, 12ºC for SG13, and 11ºC for SG45. The differences between measured liquidus temperatures for the PNNL and SRTC glasses were: 14.5ºC for SG06, 47.5ºC for SG12, 41ºC for SG13, and 7.5ºC for SG45, where the average measured liquidus temperature was higher for the glasses fabricated using the PNNL method (which may be accounted for by the higher relative Fe_2O_3 concentrations in the PNNL glasses as indicated in Table XXIV) than for the corresponding glasses made using the SRTC method. Thus there is the possibility of some effect (e.g., cooling rate) on liquidus temperature, but any such effect does not appear to be significant relative to the liquidus temperature measurement error. Furthermore, as indicated in Table XXIV, there were significant composition differences (in, at least, the Fe_2O_3 concentrations) in the SG1 glasses corresponding to the SG06 and SG12 glasses (and less so in those corresponding to the SG13 and SG45 glasses) which may have accounted for at least a portion of the observed measured liquidus temperature differences.[††] Therefore, there appears to be no reason concerning melt temperature or other potential such effects that would cause the original SG Study data to be omitted from modeling consideration. However, these results indicate that the SG1 Study data should only be used with caution.

[†] The SP-1 glass was used by PNNL during the SG Study to correct the liquidus temperature measurements on a furnace to furnace basis by between 1 and 33ºC. The accepted value for the SP-1 glass is 1040ºC [9].

[††] Two of the SG1 Study glasses (i.e., those corresponding to the original SG06 and SG13) were selected for more detailed composition examination. The SRTC-ML results for these glasses are provided in Table XXV and Table XXVI in the appendix; these results confirm the composition differences previously mentioned.

Table V. Raw Liquidus Temperature Measurements to Illustrate Possible Measurement Impacts*

SG ID	SG1 ID	Glass ID	Melt Protocol	T_M(°C)	PNNL Furnace	T_A(°C)	T_C(°C)	Phase	T_L(°C)
SG06	SG1-15	SG06-PNNL-1	PNNL	1322	F8	975	973	S	974
SG06	SG1-20	SG06-PNNL-2	PNNL	1322	F8	992	984	S	988
SG06	SG1-07	SG06-SRTC-1	SRTC	1150	F8	973	963	S	965
SG06	SG1-08	SG06-SRTC-2	SRTC	1150	F8	973	963	S	968
SG12	SG1-19	SG12-PNNL-1	PNNL	1384	F5	1094	1084	S	1090
SG12	SG1-03	SG12-PNNL-2	PNNL	1384	F5	1094	1084	S	1090
SG12	SG1-12	SG12-SRTC-1	SRTC	1150	F5	1041	1032	S	1039
SG12	SG1-13	SG12-SRTC-2	SRTC	1150	F5	1051	1041	S	1046
SG13	SG1-06	SG13-PNNL-1	PNNL	1400	F5	955	948	S	952
SG13	SG1-11	SG13-PNNL-2	PNNL	1400	F5	968	961	S	964
SG13	SG1-10	SG13-SRTC-1	SRTC	1150	F5	945	937	S	941
SG13	SG1-02	SG13-SRTC-2	SRTC	1150	F5	897	886	C,S	893
SG45	SG1-21	SG45-PNNL-1	PNNL	1317	F8	1076	1068	S	1072
SG45	SG1-16	SG45-PNNL-2	PNNL	1317	F8	1086	1079	S	1083
SG45	SG1-04	SG45-SRTC-1	SRTC	1150	F8	1075	1065	S	1070
SG45	SG1-18	SG45-SRTC-2	SRTC	1150	F8	1075	1065	S	1070

* The temperatures represent that (T_M) at which the glass was melted, the lowest temperature (T_A) measured that the glass was amorphous, the highest temperature (T_C) measured at which the glass was crystallized, and the liquidus temperature (T_L) estimated by PNNL from T_A and T_C. The phases represent spinel (S) and clinopyroxene (C).

However, before using the SG1 Study data for DWPF liquidus temperature modeling, the six glasses other than those presented in Table V from the SG1 Study must be examined. These results and the pertinent comparisons to the corrected, original SG Study results are provided in Table VI. It should also be noted that the SG1 Study tests were only conducted after the NBS777 standard glass liquidus temperature was reproduced in each furnace used to within ±5°C. From the data in Table VI, it appears that the long-term effects on the liquidus temperature measurements are much greater than can be tolerated for a revised DWPF model. For example, the liquidus temperature measurements for both samples of the SP-1 glass, which was used for bias correction in the SG Study, were 29 and 30°C higher than the accepted PNNL value of 1040°C. The other values were between 0 and 62°C higher than the original SG Study measurements. Therefore, it was decided (especially because the measurements of the NBS777 and SP-1 glasses disagreed) that the SG1 Study data were not sufficiently accurate to use in revising the DWPF liquidus temperature model. On the other hand, because the measurements for the NBS777 and SP-1 glasses for the SG Study agreed [9], these data, including those melted at temperatures greatly different from the nominal DWPF melt temperature, were considered for modeling. Furthermore, despite there being large differences in some of the CELS data (as indicated in Table III), those CELS data where two of the three measurements agreed, within reason, were used for modeling.

Table VI. Long-term Comparisons of the Original, Corrected SG and New SG1 Study Data*

		SG1 Raw Measurements			SG Corrected Values			Diff.
GlassID	Furnace	T_A(°C)	T_C(°C)	T_L(°C)	T_A(°C)	T_C(°C)	T_L(°C)	T_L(°C)
SP-1	F8	1066	1075	1070	n/a	n/a	1040	+30
SP-1	F5	1065	1074	1069	n/a	n/a	1040	+29
SG06	F8	970	975	973	906	915	911	+62
							929	+44
SG12	F5	1084	1090	1087	1025	1034	1030	+57
SG13	F5	1076	1082	1079	1060	1065	1063	+16
SG45	F8	931	941	936	932	941	936	0

* The temperatures represent the lowest temperature (T_A) measured that the glass was amorphous, the highest temperature (T_C) measured at which the glass was crystallized, and the liquidus temperature (T_L) estimated by PNNL from T_A and T_C. Spinel was observed as the primary phase for each glass.

The only remaining issue is that both clinopyroxene and spinel were observed at the liquidus temperature (T_L) for the SG Study glasses. However, since the primary focus for this report is the spinel phase normally observed at T_L for DWPF glasses, only those SG Study glasses exhibiting spinel[†] will be used for modeling; the other seven glasses will be omitted from modeling consideration as indicated in Table XXIII. (The impact of omitting these glasses will be examined subsequently after model development.) This results in 59 measured liquidus temperatures for 44 additional glass compositions from a designed study [10] being available for modeling.

However, the SG1 Study results indicate that the long-term effects on the liquidus temperature measurements are much larger than the short-term effects. Thus, as in Section 3.1.1 for the SRTC model data, the short-term PNNL liquidus temperature measurements from the SG Study will be averaged. Thus the individual PNNL T_L measurements for the SG06(2), SG18(7), SG18B(5), SG25(2), and SG37(2) glasses will be averaged to represent these data. The seven SG18 and five SG18B measurements were averaged over the various PNNL furnaces used for heat-treatment into two sets of three values each because it was hypothesized that furnace recalibration (or, alternatively, use of a different furnace) might introduce the observed long-term effects. This results in an additional 50 liquidus temperatures for modeling from a designed study [10] representing coupled DWPF operation; the ranges for these 50 compositions are provided in Table VII. There were no REDOX measurements for these glasses so only the $(\Sigma Fe)_2O_3$ values are provided. Thus a total of 105 data (i.e., 55 SRTC and 50 SG Study) are available for DWPF liquidus temperature modeling where the SG Study data were designed.

Table VII. SG Study Data Composition Region

	Al_2O_3	B_2O_3	CaO	Cr_2O_3	$(\Sigma Fe)_2O_3$	K_2O	Li_2O	MgO
Maximum	8.364	11.536	2.007	0.301	15.17	3.885	6.158	2.650
Minimum	2.500	4.893	0.305	0.082	5.784	1.444	2.651	0.490
	MnO	Na_2O	NiO	SiO_2	TiO_2	U_3O_8	ZrO_2	
Maximum	2.966	11.28	2.145	58.230	0.659	5.138	0	
Minimum	0.955	5.99	0.038	41.795	0.159	0.259	0	

3.2. Liquidus Temperature Measurement Methodologies

Method A of the ASTM gradient furnace method [22] was used by CELS and Sharpe-Shurtz to measure liquidus temperatures for the glasses in Table XXI. PNNL procedure GDL-LQT, "Liquidus Temperature Measurement Procedure," which has been submitted to ASTM for approval, was used by PNNL to provide repeated liquidus temperature measurements for five of the glasses in Table XXI as well as all the glasses in Table XXIII. The ASTM gradient furnace procedure states that a precision of ±10°C is achievable in the liquidus measurement with clear glasses tested in the same furnace; no precision is given for glasses tested in different furnaces or for opaque glasses such as those produced in DWPF. An estimate of ±25°C was reported in CELS Report 009 for a number of DWPF (opaque) glasses. The precision of the PNNL uniform temperature method was believed to be ±12°C for bias-corrected liquidus measurements [9]. However, this error estimate was not statistically determined and based upon the SG1 Study results appears to reflect only short-term errors.

4. MODELING LIQUIDUS TEMPERATURE AS A FUNCTION OF COMPOSITION

As illustrated in Section 2, the liquidus temperature of a DWPF glass should be a strong function of molar composition. A total of 105 liquidus temperature-composition data pairs have been identified that appear reasonable for modeling the DWPF liquidus temperature response as a function of composition. These model data were generated primarily by CELS and PNNL and validated (to the extent possible) by SRTC and PNNL. The glasses measured by CELS were fabricated with waste loadings on an oxide basis between 25 and 35 wt% from high Fe_2O_3 containing Purex sludge, high Al_2O_3 containing HM sludge, and average sludge waste based upon waste types and frits. The glasses measured by PNNL were based upon a designed study [10] covering

[†] As in one of the SRTC model data (i.e., one of the DWPF Startup Frit glasses), some of the glasses exhibit both spinel and (clino)pyroxene to the resolution of the liquidus temperature measurement.

expected DWPF coupled glass compositions. The glasses were made in both reduced and oxidized states spanning $Fe^{+2}/\Sigma Fe$ ratios of 0.005 to 0.47. However, since liquidus measurements were not carried out in a controlled environment (and the resulting T_L samples not analyzed for REDOX), there was no way to know what the REDOX values were at the liquidus temperatures. Thus any REDOX effects are ignored in the subsequent modeling. Fifty of the glass compositions were obtained from the statistically designed SG Study [10]; the remaining 55 extended beyond the anticipated DWPF glass composition extremes but lacked individual variations amongst individual components. How well these data cover the important composition effects in the liquidus temperature response will subsequently be verified as part of the modeling task.

4.1. Design Efficiency of the Model Data

The SG Study data were obtained from a designed study [10] whereby 51 compositions were generated to cover expected DWPF glasses based upon DWPF Chemical Process Evaluation System (CPES) projections. The compositions for these glasses were measured by the SRTC-ML and the average compositions are provided in Table XXIII. The SRTC glasses were fabricated to extend well beyond the expected component ranges but were based upon waste and frit types and thus the individual concentrations are often highly correlated. Furthermore, the glasses include different sets of components (e.g., many SG Study glasses contained U_3O_8, but the SRTC glasses were all non-radioactive, but contained some ZrO_2). To determine the effects of such issues on modeling, the glasses were first normalized to a consistent and common set of major component oxides (i.e., Al_2O_3, B_2O_3, CaO, Cr_2O_3, Fe_2O_3, K_2O, Li_2O, MgO, MnO, Na_2O, NiO, SiO_2, and TiO_2). The D-efficiencies[†] were then computed for various subsets of model data and were 9.0760 for the 53 measured SG Study compositions, 8.4908 for the 46 measured SG Study compositions containing spinel (and no clinopyroxene) at the liquidus temperature, and 6.0246 for the 101 measured compositions for the model glasses (i.e., both PNNL and SRTC). Therefore, as expected, including the SRTC data does reduce the efficiency of the model data; however, this decrease in efficiency is offset by broader coverage of the extremes of the expected DWPF composition region and all 105 data will be used for modeling.

4.2. The Original, DWPF Liquidus Temperature Model

A subset of 22 of the 55 CELS liquidus temperature data were used to develop the original DWPF liquidus model [23]:

Equation 14 $$\hat{T}_L(^oC) = 803.6 + 2277\kappa \quad \text{where} \quad \hat{e} \equiv \frac{(-134\text{kcal/mol})[Fe_2O_3]}{(-156\text{kcal/mol})[SiO_2] - (-360\text{kcal/mol})[Al_2O_3]}$$

and the coefficients in κ represent the free energies of formation for amorphous silica and the observed liquidus phases, spinel and nepheline, at the liqudus temperature limit (or 1050°C) for the DWPF melter. Since the concentrations, x_i, in Table XXII and Table XXIII were provided on a gram oxide per 100 gram glass basis, each concentration was divided by its corresponding molecular weight, M_i, to provide the molar oxide concentrations, $[*] = x_i/M_i$, necessary to compute κ in Equation 14. At the time the model in Equation 14 was developed, only as-batched compositions were available.

For DWPF waste glass formulations, Fe_2O_3 and Al_2O_3 were considered the major waste oxides and SiO_2 was considered the major frit oxide (or solvent) in the glass. Fe_2O_3 and Al_2O_3 were likely the oxides primarily promoting spinel and nepheline precipitation, respectively. In the precipitation reaction controlling production of spinel, the glass was considered a mixture of silicate and oxide species, and the predominant solvent in the glass was considered to be amorphous SiO_2 depleted by the amount of SiO_2 needed to form $NaAlSiO_4$ (which was assumed dominated by the amount of Al_2O_3 present). The competition between the solvent and spinel precipitation was represented by the pseudo-equilibrium constant, κ, in Equation 14.

[†] The D-optimal design seeks to minimize the determinant of the product moment matrix, $(\mathbf{X}^T\mathbf{X})^{-1}$ where each row of $\mathbf{X}$ is a design point and is reasonable for comparing the optimality of different sets of candidate design points for a given experiment. D-efficiency is the objective of this design, and the higher the value the more optimal the design based upon this criterion.

Figure 4 illustrates the large prediction biases for the new model data described in Table XXI, Table XXII, and Table XXIII when the original liquidus model form (i.e., Equation 14) is used. The various least-squares fits have the following results:

Data Set	N	R^2	RMS
SRTC	55	0.716	46°C
SG Study	50	0.198	126°C
SRTC+SG	105	0.333	94°C

where RMS is the Root Mean Square (RMS) Error or s_r. These results do not compare favorably to those obtained from the original 22 data (i.e., $R^2 = 0.769$ and $s_r = 37$°C) [23]. Even though there are more data, this increase in the number of model data does not offset the huge increase in prediction biases; furthermore, the current model form does not appear to represent the liquidus temperature response for the new model data, which cover the expected DWPF compositions. It was intended that improvement of the liquidus temperature prediction would translate into a significant waste loading increase and a corresponding reduction in ultimate production and storage costs for DWPF. Because the current model form (i.e., that described in Equation 14) does not provide accurate predictions and will not provide the desired improvement in waste loading for DWPF, the model presented in Section 2 will be examined to see if it can provide the desired model improvements.

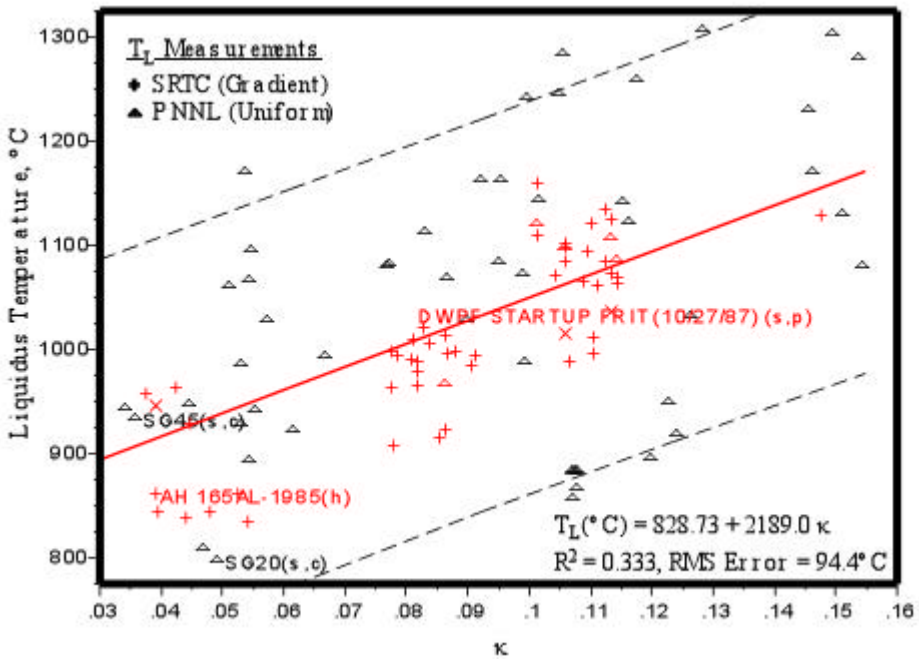

Figure 4. This figure shows the relationship between measured liquidus temperature (in °C) and the pseudo-equilibrium constant, κ, for the 105 DWPF model glasses. The dotted lines represent the 95% confidence curves about the individual data.

4.3. Alternative Mechanistic-Based Liquidus Temperature Model

As indicated in Equation 13, an alternative model based upon the formation of melt phase complexes or precursors analogous to a pyroxene-like intermediary can be used as a basis for relating liquidus temperature to a function of composition. However, before this relationship can be used, the manner in which the constituent components of the molten glass are distributed into melt phase complexes or precursors just prior to pyroxene formation must be discussed.

4.3.1. Melt Phase Speciation Just Prior to Pyroxene Formation

It is hypothesized that melt phase complexes or precursors analogous to a pyroxene-like intermediate (that incongruently melts to form hematite or primarily spinel) control crystallization in DWPF glasses. This led to the further proposal that the solution (i.e., Equation 13) to the solubility (or freezing point depression) problem in the appropriate pyroxene-substituted nepheline field would provide a reasonable basis for relating liquidus temperature to glass composition. However, this relationship involves speciating or distributing the constituent components in the molten glass just prior to pyroxene formation. This speciation has been defined in such a way as to account for the various issues regarding the pyroxene structure as illustrated in Table I and Table II. One such speciation based upon the information in Table II is provided in Table VIII.

The speciation provided in Table VIII was obtained by adhering to the limitations indicated in Table II; that is, the molar contributions of the various cations were constrained based upon the site information in Table II. For example, the available Si^{4+} cations (corresponding to moles of SiO_2) were initially distributed equally among the MT, T2, and T3 tetrahedral sites and the Al^{3+} cations (corresponding the moles of Al_2O_3) were distributed equally among the MT, M1, T2, and N2 sites. Because there are no data on how such cations are distributed in molten glass, a trial-and-error method was used to improve the initial estimates of the cation distributions using the SG Study data (because this was a designed set of data describing expected DWPF compositions). In other words, it was hypothesized that the model represented in Equation 13 would be reasonable for DWPF glasses and distribution of the cations were varied systematically (while constrained by the information in Table II) until the resulting model described the SG Study data with no lack-of-fit at the 95% confidence level[†]; the estimated distributions for this model are provided in Table VIII. Thus if 1) the model in Equation 13 is descriptive and 2) the distributions obtained from the 50 SG Study data (which were designed over the expected DWPF composition region) were reasonable, then the model in Equation 13 using the distribution information in Table VIII would also describe the remaining 55 model data (and pertinent validation data).

Table VIII. Distribution in DWPF Molten Glass Just Prior to Crystallization*

	Pyroxene-like Precursors			Nepheline-like Precursors		
	M2	**M1**	**MT**	**N1**	**T2**	**SUM**
Al_2O_3	0	0.0607	0.9393	0	0	1.0000
B_2O_3	0	0	0	0	0	0.0000
CaO	0.029	0	0	0	0	0.0290
Cr_2O_3	0	0.9202	0	0	0	0.9202
Fe_2O_3	0	0.1079	0.0193	0	0.6094	0.7366
K_2O	0.3041	0	0	0.1049	0	0.4090
Li_2O	0.1745	0	0	0.1068	0	0.2813
MgO	0.0167	0.0223	0	0	0	0.0390
MnO	0.994	0.00603	0	0	0	1.0000
Na_2O	0.1671	0	0	0.2518	0	0.4189
NiO	0	0.1079	0	0	0	0.1079
SiO_2	0	0	0.0193	0	0.0133	0.0326
TiO_2	0	0.0568	0	0	0.5667	0.6235
U_3O_8	0	0	0	0	0	0.0000
ZrO_2	0	0.0458	0	0	0	0.0458

[†] When there are repeated measurements, the lack-of-fit (LOF) test for a given model provides an assessment of the possible misspecification in (or what might be missing from) the model at a given confidence level. This test is performed by comparing the residual and replicate standard deviations. It should be noted that this test is often not very powerful because many fewer trials are normally available to estimate the replicate standard deviation. Therefore, a missing LOF warning should not alone be interpreted to mean that the model adequately fits the data—it most likely indicates that there is insufficient evidence for lack-of-fit if it is actually present.

* Note that the DWPF glasses studied in this report contain little or no ZnO and thus this component has been omitted from the model presented in this report.

Using the model in Equation 13 and the speciation in Table VIII, the following relationship between $(1/T_L)$ and composition is obtained for the 50 SG Study data (△):

Equation 15

$$\frac{1}{T_L(K)} = -0.000260\ln(M_2) - 0.000587\ln(M_1) - 0.000149\ln(M_T) - 0.00150$$
$$= \ln\left\{(M_2)^{-0.000260}(M_1)^{-0.000587}(M_T)^{-0.000149}\right\} - 0.00150$$

as illustrated in Figure 5; the 55 SRTC/CELS data (+) are also shown. (The complete regression analysis obtained from JMP® [24] for the model presented in Figure 5 is provided in Exhibit 1.) Note that the model using this speciation has no significant lack-of-fit at the 95% confidence level and does an admirable job of describing the CELS data; this is despite the fact that the CELS data cover a much broader composition region than the SG Study data. However, it is true that for the SRTC model data, there are very high pair-wise correlations between the mass concentrations for Al_2O_3 and Fe_2O_3 (-0.97), K_2O and TiO_2 (+0.96), K_2O and ZrO_2 (-0.95), TiO_2 and ZrO_2 (-0.96), NiO and Fe_2O_3 (+0.84), etc. These high pair-wise correlations may lead to accurate T_L predictions for these glasses when using the model developed from the SG Study glasses. From the information in Table VIII, it appears likely that the large negative correlation between the Fe_2O_3 and Al_2O_3 concentrations in the SRTC glasses likely allows these glasses to be accurately predicted by the model presented in Figure 5; the other constituents have smaller correlations, generally smaller concentrations in the glasses, and thus likely smaller effects based upon the parameters in Table VIII. Thus, because the model in Figure 5 does such an admirable job of describing the remaining SRTC data (under the conditions described above which should apply to expected DWPF operation), it appears reasonable to use all 105 (i.e., 50 SG Study and 55 SRTC) data in model development.

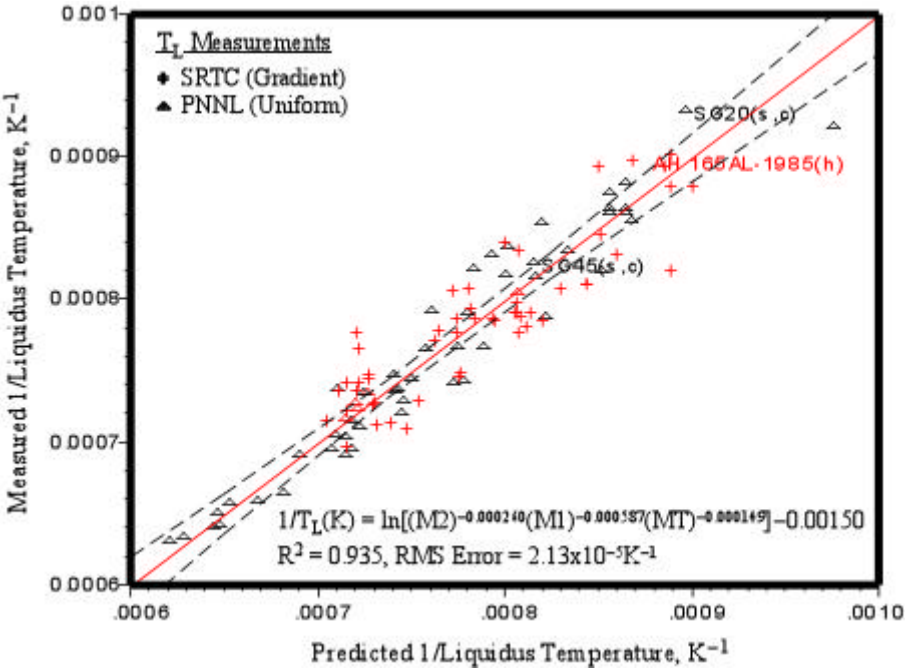

Figure 5. This figure shows the relationship between measured reciprocal liquidus temperature (K^{-1}) and that predicted from Equation 13 using the parameters in Table VIII for the 50 SG Study data. The dotted lines represent the 95% confidence curves about the fitted line.

4.3.2. Speciation is Not Merely "Hiding Model Parameters"

One obvious issue concerning the use of a "speciated" composition basis for DWPF liquidus temperature prediction is that it may appear to the casual observer that distributing the molar composition as indicated in Table VIII may merely be a way to hide fitted parameters without accounting for them in estimating prediction uncertainty. This is considered not the case for a number of reasons. First, such a speciation is considered not significantly different (and in some ways better) than assuming a glass is comprised of oxides (and/or silicates) as done in a number of models used for predicting critical glass properties (e.g., durability, melt viscosity, liquidus temperature, etc.). In many of these models, such a simplification of the glass composition was not taken into account when estimating prediction uncertainty. Furthermore, there is growing evidence that glasses are not composed of such simple structures; thus the proper composition basis is likely more complicated than in existing models. The composition basis for the liquidus temperature model presented in this report is an attempt to capture such information regarding the more complicated molten glass structure upon which properties such as crystallization should, in fact, be based.

Second, the distribution information presented in Table VIII was not obtained from a least-squares regression of available data (although the regression analysis for the SG Study data is presented in Exhibit 1 for reference purposes). There exist alternate cation distributions that describe the SG Study data as well as those presented in Table VIII; however, these alternate distributions do not agree as well with either the information in Table II or other known information concerning pyroxenes. The distributions in Table VIII were defined primarily based upon the pyroxene cation distributions presented in Table II with some regard to the ability of the resulting parameters to describe the aforementioned SG Study data. However, it is the ability of any model to provide *unbiased* descriptions of the 50 SG Study data, the 55 SRTC model data, and any pertinent validation data that will determine whether or not the model presented is appropriate for DWPF process control.

4.3.3. Proposed Semi-Empirical Model for DWPF Liquidus Temperature Prediction

Because the relationship using the distribution information in Table VIII appears to describe both the 50 SG Study data and the 55 SRTC CELS data (which have high, negative Al_2O_3-Fe_2O_3 correlations among others), these data are combined for model development (because they have similar pedigrees including the use of standards and measured compositions and expected DWPF compositions are anticipated to have the same kinds of correlations as seen in the SRTC model data). Figure 6 illustrates the least-squares relationship for (reciprocal) liquidus temperature as a function of composition for the 105 model data. This relationship has four fitted parameters and has the form:[†]

Equation 16

$$\frac{1}{T_L(K)} = -0.000260\ln(M_2) - 0.000566\ln(M_1) - 0.000153\ln(M_T) - 0.00144$$
$$= \ln\left\{(M_2)^{-0.000260}(M_1)^{-0.000566}(M_T)^{-0.000153}\right\} - 0.00144$$

where the new coefficients were obtained from the multi-linear regression of $(1/T_L)$ as the dependent variable and $\ln(M_2)$, $\ln(M_1)$, and $\ln(M_T)$ as the independent variables based upon the speciation provided in Table VIII and the 105 SG Study and SRTC model data; the least-squares results are $R^2 = 0.891$ and $s_r = 2.28\text{x}10^{-5}K^{-1}$ for this information. (The complete JMP® [24] output for this regression analysis is provided in Exhibit 2 and the measured liquidus temperatures versus those predicted using the proposed and current DWPF model are provided in Table XXIX in the appendix in Section 18.) Note the small differences in the coefficients between Equation 15 and Equation 16 as well as the large differences in the abilities of the mechanistic-based relationships (i.e., Figure 5 and Figure 6) versus that of the current DWPF model form illustrated in Figure 4. Further note that, as indicated in Exhibit 2, the relationship in Equation 16 does not exhibit a significant lack-of-fit for the model data. The fact that there is no lack-of-fit is reassuring, but not critical, because many of the data were not obtained from designed studies and thus the lack-of-fit results may be understated.

[†] Note the logarithmic expansion was used:
$\ln\{[M_2^a][M_1^b][M_T^c]\} = \ln(M_2^a) + \ln(M_1^b) + \ln(M_T^c) = a\ln(M_2) + b\ln(M_1) + c\ln(M_T)$.

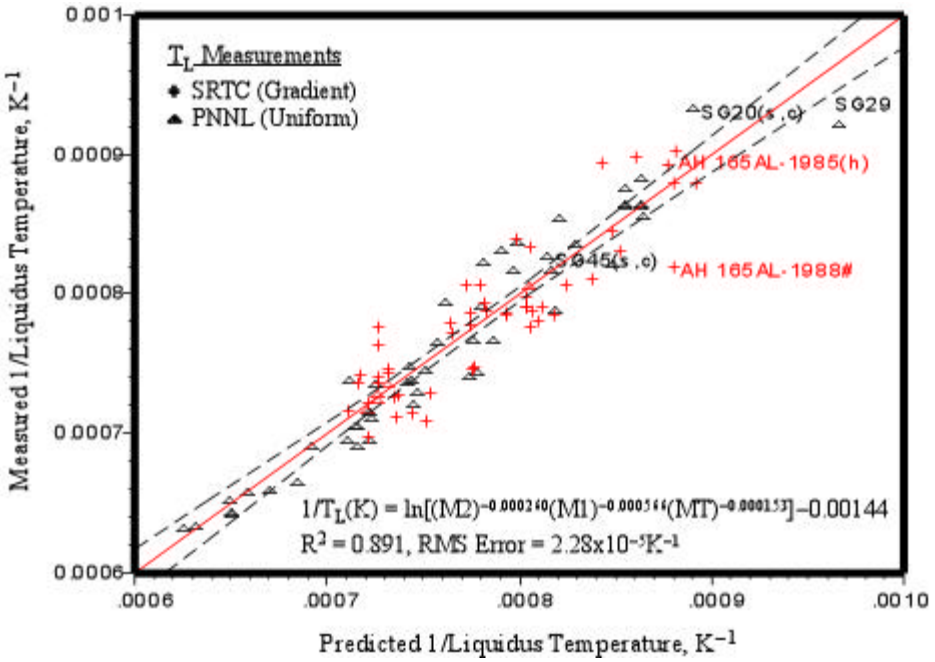

Figure 6. This figure shows the relationship between reciprocal liquidus temperature (K^{-1}) and the composition term from Equation 13 for the 105 DWPF model data. The dotted lines represent the 95% confidence curves about the fitted line.

From Equation 13 (and a little algebra), the new relationship can also be expressed as:

Equation 17

$$\frac{1}{T_L(K)} \approx -\frac{R}{\Delta\overline{H}_{fus,P}\left(T_P^*\right)}\ln\left\{(M_2)^a(M_1)^b(M_T)^c\right\}+\left\{\left(\frac{1}{T_P^*}\right)-\frac{R\ln(K_P)}{\Delta\overline{H}_{fus,P}\left(T_P^*\right)}\right\}.$$
$$= \ln\left\{(M_2)^{a'}(M_1)^{b'}(M_T)^{c'}\right\}+d$$

where

$$a' \equiv -a\left[\frac{R}{\Delta\overline{H}_{fus,P}\left(T_P^*\right)}\right],\ b' \equiv -b\left[\frac{R}{\Delta\overline{H}_{fus,P}\left(T_P^*\right)}\right],\ c' \equiv -c\left[\frac{R}{\Delta\overline{H}_{fus,P}\left(T_P^*\right)}\right],\ \text{and}$$

a, b, and c are the parameters presented in Equation 13. However, there are too many degrees of freedom in the above expression to solve explicitly for the fundamental parameters. Additional information, likely in the form of estimates of one or more of the above parameters, will be necessary to estimate the fundamental parameters.

There is an assumption implicit in Figure 6 and Exhibit 2 since unweighted least squares regression was used to fit the model to data. The use of this technique requires that the errors in ($1/T_L$) be stable over the range considered which is possibly important since T_L and not ($1/T_L$) is actually measured. The residuals from the model fit are shown in Exhibit 2; these indicate no instability in the residuals in the predicted ($1/T_L$) values for the model data.

There is another interesting feature of the cation distribution information in Table VIII and the resulting liquidus temperature model in Equation 16: neither B_2O_3 nor U_3O_8, which are major species in a number of glasses, are used to describe the T_L response as a function of composition. That is, because no known site information suggests that these cations should be incorporated into the pyroxene-like precursors, they were omitted from the resulting model described by Figure 6. If these components were important to describing the liquidus temperature for the glasses studied, then it is likely that the residuals from the model fit would be described by

the concentrations of B_2O_3 and U_3O_8 in the model glasses. A response surface model in molar B_2O_3 and U_3O_8 was used to attempt to describe the 105 model data residuals. The results indicated that none of the B_2O_3 and/or U_3O_8 terms were significant (at the 5% significance level) in describing the residuals. Therefore, it appears as though the proposed liquidus temperature model more than adequately describes the model data using the 13 components presented in Table VIII.

The model presented in Equation 16 appears to describe the general relationship between (reciprocal) liquidus temperature and composition for the DWPF model data; however, it remains to determine whether or not this model is significantly better than the current DWPF model (although Figure 4 clearly demonstrates the inadequacy of the current model for the expanded glass composition region). One of the reasons for revising the liquidus temperature model is to decrease the prediction uncertainty, which should, all other things being equal, correspondingly allow increased DWPF waste loading. For example, the RMS Error, s_r, for the current DWPF model using the original 22 data was approximately 37°C although the prediction uncertainty for the model generated from the data in this report is almost 95°C. The value of s_r provided from the regression results for Equation 16 was $2.28 \times 10^{-5} K^{-1}$ and thus cannot be compared directly. Using error propagation, the approximate error in the reciprocal liquidus temperature can be related to that in the liquidus temperature measurement by:

Equation 18
$$\sigma_{T_L} \approx \left[\left(\overline{T_L^{-1}}\right)\right]^{-2} \sigma_{T_L^{-1}}$$

From the regression results (where the mean reciprocal liquidus temperature is $0.0007737 K^{-1}$), the r_s value of $2.28 \times 10^{-5} K^{-1}$ translates into approximately 38.1°C (using Equation 18) which is only slightly larger than that for the current model (which is applicable to a much smaller composition region). This indicates that significant improvement in prediction (and thus higher waste loading) can be expected from the mechanistic-based model provided in Equation 16.

4.4. Outlier Analysis and Lack-of-Fit in the DWPF Spinel Liquidus Temperature Model

However, because the model data were not all collected as part of an experimental design, there may be data that are outlying or highly influential on the fit illustrated in Figure 6. Cook's D statistic is a metric that identifies points of high influence in least-squares fits: large values of the Cook's D statistic indicate high influence on the least-squares fit based upon a linear effects model. The Cook's D values for the 105 model data ranged up to a value of 0.124 (as compared to a maximum of 0.648 for the 50 SG Study data exhibiting spinel [9], which were taken from a designed study). However, because the Cook's D values are most legitimately compared within a set of data, the model datum (i.e., AH 165AL-1988) with the largest Cook's D value (of 0.124) was removed from the data set and the fit recomputed using the resulting 104 Model Data. The maximum difference in predicted liquidus temperatures for the model data is less than 0.47%. Therefore, no model data are excluded for purely data-driven reasons.

From Exhibit 2 there is another aspect of the model in Equation 16 that must be examined: this model has no apparent significant lack-of-fit (LOF) at a 95% confidence level for the model data. Part of the reason for this may be that many of the repeated measurement were averaged because of the observed differences between long and short-term errors. However, because many of the data were not obtained from studies designed to capture all sources of variation, it is unlikely that the model data captured all sources of variation. Thus the estimate of "pure" error provided in the JMP® analysis would be an underestimate of the true "pure" error in the liquidus temperature measurements; this would make it more likely that a significant LOF determination would be identified for the model. It was assumed that the latter condition (i.e., underestimating the "pure" error) would at least compensate for the former (i.e., impact of short-term errors) in the LOF determination for the model.

Another contribution to the possible LOF for any model is that the model may not capture all composition effects important to liquidus temperature prediction. One method for examining this possibility for Equation 16 is by determining whether the liquidus temperature residuals (i.e., measured versus predicted T_L) are highly correlated with any other composition term. Such a high correlation may indicate that other composition terms may be introduced to improve the model fit; however, there must also be a legitimate corresponding mechanistic reason for inclusion of such terms before they can be included in the liquidus model. The fact that additional

model terms may help reduce prediction variation (i.e., potentially better describe the variation in the system) is not a sufficient reason for their inclusion. Such considerations will be pursued later in this report when the SRTC data are examined.

Variations in pyroxene properties will result in biases in the predictions made using Equation 16.† Since only random prediction uncertainties are currently considered in the DWPF process control scheme, such prediction biases must be small for the model presented in Equation 16 to be useful for DWPF process control using the current control system. Validation data will be examined below to assure that these biases are indeed likely to be sufficiently small.

4.5. Applicability of the DWPF Spinel Liquidus Temperature Model

The model presented in Equation 16 appears to describe the relationship between liquidus temperature (for DWPF glasses exhibiting spinel) and composition for the 105 model data. Since the melt temperature, enthalpy of fusion, and equilibrium constant were unavailable for the pyroxene-like melt phase complexes or precursors assumed to control crystallization in DWPF glasses, these parameters were estimated using least-squares. Thus the model in Equation 16 is semi-empirical (or preferably "semi-mechanistic") in the sense that the model form is based upon mechanistic information; however, necessary coefficients were estimated from appropriate experimental data. Table IX and Table X provide the pertinent mass and molar oxide component ranges, respectively, from which Equation 16 was obtained and thus describe the region of applicability of the model. Considering Table IX, all concentrations for these glasses fall within the DWPF range as specified in Reference 9.

Table IX. SG Study and SRTC Model Data Composition Ranges in Weight Percent (on a Glass Basis)

	Al_2O_3	B_2O_3	CaO	Cr_2O_3	FeO	Fe_2O_3	$(\Sigma Fe)_2O_3$	K_2O	Li_2O
Maximum	14.162	12.652	2.007	0.3008	6.901	16.977	17.60	3.8846	6.1576
Minimum	0.99	4.893	0.3053	0	0.0161	3.427	3.452	0	2.4901
	MgO	MnO	Na_2O	NiO	SiO_2	TiO_2	U_3O_8	ZrO_2	Total*
Maximum	2.6502	3.25	14.901	3.045	58.230	1.8549	5.1378	0.97	94.5479
Minimum	0.470	0.7392	5.989	0.0379	41.795	0	0	0	81.5746

* The shaded components are included in the proposed DWPF liquidus temperature model. As indicated in the Total column, they constitute between approximately 81.6 and 94.5% of the model glasses by weight.

Table X. Model Data Ranges for the Proposed Pyroxene-like Terms

	M_2	M_1	M_T
Maximum	0.394	0.0719	0.441
Minimum	0.218	0.0323	0.108

There is another characteristic of the model data (other than the design efficiency described in Section 4.1 and the composition ranges shown in Table IX and Table X) that indicates how well the data describe expected DWPF glasses: the pair-wise correlations between concentrations. For example, a high degree of correlation between concentrations will make it difficult to separate effects significant to the liquidus temperature response. Exhibit 3 provides the pair-wise correlations and corresponding scatterplots representing the model mass oxide concentrations. (The concentrations for the 13 oxides shaded in Table IX were selected and normalized to 100% for consistency of comparison.) Because of the manner in which many of the model data were targeted, it is not surprising that the degrees of correlation among many of the pairs of components in the model data are relatively high. However, these high degrees of correlation are 1) for minor components or 2) expected in actual DWPF

† As will be described below, a brief analysis of the prediction residuals as a possible function of the major oxides (i.e., B_2O_3 and U_3O_8) omitted from modeling consideration indicated that neither were significant in describing the residuals.

glass. Exhibit 4 provides similar information for the melt phase complexes described in Table X. Note that the high correlation between the M_1 and M_T terms appears to be largely driven by the SRTC data.

The design efficiencies of the various subsets of data for the terms (i.e., M_2, M_1, and M_T) representing the melt phase complexes can also be computed . The D-efficiencies were computed for various subsets of model data pyroxene-like terms (corresponding to Table VIII) and were 24.9021 for the 53 SG Study compositions (which correspond to 57 liquidus temperatures), 26.3563 for the 46 SG Study compositions (corresponding to 50 liquidus temperatures) exhibiting spinel at T_L, and 22.0886 for the 101 measured compositions for the model glasses (corresponding to all 105 model liquidus temperatures). Therefore, including the SRTC data, in this case, did not significantly decrease the efficiency of the design.

4.6. Prediction Uncertainties and Empirical Relationships

There are two ends to the modeling spectrum [25]: empirical at one end and completely mechanistic at the other[†]. In an attempt to reduce prediction bias (as required by the statistical methods normally employed), many terms (including non-linear ones) must often be included in empirical models for complex systems; this results in large prediction uncertainties. Mechanistic model forms (i.e., those based upon first-principles), which have often been developed with parsimony in mind, can be inflicted by large prediction biases. Historically, both methods have been used to develop models for liquidus temperature prediction from composition with varying degrees of success [9,23,26,27,34]. The methods employed in this report to develop the new liquidus temperature model fall in-between because, even though the forms of the models were developed using mechanistic information, essential parameters had to be estimated from least-squares fits. Since the new model was developed with parsimony in mind, it will subsequently be determined (via validation data) whether the new liquidus temperature model appears to be inflicted by excessive prediction biases.

Similarly, there is a spectrum of data generation techniques: on the one hand, there are statistically-designed studies covering all independent variables including a sufficient number of interior points to discern significant non-linear (including interaction) effects, and on the other hand, there are ad hoc sets of data derived with the best of intentions, however, without optimality in mind. Historically, data from both ends of this spectrum have been used for model development—also with varying degrees of success. Obviously, the best of all possible worlds is to possess a completely mechanistic model that accurately describes the data obtained from an optimal, designed study. However, this circumstance rarely occurs, especially in complicated systems such as waste glasses.

With these facts in mind, the new liquidus temperature model (i.e., Equation 16) can be compared to both the current DWPF model form (i.e., Equation 14) updated for the new model data as illustrated in Figure 4 and an empirical model like that developed by PNNL for the SG Study glasses that exhibited spinel as the primary liquidus temperature phase [27]. The concentrations used for the empirical model will be the normalized compositions over the same components as those used by PNNL for the SG Study glasses. The empirical model is examined to highlight the differences between a semi-empirical model form (Equation 16) based on mechanistic information and a strictly empirical model neglecting any mechanistic information. The empirical relationship that will be studied assumes that T_L (in °C) can be described by a linear combination of the normalized constituent percent mass oxide concentrations [27].

The least-squares results using the 105 model data are presented in Exhibit 5 for the proposed empirical relationship; the R^2 and RMS Error for this fit are 0.882 and 42.6°C, respectively, or, in other words, the empirical relationship presented does not do as adequate a job in describing the variance in the model data as Equation 16 (which is based upon mechanistic information). Despite having 14 fitted parameters, the empirical relationship presented in Exhibit 5 exhibits a significant lack-of-fit (LOF) unlike the mechanistic relationship in Equation 16 (as described in Section 4.4). Furthermore, the model includes three parameters with little significance in describing the relationship between liquidus temperature and the model data compositions. Therefore, there is little chance that the empirical relationship presented will shed much light on liquidus temperature prediction. Because both the revised version of the current DWPF model (i.e., Equation 14) and the

[†] As described in ASTM Standards [25], empirical analysis is performed as input to mechanistic analysis. The results from these analyses determine the type of model that will be developed.

empirical relationship presented in Exhibit 5 provide less information concerning the relationship between liquidus temperature and composition, neither will be pursued further.

However, it will be enlightening to examine the predictions and corresponding uncertainties for the semi-empirical liquidus temperature model presented in Equation 16. One metric demonstrating the utility of a model is the random uncertainty associated with predictions made using the model in question. When a model is to be used multiple times (as is the case with the T_L model), Scheffé-type prediction uncertainties [28] for the expected response can be useful:

Equation 19
$$\text{Prediction} \pm s_r \sqrt{pF_{\alpha}(p, n-p)} \sqrt{\underline{c}_0 \left(\mathbf{X}^T\mathbf{X}\right)^{-1} \underline{c}_0^{\,T}}$$

where s_r is the RMS Error, $F_\alpha(p,n–p)$, is the $100(1–\alpha)\%$ two-sided quantile from the F-distribution for a p parameter model estimated from n data, $\underline{c}_0$ is the vector of independent variables for which the prediction is to be made, and $(\mathbf{X}^T\mathbf{X})$ is the product moment matrix representing the independent variables in the model. Use of these prediction intervals assumes that there is no significant lack-of-fit in the model (as is the case with Equation 16). However, even if the manner in which replicate T_L measurements were made did not likely cover all possible sources of variance and the LOF for the mechanistic model understated, the resulting slight inflation of the s_r values for this model should allow coverage of the prediction uncertainty interval described by Equation 19 to be close to nominal.

It was stated above that the prediction uncertainties in Equation 19 are the two-sided intervals about the model prediction; however, there is only an upper constraint (of 1050°C or 1323K) on liquidus temperature. Because the inverse of liquidus temperature (or $1/T_L$) is predicted, this constraint translates into a lower limit on $(1/T_L)$ of approximately $7.56\text{x}10^{-4}\text{K}^{-1}$. Therefore, the test for liquidus temperature should be one-sided based upon the one-sided lower bound on the $(1/T_L)$ prediction, or:

Equation 20
$$\frac{1}{T_L(\text{K})} - s_r \sqrt{pF_{2\alpha}(p, n-p)} \sqrt{\underline{c}_0 \left(\mathbf{X}^T\mathbf{X}\right)^{-1} \underline{c}_0^{\,T}} \geq 7.56\text{x}10^{-4}\text{K}^{-1}$$

where the predicted $(1/T_L)$ is obtained from Equation 16 and 2α replaces α in the two-sided limits in Equation 19.

The Scheffé-type lower bounds on the predictions for the p=4 parameter model based upon N=105 model data presented in Figure 6 are estimated using:

Equation 21
$$\ln\left\{(M_2)^{-0.000260}(M_1)^{-0.000566}(M_T)^{-0.000153}\right\} - 0.00144$$
$$-\left(2.28\text{x}10^{-5}\right)\sqrt{pF_{2\alpha}(p, N-p)} \sqrt{\xi \begin{bmatrix} 105 & -126.56 & -309.14 & -162.47 \\ -126.56 & 154.22 & 371.50 & 194.98 \\ -309.14 & 371.50 & 913.84 & 473.73 \\ -162.47 & 194.98 & 473.73 & 265.64 \end{bmatrix}^{-1} \xi^T}$$

where ξ is defined to be the vector (i.e., $[1\ \ln(M_2)\ \ln(M_1)\ \ln(M_T)]$) of values at which to predict $(1/T_L)$. For example, the constraint test for the AH-131Fe-A and -B predictions based upon the compositions in Table XXII (and thus the values of M_2, M_1, and M_T are 0.259, 0.0677, and 0.150, respectively) is:

$$7.253\text{x}10^{-4} - \left(2.28\text{x}10^{-5}\right)\sqrt{(p)F_{2\alpha}(p, N-p)}\sqrt{0.0376} \geq 7.56\text{x}10^{-4}$$
$$7.253\text{x}10^{-4} - \left(2.28\text{x}10^{-5}\right)\sqrt{(4)(2.001)}\sqrt{0.0376} \geq 7.56\text{x}10^{-4}$$
$$7.253\text{x}10^{-4} - 2.423\text{x}10^{-6} \geq 7.56\text{x}10^{-4}$$

where 0.0376 is the product of the composition term and inverse product moment matrix from the 105 model data and $F_{2\alpha}(4,101)$ is 2.001 at the 95% (one-sided) confidence interval. The one-sided 95% lower bound for this glass translates into: $T_L \leq 1130^oC$ (which, as indicated above, exceeds the DWPF upper T_L limit of 1050^oC); the average measured value for this glass is 1108^oC.

Table XI summarizes the model prediction and corresponding uncertainty information for the model represented in Equation 16. The prediction uncertainties for the model appear to be relatively small (despite the number of parameters in the model). Thus the model should provide reasonable waste loading increases especially considering the data for which the current DWPF model no longer is valid and the revised model form would have to be used if the model form in Equation 13 was valid. As mentioned above, the prediction errors for the mechanistic model based upon Equation 16 will most likely be significantly smaller than those for the proposed empirical model (as presented in Exhibit 5) or those based upon the revised version of the current model (i.e., Equation 13). As long as the validation data suggest that there are no large prediction biases associated with the mechanistic model, then use of this model for predicting liquidus temperature should be better from a waste loading perspective. Such prediction errors (both random and systematic) must be accounted for by DWPF when determining whether a composition is likely to undergo crystallization. Therefore, one cannot determine solely from this information which of these models should be selected for DWPF process control.

Table XI. Prediction Uncertainty Results (in °C) for the DWPF Semi-Empirical Model

	Measured	Predicted	1-Sided 95% Upper Bound	1-Sided 95% Uncertainty	% of Prediction
Min	799	762	784	0.426	0.847
Max	1309.5	1322	1378	90.4	3.35

4.6.1. Composition Measurement Uncertainty

Apart from the prediction errors (as summarized in Table XI for the model data), any errors associated with measuring the composition from which the liquidus temperature must be predicted must be introduced to assure that the glass in question will not crystallize in the DWPF melter.† To estimate the relevant measurement uncertainties, the error for each measured concentration can be first propagated through the model and the resulting pair-wise covariances summed to provide an estimate of the measurement variance. For the model in Equation 16, the variance would be:

Equation 22
$$V\left(\frac{1}{T_L}\right) \approx \sum_i \sum_j \left\{ \left[\frac{\partial}{\partial [i]} \left(\frac{1}{T_L} \right)_{pred} \right] (r_i [i]) \left[\frac{\partial}{\partial [j]} \left(\frac{1}{T_L} \right)_{pred} \right] (r_j [j]) \rho_{i,j} \right\}$$

for i and j from $\{Al_2O_3, CaO, Cr_2O_3, Fe_2O_3, K_2O, Li_2O, Na_2O, MgO, MnO, NiO, SiO_2, TiO_2, \text{and } ZrO_2\}$ and

Equation 23
$$\left(\frac{1}{T_L}\right)_{pred} \equiv \ln\left\{(M_2)^{-0.000260}(M_1)^{-0.000566}(M_T)^{-0.000153}\right\} - 0.00144$$

as indicated in Equation 16. In the above expression, r_i, [i], and $\rho_{i,j}$ are the relative standard deviation, molar concentration (on a 100g glass basis), and correlation coefficient, respectively. The glass chemical composition measurement variances associated with the (reciprocal) liquidus temperature predictions for the 105 model glasses were estimated using the prototypic DWPF variance information [1]. The resulting variances range from 4.80×10^{-11} to 1.62×10^{-9} $(°C)^2$ or the standard deviations associated with the model data predictions (each from a

† All compositions used in liquidus modeling were either measured by Corning Engineering Laboratory Services (CELS) or had measurements corrected to CELS standards. These compositions had oxide sums of 100±5%. This is the same standard applied to the data used to develop the DWPF durability model.

single composition measurement) range from 6.93×10^{-6} to 4.02×10^{-5} °C or between 0.81 and 5.4% of the predicted reciprocal liquidus temperatures. Assuming four samples are used to estimate a composition (as currently is the case in DWPF to determine SME melter feed acceptability), the uncertainties[††] at the 95% confidence level associated with (reciprocal) liquidus temperature predictions would range from 0.70 to 4.7% of the corresponding predictions.

These measurement uncertainties computed above can be added to their corresponding prediction uncertainties (i.e., as summarized in Table XI); the resulting limits correspond to those used previously to define the Measurement Acceptable Region (MAR) for DWPF melter feed acceptability [1]. The differences between the predictions and the lower such (MAR) bounds for the 105 model data range from 25 to 108°C (with an average of 49°C) or between 2.5 and 9.5% (with an average of 4.7%) of the predicted liquidus temperatures. Thus even though the model represented in Equation 16 has two additional fitted parameters and includes many more components than the current model form (i.e., Equation 13), the errors corresponding to the MAR for Equation 16 are comparable to those for the current DWPF model (which are normally on the order of 50°C). The current model was shown in Section 4.2 to be inadequate for process control over the expected DWPF composition region, and it will be demonstrated below that the current model is likely very conservative for the first two macrobatches processed through DWPF.

This demonstrates that models must be evaluated in terms other than solely R^2 and s_r. The number of parameters needed to describe adequately the data plays a vital role in developing a model that can be used for process control; therefore, in this report mechanistic information was employed to the extent possible to define a parsimonious set of composition parameters to describe liquidus temperature. Empirical relationships often admirably describe the variance in the data; however, they often do so at a cost in the number of parameters needed and the resulting prediction error that must be tolerated. The semi-empirical model represented by Equation 16 has the benefits of being based upon mechanistic information and suffering from no significant lack-of-fit (i.e., no large prediction biases in the model data). It allows DWPF liquidus temperatures to be predicted with combined prediction and measurement errors comparable to the current DWPF model, which appears from Figure 4 to be inadequate to describe expected, future DWPF glass compositions.

4.6.2. "Knobs" for Adjusting Prediction and Measurement Errors and, Thus, Waste Loading

Since the liquidus temperature constraint is not waste (acceptance) affecting, there is no regulatory requirement that DWPF control this property in the melter to the 95% confidence level. A high degree of confidence (i.e., 97.5%) was used for the liquidus temperature constraint because of the sparse nature of the liquidus temperature data that existing at the time the current model was developed [1]. However, the confidence level applied to the liquidus temperature constraint is merely an assessment of the level of risk DWPF is willing to take with harming the melter during routine operation. There is no known reason that the confidence level associated with the liquidus constraint cannot be adjusted. Table XII illustrates the dramatic impact of changing the requisite confidence level for liquidus temperature on the resulting lower confidence bound on $(1/T_L)$ from Equation 19 and Equation 20 corresponding to the upper bound on T_L as indicated in Table XII. It would seem that the added confidence in the liquidus temperature predictions afforded by use of Equation 16 would allow DWPF to accept some slight additional risk in setting the confidence level, $100(1 - \alpha)\%$, for this constraint to a value lower than the current 0.05 (which translates to a 95% confidence level). Even a fairly small change in α from 0.05 to 0.10 may have a significant impact on waste loading.

[††] The prediction uncertainty can then be estimated by multiplying the square root of this variance (taking into account the number of samples) by the appropriate quantile of the Student's t-distribution for the desired significance level and degrees of freedom associated with the measurement errors.

Table XII. Effect of Confidence Level, 100(1 – α)%, on Differences (in °C) Between Predictions and Upper Prediction and Total (Prediction and Measurement) Bounds for the Model Data

α	0.25		0.20		0.15		0.10		0.05		0.01	
	Pred.	Total	Pred.	Total	Pred.	Total	Pred.	Total	Pred.	Total	Pred.	Total
Min	7.1	12.8	7.8	15.0	8.6	17.5	9.5	20.7	10.9	25.5	13.5	35.0
Avg	13.7	24.6	15.0	28.8	16.6	33.7	18.4	39.9	21.1	49.4	26.3	68.4
Max	35.5	52.7	39.1	62.0	43.2	72.8	48.1	86.7	55.3	108.0	69.0	151.5

Using similar reasoning (i.e., having a better liquidus temperature prediction), it might also be warranted for DWPF to consider decreasing the current 100°C safety factor incorporated into the DWPF liquidus temperature constraint. In other words, the nominal operating temperature for the DWPF melter is 1150°C during routine operation and the corresponding constraint for liquidus temperature is set at 1050°C to provide additional assurance that significant crystalline material will not form and harm the melter. However, even a fairly conservative change of 25°C in this safety factor from 1050 to 1075°C has a very significant potential impact on waste loading. In fact, the potential impact may be greater than that associated with decreasing the confidence level for acceptance from 95% (or $\alpha = 0.05$) to 75% (or $\alpha = 0.25$) using Table XII as a guide. This will be investigated further during the waste loading examination.

5. FURTHER EXAMINATION OF THE DWPF LIQUIDUS TEMPERATURE MODEL

Spinel was observed at the liquidus temperature for the glasses used to generate the model data. However, nepheline has also been discovered in DWPF glasses during time-temperature-transformation (TTT) analysis of a high Al_2O_3/high Na_2O containing glass [29] when significant amounts of TiO_2 were included in the glass frit. (The TiO_2 may have promoted nepheline nucleation [30] or forced the resulting glass composition into a different primary phase field.) Furthermore, clinopyroxene was observed in other DWPF glasses [9]. However, the presence of these other phases in DWPF glasses should not present a problem for modeling DWPF liquidus temperature because 1) the spinels expected in DWPF glasses crystallize at significantly higher temperatures than these other phases and 2) spinels readily crystallize in 24 hours even without the aid of nucleating agents such as TiO_2. Because spinel is the primary liquidus phase expected in most DWPF glasses (and for a given composition the predicted spinel liquidus temperature will be higher than that for the other phases), modeling efforts can be concentrated legitimately on predicting spinel formation in DWPF glasses. Despite these facts, the glasses manifesting these other phases at the liquidus temperature will be examined.

There is an abundance of possible data from which to examine the relationship between liquidus temperature and composition for complicated glass systems. These glasses that have been measured for liquidus temperature were melted, heat treated, and quenched in a variety of ways. The measurements have been made either using a uniform temperature method (at small temperature increments and, at other times, using much larger ones) or using a gradient furnace. (For example, many of the CELS measurements for the SRTC glasses were confirmed using uniform temperature melts.) The glass compositions and their corresponding measurements as well as the liquidus temperature measurements have resulted from statistically designed experiments or were, at times, generated on an ad hoc basis because of time and resource limitations. Furthermore, the compositions of some glasses were not always measured to confirm batch accuracy. All of these factors can influence the ability to generate a reliable and accurate relationship between liquidus temperature and composition.

To reduce such nuisance variations, the model data used were selected from glasses that exhibited spinel at the liquidus temperature and whose compositions were measured (confirming batching accuracy) and represented those expected in DWPF. Measurements from both gradient furnace and PNNL uniform temperature methodologies were used since a previous study [31] suggested that there was no appreciable bias between these methods for glasses melted and quenched under similar conditions. For the validation data, such stringent selection criteria could not always be employed (e.g., not all glasses were measured for composition to confirm batching accuracy). Many of these data were generated from statistically designed studies although compositions were rarely measured to confirm batching accuracy and complete information concerning fabrication and testing was not available.

Furthermore, none of the other data available for model validation were within the model data composition space (i.e., Table IX)[†] even when the region was expanded by up to 20% on the individual concentrations. Therefore, because the semi-empirical liquidus temperature relationship in Equation 16 is based upon fitted parameters (i.e., a, b, c, and d), a case can be made that using the new liquidus temperature relationship outside the model data composition space might be problematic and any data outside the model data space may not be applicable. On the other hand, it is believed that these data can illustrate the usefulness of the new model even when applied to data outside those from which it was developed. (For example, the SRTC data were from "outside" the SG Study composition space; however, because these data were accurately predicted by the model, the data sets were combined and a new model developed.) Therefore, the methodology in this section will run somewhat counter to the norm; that is, the various other liquidus temperature data will be examined to see if the proposed model appears applicable and, if not, what might cause observed biases in predictions. This may allow even better models to be developed in the future.

5.1. West Valley Nuclear Services (WVNS) Data

The initial set of data that will be examined, denoted "WVNS" [32], were generated by Alfred University for the operation of West Valley Nuclear Fuel Services and were measured isothermally to the nearest 25°C. All 24 T_L measurements were reported as being between 950 and 975°C with spinel at the lower temperature. (The higher temperature of 975°C will be used to represent T_L because this is the highest temperature at which the glasses are known to be amorphous.) Because spinel was observed at T_L, it is possible that the proposed liquidus temperature model may predict the liquidus temperatures for the WVNS glasses without significant biases. Only as-batched compositions (summarized in Table XIII) were available for these glasses.

The 24 WVNS glasses (△) were plotted on the figure representing the proposed revised liquidus model as shown in Exhibit 6. From this exhibit, it appears that the measured (or "bounded") liquidus temperatures for the WVNS glasses are generally overpredicted (or the reciprocal of the measured liquidus temperature is underpredicted). This is not especially remarkable because of the bounding nature of the liquidus temperature data and the fact that the Cr_2O_3 concentrations for two (CR-004 and CR-005) of the glasses and the ZrO_2 concentrations for all the WVNS glasses are well above their corresponding maxima for the model data shown in Table IX (which, for Cr_2O_3, also makes them above the applicable DWPF solubility limit [1]). Thus the T_L predictions for these glasses are likely to be high. It is interesting to note, however, that the predictions tend to approach their corresponding bounded T_L values as the Cr_2O_3 concentration decreases. Because this type of prediction bias is conservative for DWPF process control, other data will be examined to discern whether they indicate similar responses.

Table XIII. Composition Ranges in Weight Percent (on a Glass Basis) for WVNS Glasses

	Al_2O_3	B_2O_3	CaO	Cr_2O_3	$(\Sigma Fe)_2O_3$	K_2O	Li_2O	MgO
Maximum	5.181	10.342	0.720	0.800	17.739	3.700	3.140	1.410
Minimum	1.680	10.282	0.370	0.000	10.389	3.640	3.140	1.330

	MnO	Na_2O	NiO	SiO_2	TiO_2	U_3O_8	ZrO_2
Maximum	2.456	11.851	1.010	45.576	1.020	0.000	3.520
Minimum	0.008	10.971	0.190	45.326	1.020	0.000	1.530

5.2. Hanford High-Iron Tank Waste Validation Data Measured by PNNL

The second series of data that will be examined were provided by PNNL. The primary liquidus temperature phase for these glasses was again spinel. These glasses, like the SG Study glasses, were melted for 1 hour in a Pt-Rh crucible where the melting temperature for each glass was chosen to give a predicted melt viscosity of 5

[†] Note that the model developed using the pertinent SG Study data was first examined using available SRTC data, which were from outside the composition space of the SG Study data but had numerous high pair-wise correlations. Because the model developed from the SG Study data accurately described the SRTC data, the SG and SRTC data were combined to define the relationship in Equation 16.

Pa•s using an empirical, PNNL model. These glasses, for which only the as-batched compositions are available [33], were quenched, ground, remelted for 1 hour, quenched again, reground, and then measured for liquidus temperature following the same uniform temperature method used to generate a number of the model data. The individual series described in this report are presented in Exhibit 6 (using the relationship in Equation 16) and are described below:

- The "SP" (▲) series of 35 glasses (corresponding to 43 T_L measurements) resulted from a study by PNNL of Hanford high-iron tank waste [33]. As illustrated in Exhibit 6, the model appears to overpredict T_L for the SP glasses. However, the compositions for these glasses are well outside those for the model data for many of the components; none of the SP glasses fall within a region 20% larger than that describing the model data. For example, all the SP data have approximately twice the amount of ZrO_2 as the maximum found in the model data (i.e., Table IX). Furthermore, seven (i.e., SP-Al-3, SP-B-1, SP-B-2, SP-Li-1, SP-Li-2, SP-Mn-3, and SP-Na-1) of the SP glasses were omitted from modeling consideration in an unpublished PNNL report[†] on T_L modeling; however, only three (i.e., SP-Al-3, SP-Mn-3, and SP-Na-1) of these were excluded based upon alternate T_L estimates or specific measurement issues. These three will also be excluded from further examination in this report. As illustrated in Exhibit 6, the remaining SP glasses are reasonably well predicted (i.e., there is a slight bias high in T_L) considering that they are all at least 20% outside the composition space describing the model data. These compositions do not have the high, negative Al_2O_3-Fe_2O_3 correlations found in the SRTC data; however, they do generally fall within the Al_2O_3-Fe_2O_3 bounds defined by the model data. Furthermore, they, like the SRTC data, have very high TiO_2-ZrO_2 correlations.

- PNNL expanded the SP study compositions by five components and the ranges of some major components; these 13 glasses were designated the "SP-3" (▲) series. Of these glasses, three (i.e., SP-B-5, SP-Li-6, and SP-Si-4) were excluded by PNNL from modeling consideration based upon model-specific criteria. As indicated in Exhibit 6, two (i.e., SP-Fe-4 and SP-Si-4) of the SP-3 glasses appear to be very poorly predicted by the proposed liquidus temperature model. The SP-Fe-4 glass was batched to have almost 23 wt% Fe_2O_3 and 1.63 wt% ZrO_2, therefore, the bias in the T_L prediction for this glass is of no great surprise as it could likely exceed the Fe_2O_3 solubility limit for this glass. For example, the maximum Fe_2O_3 concentrations in the SP and model data glasses were 15.0 and 17.6 wt%, respectively. The SP-Li-6 glass is much higher in both Li_2O and ZrO_2 than any of the model data glasses, which might account for its biased prediction. The SP-Si-4 glass was targeted to have only 30% SiO_2 (versus a lower value of 41.8 wt% for the model data) and 2.4 wt% ZrO_2 (versus a maximum of 0.97 wt% for the model data). Thus the biased prediction for this glass is also not surprising. As illustrated in Exhibit 6, the remaining SP-3 glasses are reasonably well predicted (i.e., there appears to be a slight bias low in predicted T_L) considering that all but a single SP-3 glass (i.e., SP-Others-1) is at least 20% outside the composition space describing the model data and all were targeted to have approximately twice the ZrO_2 concentration of any glass represented in the model data. For example, the SP-B-5 glass was targeted to have 20 wt% B_2O_3 but did not have a large prediction bias; this is despite the fact that B_2O_3 is not used in the proposed model. Also the SP-Ca-2 glass had well over twice the CaO than any model data glass. Based upon the composition information provided, the SP-Si-4 and SP-Fe-4 glasses will not be considered further unless other information dictates.

- The "SPx4" (▲) series of 15 glasses (and 19 T_L measurements) was based upon the SP-1 Hanford baseline glass composition (i.e., the glass used by PNNL for bias correction during the SG Study); the four components thought by PNNL to most influence T_L were varied while all other SP-1 components were held in constant relative proportions. Two (i.e., SP-LHLH(b) and SP-LHHL) of these glasses were omitted for PNNL modeling purposes as they were problematic to measure and had to be measured a second time. They have not been excluded from the SPx4 series as their predictions do not appear to be any more or less biased than the other SPx4 glasses as illustrated in Exhibit 6. It should be noted that all the SPx4 glasses have approximately 2.3 wt% ZrO_2 and six have targeted Cr_2O_3 concentrations of 0.6 wt% (or twice the DWPF limit). It appears from the

[†] Vienna, J. D., Hrma, P., Crum, J. V., and Mika, M. "Liquidus Temperature-Composition Model for Multi-Component Glass in the Fe, Cr, Ni, and Mn Spinel Primary Phase Field," Unpublished PNNL Report, Version 5, 2001.

information examined thus far that the proposed model may underpredict T_L for those glasses with higher ZrO_2 than in the model data. This should not be problematic for DWPF as such glasses are not expected to be feasible in DWPF based upon the most recent information available. It may be possible in the future to adjust the ZrO_2 terms in Table VIII to account for these prediction biases.

- A small study of eight glasses denoted "SP-MC" (▵) was designed to provide better coverage of the combined SP and SG composition region. However, only five of the glasses exhibited spinel at T_L, and only a single glass (i.e., SP3-1(env.D)) was used by PNNL for subsequent liquidus modeling. Surprisingly, only a single glass, SP-MC-8, has a large prediction bias based upon the proposed liquidus temperature model (as illustrated in Exhibit 6). The fact that SP-MC-8 has a large prediction bias is not surprising as it was targeted to have almost no Al_2O_3[†] or B_2O_3 and high CaO, TiO_2, and ZrO_2 and is, therefore, likely to have a large prediction bias. What is surprising is that there are relatively small prediction biases for the other four SP-MC glass exhibiting spinel at T_L. The SP-MC-2 glass is targeted to have no Al_2O_3 and high Cr_2O_3 (1 wt%), TiO_2 (5 wt%) and ZrO_2 (8 wt%) concentrations. This appears to disagree with the other glasses studied whereas the T_L predictions for the other glasses with higher ZrO_2 than those in the model glasses appeared to have been biased high. It may be, for example, that this glass has a high Cr_2O_3 concentration and the two cancel each other. The SP3-1(env.D) glass has high CaO and Fe_2O_3 and low SiO_2 concentrations relative to the model data glasses. As a matter of fact, SP3-1(env.D) has the same target Fe_2O_3 and SiO_2 concentrations as the SP-Fe-4 and SP-Si-4 glasses from the aforementioned SP Study glasses, respectively, which were excluded previously. Without additional information (e.g., measured compositions, repeated measurements, etc.), it cannot be determined whether or not the proposed model should be applicable to the SP3-1(env.D) or SP-MC-2 glasses (despite the small prediction biases). These two glasses obviously provide interesting information; however, they are not pertinent to DWPF waste glasses. The SP-MC-1 glass was likely only high in TiO_2 (5 wt%) whereas the SP-MC-9 glass was targeted to be high in CaO (5 wt%), Cr_2O_3 (1 wt%), and TiO_2 (5 wt%). These will be considered reasonable glasses to examine the model unless subsequent data indicate otherwise.

- A set of 23 glasses, designated "MS" (▵), corresponding to 31 T_L measurements was designed, fabricated, and measured for T_L by PNNL to model the behavior of spinel in high-level waste melters. Several components were varied and then a baseline glass chosen for subsequent "one-major-component-at-a-time" examination. Two (i.e., MS-5 and MS-6) of these glasses were excluded by PNNL from modeling consideration; however, all the MS glasses appear to have reasonably small prediction biases according to the proposed T_L model as illustrated in Exhibit 6. Ten of the MS glasses had Cr_2O_3 concentrations higher than the DWPF limit, and all the glasses had between 3 and 6 wt% ZrO_2. It is again surmised that the prediction biases introduced by the high Cr_2O_3 and ZrO_2 concentrations in these glasses may have cancelled.

- A set of 14 miscellaneous glasses denoted "MISC" (▵) produced and measured by PNNL were also examined. Of these glasses, only four (i.e., Nom-2, NomC-2, C106A-3, C106B-2) were used by PNNL for T_L modeling. Furthermore, it appears from Exhibit 6 as though none of the MISC glasses had large prediction biases when using the proposed T_L model. For example, the T51-Opt glass is a high Fe_2O_3 (i.e., approximately 20 wt%) glass with little Cr_2O_3 or ZrO_2 and thus is likely to have a small prediction bias. Six of the MISC glasses were targeted to have at least twice the ZrO_2 as that with the highest concentration from the model data; however, these glasses also have small prediction biases. The other seven MISC glasses do not fall with 20% of the compositions describing the model data, but they do not appear to have any constituents (e.g., Cr_2O_3, Fe_2O_3, ZrO_2, etc.) in concentrations that would result in large T_L prediction biases. Thus all these glasses will be considered.

[†] C. M. Jantzen of SRTC performed studies which confirmed that the presence of Al_2O_3 in waste glasses strongly impacted the crystallization of the glasses including what phases form. Thus glasses with little or no Al_2O_3 will likely have either different phases formed at T_L or large prediction biases. This should not be problematic because glasses with little or no Al_2O_3 are not feasible in DWPF and there is also a lower limit on Al_2O_3 to prevent amorphous phase separation.

- A set of ten glasses designated "US" (▲) were fabricated and measured by PNNL (in a "scoping" fashion) to examine any possible effects of uranium on measured liquidus temperature[†]. Of these glasses, those two corresponding to the AZ-3 glasses from the aforementioned MISC set appeared to have the largest prediction biases. These glasses were the lowest in Fe_2O_3 and highest in ZrO_2 for this set and would, therefore, be most likely to have large prediction biases based upon the proposed T_L model. Some of these data (including the DWPF glasses) were within 5% of the model data compositions and there is no obvious reason that theses data should have large prediction biases.

It is surprising that the model in Equation 16 adequately describes these PNNL glasses as these describe a much larger composition space than that expected for DWPF glasses (and covered by the model data). It is not surprising that as the concentrations of Cr_2O_3 and ZrO_2 increase above the maximum from those in model data or the Fe_2O_3 concentration falls below the minimum from the model data that large prediction biases appear. However, the above data do appear to indicate that the basic liquidus temperature response has been captured by the proposed model. That is, the proposed model, despite being semi-empirical, appears to describe adequately glasses whose compositions far exceed the model presented in Table IX (which cover the expected DWPF ranges). The composition ranges for the PNNL glasses in this section are summarized in Table XIV.

Table XIV. PNNL SP, SP-3, SPx4, SP-MC, MS, MISC, and US Composition Ranges (Weight Percent)

	Al_2O_3	B_2O_3	CaO	Cr_2O_3	$(\Sigma Fe)_2O_3$	K_2O	Li_2O	MgO
Maximum	16.374	19.996	5.003	1.2	22.992	4.002	7.499	6.02
Minimum	0	0	0	0	4.991	0	0	0

	MnO	Na_2O	NiO	SiO_2	TiO_2	U_3O_8	ZrO_2
Maximum	4.00	22.737	3.005	60.00	5.003	5.59	8.00
Minimum	0	4.996	0	29.979	0	0	0

5.3. PNNL CVS-I and CVS-II Data

Another set of data of potential interest was obtained from the PNNL Composition Variation Study (CVS) performed to support high-level waste vitrification plant at the Hanford Site [34]. This study was conducted in two major parts (designated "CVS-I" and "CVS-II") consisting of five experimental and data analysis phases. In CVS-I, 23 glass compositions were selected based on the results of previous PNNL scoping studies on compositions at the boundaries of those that might be produced from various, expected Hanford tank wastes. For these glasses, the liquidus temperatures were measured using a gradient furnace. Of these 23 glasses, only seven spinel liquidus temperatures[††] were reported [34], and these CVS-I glasses (+) are presented on Exhibit 6. The measured compositions provided by PNNL are used and the ranges for the measured compositions are provided in Table XV.

From Exhibit 6, it is apparent that there are large biases in most of the predictions. This is not surprising. Glasses CVS-I-1, CV-I-19, and CVS-I-20 contain concentrations of ZrO_2 much higher than those in the model glasses (although the biases appear to be opposite those in the PNNL glasses described in Section 5.2 which may be due to low relative Fe_2O_3 concentrations of approximately 5.5 wt%). Glass CVS-I-11 contains little Fe_2O_3 (i.e., approximately 2%) and CVS-I-17 contains no Al_2O_3. These components appear to be critical in controlling crystallization in DWPF glasses and are far outside the region describing the model data. Thus it is likely that the prediction biases for only the CVS-I-5 and CVS-I-23 would be small, which is the case. Furthermore, one recent unpublished PNNL report on liquidus temperature modeling excludes all CVS data from modeling (or validation) consideration due to quality and repeatability concerns.

[†] P. Hrma, J.D. Vienna, M. Mika, J.V. Crum, G.F. Piepel, "Liquidus Temperature Data for DWPF Glass," Draft U.S. DOE Report PNNL-11790, Pacific Northwest National Laboratory, Richland, WA (December, 1997).

[††] Other primary phases (e.g., clinopyroxene, Zr-containing crystals, etc.) were observed for the CVS-I glasses [34]; however, these other phases were discovered at lower temperatures than would be predicted for spinel. Thus focusing on spinel provides a conservative way to estimate liquidus temperature for DWPF glasses.

Table XV. Target Composition Ranges in Weight Percent (on a Glass Basis) for the CVS-I Glasses

	Al_2O_3	B_2O_3	CaO	Cr_2O_3	$(\Sigma Fe)_2O_3$	K_2O	Li_2O	MgO
Maximum	14.5	16.0	10.3	0.23	14.9	1.4	6.2	3.59
Minimum	0.0	5.13	0.104	0	2.06	0.0	0.91	0

	MnO	Na_2O	NiO	SiO_2	TiO_2	U_3O_8	ZrO_2
Maximum	0.23	15.4	1.04	56.3	0.017	0.0	4.18
Minimum	0.03	6.41	0.135	41.8	0.0	0.0	0.02

In the CVS-II study, 123 glasses were designed and fabricated in four phases; liquidus temperatures were measured only in the first three phases. In CVS-II Phase 1, 19 glasses were tested in a subregion interior to the revised experimental region (based upon CVS-I results). Of the 39 CVS-II glasses, 20 were selected from the boundaries of the revised experimental region, ten were selected in a subregion of acceptable compositions, two were retests of a glass each from CVS-I and CVS-II Phase 1, and the remaining seven glasses were based upon variations of either the SiO_2 or UO_2 concentrations or the "Others" makeup and/or concentration. The 43 glasses in CVS-II Phase 3 involved testing seven expected Hanford tank wastes and two variations of the Environmental Assessment (EA) glass. A total of 22 spinel liquidus measurements produced using a gradient furnace were reported for these 82 CVS-II glasses [34]. However, since these glasses were designed for Hanford—not DWPF—wastes, many components vary over different, and at times, much broader ranges of compositions than expected in DWPF [9]; therefore, it is highly likely that different melt phase complexes or precursors than those hypothesized for DWPF glasses may control the onset of crystallization in the CVS-II glasses. It is also likely the T_L predictions for many of the CVS-II glasses would be significantly biased when the proposed T_L model is used. The measured compositions for the CVS-II glasses are used; the ranges for the components of interest are provided in Table XVI.

The CVS-II liquidus temperature data (+) with spinel at the liquidus temperature are shown in Exhibit 6 (as well as those showing either clinopyroxene or orthopyroxene), which represents the predictions from the proposed liquidus temperature model for DWPF process control. From this exhibit, it is apparent that many of these predictions are in poor agreement with measured values reported by PNNL. (Note that PNNL has excluded the CVS data from a recent report on liquidus temperature modeling.) The large prediction biases are not surprising because many of the CVS-II data are from a composition region far outside that for DWPF (or described by the model data). For example, CVS-II-15 possessed a measured CaO concentration (i.e., 5.5% by weight) more than twice that expected in DWPF (and almost three times that of any other concentration in the model data); the Fe_2O_3 concentration (i.e., 3.8%) in this glass was also relatively low. Furthermore, four additional CVS-II glasses (i.e., CVS-II-22, -24, -46, and -74) have very low Fe_2O_3 concentrations; the other such glasses (i.e., CVS-II-21, -40, -41, -44, -45, -47, and -48) exhibited either ortho- or clinopyroxene at the liquidus temperature. The CVS-II-17 glass was also relatively low in Fe_2O_3, but high in ZrO_2 and behaved similarly to the corresponding CVS-I glasses.

The CVS-II-30 glass possessed a measured B_2O_3 concentration (i.e., 19.6% by weight) that far exceeded anything in the model data (or expected in DWPF glasses); this might be of importance as there is likely an immiscibility field in the borosilicate system at high B_2O_3 concentrations, that is, a field not currently considered in DWPF process control. However, a previous glass, SP-B-5, from the PNNL SP-3 series had a similar B_2O_3 concentration, but did not exhibit a significant prediction bias. This would appear to indicate that more work would be needed if glasses with high B_2O_3 concentrations are expected in DWPF (which at this time, they are not).

Of the remaining CVS-II glasses, only CVS-II-49 has a very large prediction bias considering the fact that none of these glasses are within 20% of the model data composition space. The CVS-II-56 glass has a Cr_2O_3 concentration more than twice the DWPF limit and almost four times the ZrO_2 than that in the model data glass with the highest concentration. These effects may again be canceling each other. Seven (i.e., CVS-II-16, -17, -18, -50, -51, -96, and -97) of the remaining 12 CVS-II glasses have ZrO_2 concentrations almost four times that of the model glass with the highest such concentration. Therefore, only the remaining five CVS-II glasses exhibiting spinel at the liquidus temperature would be reasonable for further consideration. The T_L predictions for most of these remaining glasses (and CVS-II-49 in particular) have large prediction biases. This may, in part,

be due to the difficulties PNNL discovered when using a gradient furnace to measure T_L; PNNL personnel have been developing a uniform temperature method for T_L determination (which was used to measure the SG Study glasses). Thus the CVS T_L measurements (none of which were repeated during CVS testing) may have much larger measurement errors than those for either the model data or other PNNL spinel data (that were measured using a uniform temperature method) mentioned in this section.

Table XVI. Composition Ranges in Weight Percent (on a Glass Basis) for the CVS-II Glasses

	Al_2O_3	B_2O_3	CaO	Cr_2O_3	$(\Sigma Fe)_2O_3$	K_2O	Li_2O	MgO
Maximum	10.65	20.075	7.6	0.66	12.175	3.7	7.03	7.31
Minimum	2.3	4.9	0.01	0.007	1.85	0.0	0.84	0.0

	MnO	Na_2O	NiO	SiO_2	TiO_2	U_3O_8	ZrO_2
Maximum	3.141	16.6	0.93	55.6	0.649	0.0	4.4
Minimum	0.01	5.2	0.0	43.6	0.01	0.0	0.0

5.4. The Liquidus Temperature Response for the Selected Non-Model Data

The data examined thus far in this section indicate that there are regions for which predictions from the proposed liquidus temperature model have very large biases. For example, the WVNS data in Section 5.1 indicate that one such region may be those compositions with Cr_2O_3 concentrations higher than the current DWPF solubility limit of 0.3 wt% in glass (where the maximum from the model data is 0.301 wt%). However, because such a restriction excludes many glasses that exhibit spinel (as opposed to Cr_2O_3) at T_L and appear to have small prediction biases, this constraint will not yet be imposed. On the other hand, "scoping" experiments at SRTC indicated the importance of Al_2O_3 to the crystallization behavior in DWPF type waste glasses; therefore, no glasses with Al_2O_3 concentrations outside the range from the model glasses will be considered for this examination. (This will not be a problem for DWPF process control because there already is a lower limit of 3 wt% Al_2O_3 to prevent amorphous phase separation, and the upper limit is much higher than expected for DWPF glasses.) Furthermore, because there is a known immiscibility field in borosilicate glasses that is likely to affect crystallization, those glasses with B_2O_3 concentrations outside those from the model data will not be considered (where the lower limit is to assure that borosilicate glasses are considered). Furthermore, the type of spinel normally found in DWPF glasses that crystallize are of the "high-iron" variety; therefore, it is likely that T_L predictions for those glasses with either too little or too much Fe_2O_3 will be significantly biased. As indicated in Section 5.2, the SP-Fe-4 glass appeared to indicate that predictions for glasses very high in Fe_2O_3 may be significantly biased; thus the upper limit from the model data is used to restrict the data considered. Because the Fe_2O_3 concentration is likely very important to crystallization in DWPF glasses, the minimum Fe_2O_3 concentration from the model data will also be imposed on the data for this examination. The aforementioned constraints (in wt% on a glass basis) on the non-model data are thus:

$$0.99 \le Al_2O_3 \le 14.16,\ 4.89 \le B_2O_3 \le 12.65, \text{ and } 3.43 \le Fe_2O_3 \le 16.98$$

from the model data where other data presented in this section may indicate the need for constraints on minimum SiO_2 and/or maximum CrO_2 and ZrO_2 for the proposed liquidus temperature model to be more generally applicable. At least this information will guide further development of liquidus temperature models for DWPF process control.

The predictions for the non-model spinel data after selection based on the above constraints are illustrated in Figure 7, and the composition ranges for the selected non-model data are provided in Table XVII (which again far exceed the ranges for the model data components other than those constrained above). The T_L predictions for a number of the resulting data (e.g., CVS-II-15, SP-Si-4, WNVS-005, etc.) appear to have significant biases; these glasses tend to be well outside the composition space for the model data in CaO, Cr_2O_3, Na_2O (and R_2O), SiO_2, and ZrO_2. However, no simple single-component limits for these components are apparent that do not also exclude a great many glasses that have insignificant prediction biases. Therefore, a more fundamental understanding of the liquidus temperature versus composition relationship will be needed to advance the development of the proposed T_L model to glasses outside the model region.

Table XVII. Composition Ranges for the 155 Selected Non-Model Data Represented by Figure 7

	Al_2O_3	B_2O_3	CaO	Cr_2O_3	$(\Sigma Fe)_2O_3$	K_2O	Li_2O	MgO
Maximum	13.68	12.00	5.5	1.20	16.19	4.00	7.50	6.02
Minimum	1.68	4.90	0	0	3.80	0	0	0

	MnO	Na_2O	NiO	SiO_2	TiO_2	U_3O_8	ZrO_2
Maximum	3.14	22.74	3.00	60.00	5.00	5.53	6.24
Minimum	0	6.26	0	29.98	0	0	0

However, despite the significant prediction biases illustrated in Figure 7, the relationship in Equation 16 does appear to describe the general trend of $(1/T_L)$ as a function of composition (within the restricted composition space described above). This relationship appears to describe the selected data from PNNL and West Valley studies. However, if such glasses outside the composition space for the model glasses become likely in DWPF, the model may have to be adjusted considering such components as CaO, Na_2O, SiO_2, and ZrO_2 (where Cr_2O_3 has been excluded because there is already a solubility limit on this component).

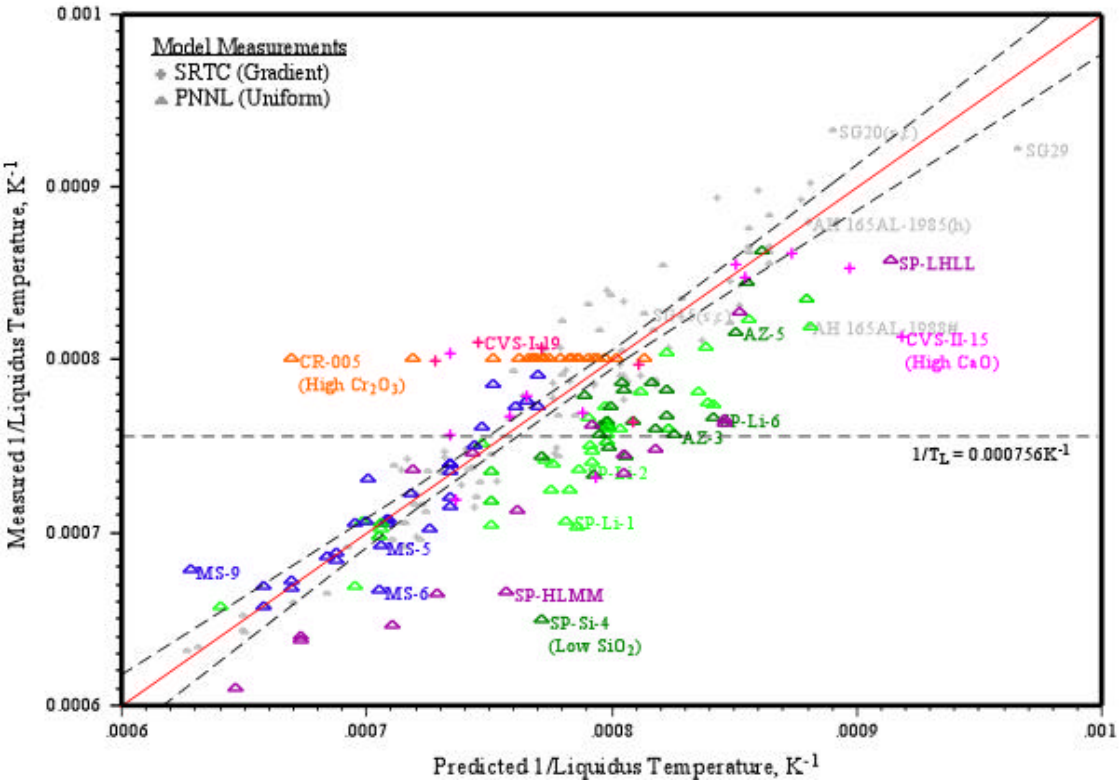

Figure 7. This figure shows the new DWPF liquidus temperature model including pertinent WVNS (△) and PNNL SP (△), SP-3 (△), SPx4 (△), MS (△), MISC (△), US (△), CVS-I (+) and CVS-II (+) data that exhibited spinel at T_L. Note that no SP-MC (△) are visible as they do not meet the Al_2O_3, B_2O_3, and Fe_2O_3 limits imposed on the data in Exhibit 6 (k). The dotted lines represent the 95% confidence curves about the regression line fitted from the model data (which have been grayed).

5.4.1. MgO Study Data

Because of the nature of the other spinel data presented in Figure 7, it is prudent to assure that the proposed liquidus temperature model (i.e., Equation 16) describes other data pertinent to DWPF. Such a set of data was generated in studying the possible effect of MgO on the crystallization of DWPF glasses [35]. An interim model using a subset of the model data in this report indicated that the addition of a significant amount of MgO (i.e., enough to change the predicted T_L by more than the nominal measurement error) as part of the DWPF frit might

increase the liquidus temperature of DWPF glasses. Thus removal of the MgO from the frit might increase the DWPF operating window.

A study [35] was designed and executed to examine the potential effect of MgO on the crystallization of DWPF glasses. In this study, the four standard, DWPF glass compositions (i.e., WCP PUREX, WCP HM, WCP BLEND, and the DWFP Startup Frit) provided in Table XXVII were rebatched by replacing MgO with B_2O_3 and SiO_2 so that the predicted melt viscosity and durability would be the same. Based upon an interim model in a previous draft modeling report, it was expected that these changes would produce liquidus temperature differences of between 70 and 100°C (i.e., significantly higher than the T_L measurement error); however, when the model presented in Equation 16 was applied to the compositions presented in Table XXVII, the differences in prediction for these four pairs of glasses were between 23 and 50°C (i.e., the liquidus temperatures would be lower in the glasses without MgO). It should be noted that the four original compositions were within the composition space defined by the model data[†]; however, the four corresponding glasses fabricated without MgO were not within the composition region describing the model data; however, the other information in this section would suggest that large prediction biases should not be expected for these glasses. Unfortunately, this range of differences in predictions was well within that for the measurements made during the MgO Study because the isothermal melts were performed in 25 to 50°C steps. As expected, no significant differences were observed between the pairs of glasses in the MgO Study.

6. MODEL ASSUMPTIONS AND LIMITATIONS

A semi-empirical model form (i.e., Equation 16) describing the relationship between liquidus temperature and composition was derived using mechanistic information (e.g., solubility definition, site information, etc.) where possible. The major assumptions involved in deriving the relationship in Equation 16 were that

1) melt phase complexes or precursors analogous to pyroxene-like groups control the onset of spinel crystallization in DWPF glasses (i.e., spinel forms from these pyroxene-like precursors in a way analogous to spinel formation from the incongruent melting of acmite);
2) the differences in properties of the aforementioned pyroxene-like melt phase precursors formed in DWPF glasses are sufficiently small that such differences could be “averaged over” for modeling purposes with small impact;
3) the system behaved close enough to ideality that activities could be closely approximated by their corresponding molar melt concentrations;
4) any REDOX effect on T_L was negligible for glasses expected in DWPF when compared to the uncertainty introduced in the T_L prediction by its inclusion;
5) the proposed pyroxene-substituted nepheline pseudobinary composition space was adequate to describe the melt compositions needed to predict liquidus temperature for expected DWPF glasses; and
6) the compositions of the glasses that will be made in DWPF, or more specifically, the glass compositions from which liquidus temperature will be predicted do not deviate significantly from the ranges provided in Table IX especially for the Al_2O_3, B_2O_3, and Fe_2O_3 (and is likely true for the case of significant ThO_2 additions to DWPF glasses).

The fact that the model in Equation 16 describes both the model data well and the overall trend in the selected other data indicates that none of the assumptions made above will likely deleteriously affect model performance or introduce significant prediction biases for expected DWPF glass compositions.

Many of these assumptions involve the manner in which the model was derived as the solution to a well-known solubility problem. To describe the model data adequately, a set of pyroxene-like melt phase complexes or precursors with reasonably similar properties appears to be present in the model data glasses at temperatures just higher than the liquidus temperatures. If different melt phase complexes with highly variable properties were formed in the melt, then there would be little chance of modeling the resulting data in such a manner. Such behavior is not indicated in Figure 7 as the general trend in the selected data is also well described. Also, if the

[†] The K_2O concentration for the WCP BLEND glass from Table XXVII was 3.9 wt% versus the upper value of 3.8846 wt% from Table VII, which is considered too close (i.e., less than 0.5%) to reject.

heat capacity of the melt pyroxene phase was not negligible compared to the enthalpy of fusion, then the relationship in Figure 6 would not likely appear linear over the range of DWPF compositions that are considered. Finally, if the system did not behave sufficiently close to ideality over the conditions observed in the model data, then again there would be little chance of employing such a model for liquidus temperature prediction.

7. RAMIFICATIONS OF USING A "SPINEL-ONLY" MODEL FOR DWPF PROCESS CONTROL

Only a single criterion (i.e., spinel observed at T_L) was imposed upon the selection of model data for this report: spinel had to be observed at the measured liquidus temperature. However, there were glass compositions tested during the SG Study [9] (i.e., in the composition region of interest for DWPF) that exhibited clinopyroxene at the liquidus temperature. Glasses exhibiting both clinopyroxene and orthopyroxene were also discovered during CVS-II testing [34]. The predictions for the SG Study and CVS-II glasses exhibiting pyroxenes at T_L are represented in Figure 8 versus both the model and selected spinel data.

Two results should be obvious from Figure 8: the glasses exhibiting pyroxenes at T_L do not have significantly larger prediction biases than the spinel data and the liquidus temperatures for the glasses exhibiting pyroxenes are generally much lower than the DWPF limit (which would translate to a value of 0.000756 K^{-1} on Figure 8). It is true that the predictions for some of the glasses are likely unacceptable; however, these glasses have liquidus temperatures far below the DWPF limit. Therefore, even though the liquidus temperatures for these glasses may possess unacceptable biases from a statistical perspective, they are not likely of practical concern for process control purposes.

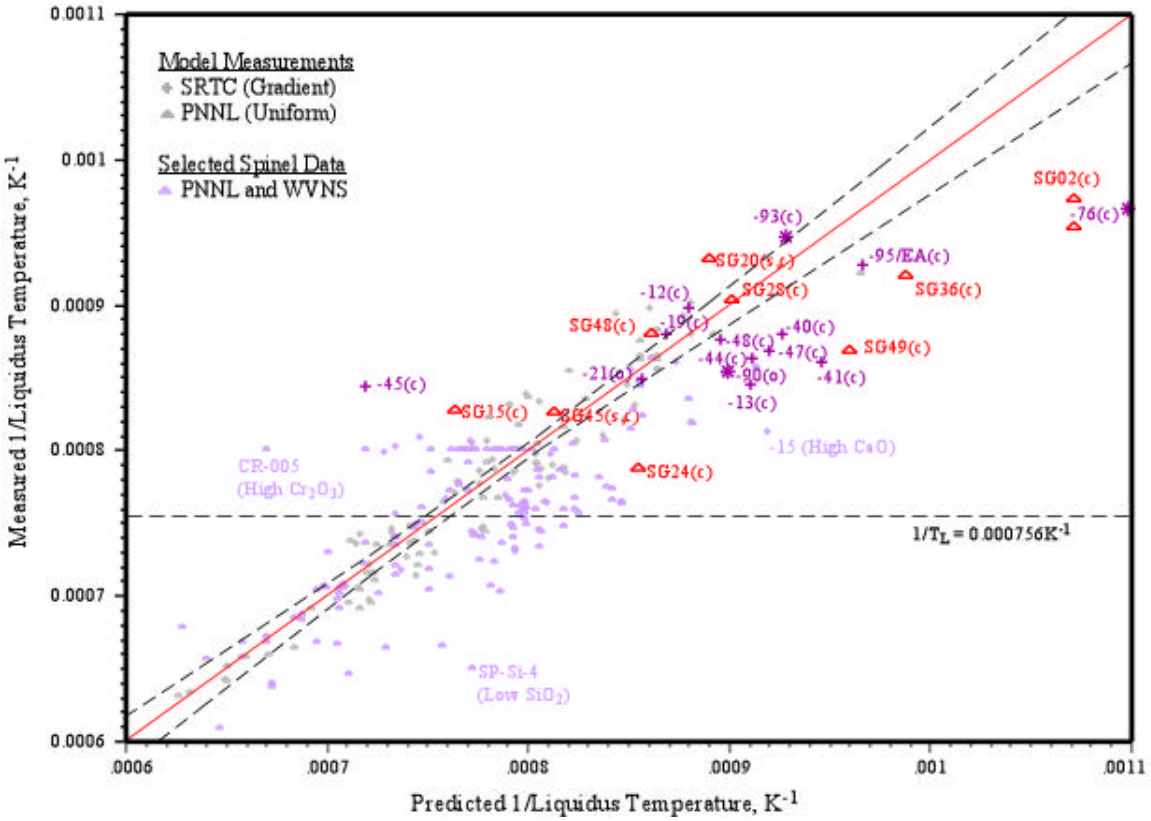

Figure 8. This figure shows the predictions from the proposed DWPF liquidus temperature model for those SG Study (△) and CVS-II (+ for measured and ✸ for target composition) glasses exhibiting pyroxene (p), clinopyroxene (c), and orthopyroxene (o) phases at T_L. Some glasses had both spinel (s) and one of the other phases near T_L as indicated. The dotted lines represent the 95% confidence curves about the regression line fitted from the model data which have been grayed.

8. WASTE LOADING IMPACT OF THE REVISED LIQUIDUS TEMPERATURE MODEL

However, the bottom line for improving liquidus temperature prediction is determining how the new model impacts waste loading for DWPF. Because the liquidus temperature prediction is related to the amount of risk DWPF is willing to take with their melter, DWPF may choose to not implement the new model if it does not significantly improve waste loading (despite the problems illustrated with the current model in Section 4.2 and especially Figure 4). It will thus be determined if the proposed semi-empirical liquidus temperature model, despite providing more accurate predictions for expected DWPF waste compositions, will also provide a significant impact on waste loading for DWPF.

Historically, the liquidus temperature and other process and product control constraints were translated into linear constraints on composition [1]. That is, the original T_L model represented in Equation 14 was used to translate the $T_L \le 1050^oC$ constraint on liquidus temperature into the following linear constraint on composition:

Equation 24
$$\begin{aligned} \underline{z}_c^T \underline{a}_c &\ge 0 \\ \underline{z}_c &\equiv \left[z_{Fe_2O_3} \quad z_{SiO_2} \quad z_{Al_2O_3} \right] \\ \underline{a}_c &\equiv \left[-134.0 \quad 155.6c_c^* \quad -359.88c_c^* \right] \end{aligned}$$

where c_c^* corresponds to a new limit obtained from the relationship and regression information from the liquidus temperature-composition data at a given confidence level, $100(1-\alpha/2)\%$[1]. (As indicated above, the current constraint on liquidus temperature is based on a two-sided confidence interval on the predictions as opposed to the one-sided interval used for the proposed liquidus temperature model.) In the current Product Composition Control System (PCCS), this defines a new limit, referred to as the Property Acceptable Region or PAR limit, based upon prediction uncertainty in the model. The measurement uncertainty, U_c, at the same confidence level is obtained in a fashion similar to that expressed in Equation 22 (whereas the partial derivatives for the linear PAR constraint in Equation 24 are much simpler to derive than those for the model in Equation 16 as provided in Section 16). The composition is then tested introducing the appropriate measurement uncertainty using:

Equation 25
$$\underline{z}_c^T \underline{a}_c - U_c \ge 0$$

which is commonly referred to as the Measurement Acceptability Region or MAR test. If a given composition satisfies the MAR test (which implicitly satisfies the PAR test), it is considered acceptable for processing in the DWPF melter (for the corresponding property).

However, it is likely immediately apparent that the new liquidus temperature model described by Equation 16 cannot be managed in a similar manner. The new constraint cannot be simply linearized and incorporated directly into the current version of PCCS—such implementation issues will be discussed in Section 9. For the sake of continuity, allow that discussion to wait until after the issues related to waste loading are examined.

As described in Equation 16, the new liquidus temperature model relates the reciprocal of liquidus temperature (in K) to a function of composition. Thus the limit for this model is $0.000756\ K^{-1}$. Because it is the reciprocal liquidus temperature that is predicted using the new model, the original $T_L(^oC) \le 1050^oC$ processing constraint becomes $1/T_L(K) \ge 0.000756\ K^{-1}$ for the new model. Thus, at a given composition $\underline{z}$, if $P_n(\underline{z})$ and $U_n(\underline{z})$ are the relevant prediction and measurement uncertainties, respectively, obtained from the information in Equation 21 and Equation 22 for this composition, the prediction, $\hat{\Pi}(\underline{z})$, from the new model in Equation 16 (and thus the composition) is deemed acceptable (at either the PAR or MAR limit) when it satisfies the following tests:

Equation 26
$$\begin{aligned} \text{PAR}: &\quad \hat{\Pi}(\underline{z}) - P_n(\underline{z}) \ge 0.000756\,K^{-1} \\ \text{MAR}: &\quad \hat{\Pi}(\underline{z}) - P_n(\underline{z}) - U_n(\underline{z}) \ge 0.000756\,K^{-1} \end{aligned}$$

These types of constraints are different in one significant way from the existing PCCS constraints in the fact that the prediction error (like the measurement error) is a function of composition. This will be considered during implementation below.

The constraint information now exists to estimate the impact of the proposed liquidus temperature model on past and future DWPF waste loading. Table XVIII provides relevant sludge and frit composition information on a normalized mass oxide basis. The median SRAT Product compositions from vitrification of the first two DWPF sludge batches (i.e., SB1a and SB1b) are provided. Three compositions for the next DWPF sludge batch (denoted SB2), based on the most current Waste Acceptance Characterization (WAC) sample results [36] at various washing endpoints (i.e., 6, 7.5, and 9% Na in the final washed totals solids) are provided in this table. The centroids from a designed set of compositions representing the subsequent sludge-only batches (i.e., SB3 and SB4) based upon Version 12 of the DWPF system plan[†] are also provided. The frit information includes compositions for a sludge-only frit, namely, Frit 165, the current Frit 200, and the proposed frit, Frit 320, to increase melt rate for DWPF macrobatch 3.

Table XVIII. DWPF Compositions (wt% oxides or glass) for Waste Loading Comparisons

	DWPF Sludge Batch (SB)							Frit		
	SB1a	SB1b		SB2*		SB3	SB4	165	200	320
Type	Med.	Med.	6Na	7.5Na	9Na	Cent.	Cent.	Nom.	Nom.	Nom.
Al_2O_3	17.45	20.71	13.76	13.55	13.36	11.80	11.55			
B_2O_3		0.05	0.03	0.03	0.03	0.04	0.04	10.0	12.0	8.0
CaO	4.19	4.68	4.29	4.17	4.04	4.28	4.05			
Cr_2O_3	0.35	0.28	0.40	0.39	0.38	0.36	0.36			
Fe_2O_3	49.71	42.18	45.08	43.80	42.45	45.26	41.83			
K_2O										
Li_2O		0.03	0.20	0.19	0.19	0.20	0.20	7.0	5.0	8.0
MgO	2.35	2.66	4.21	4.09	3.96	1.30	1.82	1.0	2.0	
MnO	4.69	5.93	5.55	5.39	5.23	5.74	9.90			
Na_2O	13.83	13.55	9.20	11.60	14.09	12.77	12.84	13.0	11.0	12.0
NiO	0.51	0.58	2.02	1.97	1.91	2.56	2.04			
SiO_2	2.11	4.34	0.92	0.89	0.87	2.21	4.35	68.0	70.0	72.0
ThO_2						0.05	0.05			
TiO_2	0.03	0.04	0.04	0.04	0.04	0.04	0.04			
U_3O_8	4.64	4.58	11.52	11.19	10.85	11.05	8.58			
ZrO_2	0.03	0.11	0.05	0.05	0.05	0.13	0.13	1.0		
Total	99.89	99.73	97.28	97.35	97.43	97.78	97.78	100.0	100.0	100.0

* For the SB2 compositions, these compositions represent those obtained by washing the SB2 sludge to endpoints of 6, 7.5, and 9% Na per 100 grams of resulting total sludge solids.

Thus the waste loading or maximum mass percentage of a given sludge relative to glass (i.e., sludge + frit) will be determined for the various combinations of sludge and frit in Table XVIII. That is, waste loading in this report is defined as the grams of oxides for a sludge given in Table XVIII per 100 grams of sludge plus frit, such issues as Na remaining from additional sludge washing is not taken into account. Historically, many DWPF liquidus temperature data were collected on glasses containing PHA and thus had significant concentrations of K_2O and TiO_2, which are either small or absent in the sludge compositions in Table XVIII. However, the model data include 24 measurements (or 23%) with concentrations of K_2O and TiO_2 of less than 0.23 and 0.17%, respectively. Thus there appears to be no reason that use of Equation 16 will be inappropriate for sludge-only operation in DWPF.

[†] The system plan information was used by T. B. Edwards of SRTC to design compositions needed to reduce the number of constraints associated with DWPF durability prediction. The sludge information in the table represents the centroids from the extreme vertices from the SB3 and SB4 designs.

The maximum waste loadings for both the current (or "Old") and proposed (or "New") liquidus temperature models (when α = 0.05) are provided in Table XIX for the possible combinations of sludge and frit compositions in Table XVIII. In Table XIX, "EPAR" refers to constraints considering no prediction or composition measurement uncertainties, "PAR" to constraints incorporating only prediction uncertainties, and "MAR" to constraints where both prediction and composition measurement uncertainties are introduced. First note that, despite the issues raised in Section 4.2 concerning the current model, the predictions for the first two sludge batches processed through DWPF appear to have been very conservative. Also note that only the combinations of Frit 200 with the "average" and "more-washed" SB2 sludge compositions (i.e., SB2-7.5Na and SB2-6Na, respectively) would have higher waste loadings with the current model than with the proposed model. Even accounting for these cases, the SB2 through SB4 glasses would have higher waste loadings by between 0.9 and 7.3 kg of sludge per 100 kg of glass produced (or by between 3.0 and 24.1% higher waste loadings than those based upon the current T_L model both at α = 0.05).

Table XIX. Waste Loadings for Various DWPF Sludge-Frit Combinations when α = 0.05

	Frit 165						Frit 200						
	EPAR		PAR		MAR			EPAR		PAR		MAR	
	Old	New	Old	New	Old	New		Old	New	Old	New	Old	New
SB1a-Med	28.4	37.7	26.6	36.4	25.8	35.2	**SB1a-Med**	29.0	33.2	27.1	31.9	26.4	30.7
SB1b-Med	31.1	39.7	29.1	38.5	28.4	37.3	**SB1b-Med**	31.7	35.2	29.8	33.9	29.0	32.7
SB2-6Na	30.7	33.6	28.7	33.0	28.0	31.6	**SB2-6Na**	31.3	29.3	29.3	28.6	28.6	27.3
SB2-7.5Na	31.3	35.7	29.3	35.0	28.5	33.5	**SB2-7.5Na**	31.9	31.2	29.9	30.4	29.1	29.0
SB2-9Na	31.9	38.1	29.9	37.3	29.1	35.7	**SB2-9Na**	32.6	33.4	30.5	32.6	29.7	31.0
SB3-Cent	31.2	38.1	29.1	37.2	28.4	35.6	**SB3-Cent**	31.8	33.3	29.7	32.5	29.0	30.9
SB4-Cent	33.2	41.6	31.0	40.1	30.2	38.4	**SB4-Cent**	33.8	36.4	31.6	35.1	30.8	33.6

	Frit 320					
	EPAR		PAR		MAR	
	Old	New	Old	New	Old	New
SB1a-Med	29.6	40.0	27.7	38.8	26.9	37.5
SB1b-Med	32.3	42.1	30.4	41.0	29.6	39.7
SB2-6Na	32.0	35.8	29.9	35.2	29.1	33.8
SB2-7.5Na	32.6	37.9	30.5	37.2	29.7	35.8
SB2-9Na	33.2	40.3	31.1	39.5	30.3	38.0
SB3-Cent	32.5	40.3	30.3	39.5	29.5	37.9
SB4-Cent	34.4	43.9	32.2	42.5	31.4	40.8

The proposed liquidus model provides the same waste loading for the SB2-6Na case as the current model only if $\alpha \approx 0.30$ (or only 70% confidence) at a limit of 1050°C. However, as suggested in Section 4.6.2, if the T_L limit is raised by only 25°C to 1075°C (because of the more accurate predictions provided by the proposed model) the same waste loading is obtained for the SB2-6Na sludge composition. Therefore, since the constraint on T_L is process and not product related and corresponds to the risk DWPF is willing to take while processing, such an adjustment to the T_L limit should be considered for future DWPF operation.

Thus, in general, the processing constraints generated using the proposed liquidus temperature model would be less restrictive than those obtained using the current DWPF model. The prediction properties of the 21 glasses at the highest MAR waste loadings are provided in Table XX. Because the prediction properties in this table (even at very high waste loadings) satisfy the other process and product constraints [1], use of the proposed T_L model would also help increase the operating window for future DWPF operation. Despite these results, it would be prudent to test glasses (e.g., using uniform temperature melts bracketing the predicted T_L) above 35% loading because this is the highest waste loading tested for DWPF glasses (even though such considerations are highly dependent upon waste and frit compositions).

Table XX. Predicted Properties for the Waste Loading Study Glasses

GlassID	Frit Used	w	Current T_L(C)	Proposed T_L(C)	Viscosity (Poise)	Homog.	DG_p	NL[B(g/L)]	SR_2O (wt%)	Al_2O_3 (wt%)
SB1a-Med	165	35.2	1158.2	1017.6	23.8	252.7	-10.233	0.894	17.83	6.14
SB1b-Med	165	37.3	1148.0	1021.3	31.2	251.6	-9.918	0.784	17.61	7.73
SB2-6Na	165	31.6	1061.0	1014.0	32.5	225.4	-10.342	0.935	16.65	4.35
SB2-7.5Na	165	33.5	1079.0	1014.9	27.2	227.7	-10.853	1.157	17.25	4.54
SB2-9Na	165	35.7	1101.8	1015.7	21.8	230.4	-11.447	1.482	17.96	4.77
SB3-Cent	165	35.6	1109.8	1014.4	22.1	233.2	-11.021	1.241	17.5	4.2
SB4-Cent	165	38.4	1119.8	1008.1	22.1	232.1	-11.468	1.495	17.33	4.44
SB1a-Med	200	30.7	1072.8	1015.8	55.0	240.5	-8.699	0.472	15.33	5.36
SB1b-Med	200	32.7	1062.8	1019.7	67.3	240.0	-8.465	0.428	15.21	6.77
SB2-6Na	200	28.6	1015.8	1037.6	67.9	218.9	-8.624	0.457	14.11	3.94
SB2-7.5Na	200	29.1	1015.1	1016.0	61.5	218.4	-9.205	0.582	14.78	3.94
SB2-9Na	200	31.0	1030.0	1014.4	52.0	220.8	-9.776	0.739	15.47	4.14
SB3-Cent	200	30.9	1037.9	1014.2	52.2	223.2	-9.404	0.632	15.06	3.65
SB4-Cent	200	33.6	1047.0	1011.6	51.2	222.7	-9.853	0.763	15	3.88
SB1a-Med	320	37.5	1176.8	1017.0	26.6	260.9	-9.604	0.688	17.69	6.54
SB1b-Med	320	39.7	1168.0	1020.6	35.1	259.6	-9.287	0.603	17.45	8.22
SB2-6Na	320	33.8	1073.8	1014.4	36.8	232.3	-9.682	0.71	16.42	4.65
SB2-7.5Na	320	35.8	1093.5	1015.9	30.5	234.6	-10.245	0.898	17.06	4.85
SB2-9Na	320	38.0	1116.6	1015.8	24.3	237.1	-10.904	1.182	17.82	5.08
SB3-Cent	320	37.9	1124.6	1015.0	24.6	240.1	-10.448	0.978	17.33	4.47
SB4-Cent	320	40.8	1135.4	1008.7	24.5	238.7	-10.948	1.204	17.16	4.71

9. IMPLEMENTATION OF THE PROPOSED LIQUIDUS TEMPERATURE MODEL

Because the constraint on liquidus temperature normally restricts loading in DWPF, use of the proposed liquidus temperature model (i.e., Equation 16) will generally allow much higher waste loading to be realized in DWPF. As mentioned above, the proposed model has one drawback—it cannot be easily linearized (like the current model) and placed directly into the current version of PCCS. However, as long as the proposed model can be implemented, the trade-off appears beneficial.

DWPF personnel no longer use the LISP-based PCCS developed by SRTC for waste acceptance determination; instead a spreadsheet based upon one developed by T. B. Edwards for test case definition is used. In this spreadsheet, the liquidus temperature prediction as well as the PAR and MAR test results are reported. Therefore, it will be necessary to provide the ability to compute the same information for the proposed liquidus temperature model. As illustrated in Appendix 17, Visual Basic® functions can be defined in Excel® and called from the appropriate locations in the DWPF SME Acceptability spreadsheet to provide this information. These functions are fairly complex, but this complexity is removed from the user and the output appears as before. Therefore, implementation (as it has already been done in the course of this report) should not present any significant problems, other than those related to documentation, for DWPF—especially as the liquidus temperature constraint is not waste affecting.

10. CONCLUSIONS

The liquidus temperature (T_L) for a glass is the *maximum* temperature at which the molten glass and primary crystalline phase (e.g., spinel for DWPF) are at equilibrium. The constraint on liquidus temperature in the DWPF melter prevents melt pool crystallization during routine operation. This type of crystallization can involve almost simultaneous nucleation of the entire melt pool volume. Furthermore, once formed in the DWPF melter, spinel crystals are refractory and cannot be redissolved into the melt pool. When a significant amount of volume crystallization has occurred and the material has settled to the floor of the melter, the pour spout may become partially or completely blocked. In addition, the melt pool may no longer be able to sustain Joule heating which would cause the melt pool to solidify. Finally, minimizing volume crystallization simultaneously minimizes subsequent devitrification of the glass once it is poured into a canister.

Glasses produced in DWPF must have liquidus temperatures below 1050°C; this limit was defined to be safely below the nominal DWPF melter operating temperature of 1150°C. However, the liquidus temperature of a glass cannot be measured in situ. Modeling the tendency of DWPF glasses to undergo crystallization was pursued employing mechanistic information where possible to minimize the number of parameters in the model, which, for a reasonable statistical fit showing no significant prediction bias (or lack-of-fit), should decrease the confidence bands associated with random prediction error. In turn, this should maximize the available glass processing window. The proposed four parameter liquidus temperature model developed in this study takes the form:

$$\frac{1}{T_L(K)} = \ln\left\{(M_2)^a (M_1)^b (M_T)^c\right\} + d = a\ln(M_2) + b\ln(M_1) + c\ln(M_T) + d$$

or

$$T_L(^oC) = \left\{a\ln(M_2) + b\ln(M_1) + c\ln(M_T) + d\right\}^{-1} - 273$$

where

$$\Sigma_{MT} \equiv \phi_{T,SiO_2} z_{SiO_2} + \phi_{T,Al_2O_3} z_{Al_2O_3} + \phi_{T,Fe_2O_3} z_{Fe_2O_3}$$

$$\Sigma_{M1} \equiv \phi_{M1,Al_2O_3} z_{Al_2O_3} + \phi_{M1,Fe_2O_3} z_{Fe_2O_3} + \phi_{M1,TiO_2} z_{TiO_2} + \phi_{M1,Cr_2O_3} z_{Cr_2O_3} + \phi_{M1,ZrO_2} z_{ZrO_2} + \phi_{M1,NiO} z_{NiO} + \phi_{M1,MgO} z_{MgO} + \phi_{M1,MnO} z_{MnO}$$

$$\Sigma_{M2} \equiv \phi_{M2,NiO} z_{NiO} + \phi_{M2,MgO} z_{MgO} + \phi_{M2,MnO} z_{MnO} + \phi_{M2,CaO} z_{CaO} + \phi_{M2,K_2O} z_{K_2O} + \phi_{M2,Li_2O} z_{Li_2O} + \phi_{M2,Na_2O} z_{Na_2O}$$

$$\Sigma_{T1} \equiv \phi_{T1,SiO_2} z_{SiO_2} + \phi_{T1,Al_2O_3} z_{Al_2O_3} + \phi_{T1,Fe_2O_3} z_{Fe_2O_3} + \phi_{T1,TiO_2} z_{TiO_2}$$

$$\Sigma_{N1} \equiv \phi_{N1,K_2O} z_{K_2O} + \phi_{N1,Li_2O} z_{Li_2O} + \phi_{N1,Na_2O} z_{Na_2O}$$

and

$$M_2 \equiv \frac{\Sigma_{M2}}{\Sigma}, M_1 \equiv \frac{\Sigma_{M1}}{\Sigma}, M_T \equiv \frac{\Sigma_{MT}}{\Sigma}, \text{and } \Sigma \equiv \Sigma_{M2} + \Sigma_{M1} + \Sigma_{MT} + \Sigma_{T1} + \Sigma_{N1}$$

The ϕ coefficients indicating the distribution of the various species are provided in Table VIII. The least-squares results for the $(1/T_L)$ versus the above expression for 105 model data representing DWPF compositions were used to estimate the parameters in the above model; these were a = –0.000260, b = –0.000566, c = –0.000153, and d = –0.00144 for the model data. The predictions for the model are provided in Table XXIX. The summary statistics for the least-squares fit obtained were R^2 = 0.891 and $s_r = 2.28\text{x}10^{-5}K^{-1}$. The model indicated no significant lack-of-fit; furthermore, relevant WVNS and PNNL data confirm that any prediction biases are tolerably small and the model will adequately describe the liquidus temperature phenomenon for DWPF glasses.

The impact of the proposed liquidus temperature model on past and future DWPF waste loading was estimated. The compositions from vitrification of the first two DWPF sludge batches (i.e., SB1a and SB1b) were examined as were three compositions for the next DWPF sludge batch (denoted SB2), based on the most current Waste Acceptance Characterization sample results at various washing endpoints. Compositions representing the remaining sludge-only batches (i.e., SB3 and SB4) were also studied. The frit information includes compositions for a sludge-only frit, namely, Frit 165, the current Frit 200, and a frit, Frit 320, proposed to increase melt rate. The predictions for the first two DWPF sludge batches appear to have been conservative. Also note that only the combinations of Frit 200 with the "average" and "more-washed" SB2 sludge compositions would have higher waste loadings with the current model than with the proposed model. The SB2 through SB4 glasses would have higher waste loadings by between 0.9 and 7.3 kg of sludge per 100 kg of glass (or between 3.0 and 24.1% higher waste loadings than those based upon the current T_L model). The proposed liquidus model would only provide the same waste loading for the worst SB2 case if the confidence is decreased from 95 to 70% at a limit of 1050°C. However, as suggested in this report, if the T_L limit is raised by 25°C to 1075°C (because of the more accurate predictions provided by the proposed model), the same waste loading is obtained for the worst-case SB2 sludge composition. Therefore, since the constraint on T_L is process and not product related and corresponds to the risk DWPF is willing to take while processing, such an adjustment to the T_L limit should be considered for future DWPF operation.

Thus modeling volume crystallization in the DWPF melt ensures that gross crystallization will not affect operation of the facility while simultaneously allowing DWPF to increase waste loadings and reduce the number of canisters produced. The cost savings specifically expected based upon use of this model are outside the scope of this report; however, indications are that the new model will significantly increase waste loading for DWPF glasses by even more than that used to provide estimates of $100 million to $533 million savings over the lifetime of the DWPF[†].

11. ACKNOWLEDGEMENTS

The authors wish to thank the following persons for their assistance in preparation and review of this report: T. B. Edwards, A. D. Cozzi, and D. K. Peeler of the Savannah River Technology Center and J. D. Vienna and J. Crum of the Pacific Northwest National Laboratory. This study was funded by the Department of Energy, EM-50, Mixed Waste Focus Area, Tanks Focus Area, DWPF, and SRTC.

12. REFERENCES

1. Brown, K. G. and Postles, R. L. “SME Acceptability Determination for DWPF Process Control,” WSRC-TR-95-0364, Rev. 3, February 1, 1996.
2. M.J. Plodinec, “Long-Term Waste Management Progress Report Small-Scale Electric Melter,” II. Slag Formation, U.S. DOE Report DPST-78-453, E.I. du Pont de Nemours & Co., Savannah River Laboratory, Aiken, SC (August, 1978).
3. M. J. Plodinec and J.R. Wiley, “Viscosity and Electrical Conductivity of Glass Melts as a Function of Waste Composition,” **Proceedings International Symposium on Ceramics in Nuclear Waste Management**, CONF-790420, U.S. DOE, Cincinnati, OH, 210-212 (1979).
4. M. J. Plodinec, “Long-Term Waste Management Progress Report Small-Scale Electric Melter, IV. Effects of Feed Mixing and Segregation on Glass Melting,” DPST-79-227, E.I. du Pont de Nemours & Co., Savannah River Laboratory, Aiken, SC (January, 1979).
5. G.G. Wicks and W.N. Rankin, “Microstructural Analysis of Slag Formation in Battelle’s Calcine Fed Ceramic Melter (CFCM), DPST-79-372, E.I. du Pont de Nemours & Co., Savannah River Laboratory, Aiken, SC (April, 1979).
6. J.P. Moseley and M.B. Cosper, “An Analysis of Spinel Deposition in the 1941 Melter, DPST-81-587, E.I. du Pont de Nemours & Co., Savannah River Laboratory, Aiken, SC (July, 1981).
7. This is taken from WSRC-IM-93-39, “DWPF Process and Equipment Description Manual,” Rev. 0, Vol. I (February 23, 1993).
8. C. M. Jantzen, K.G. Brown, K.J. Imrich, and J.B. Pickett. “High Cr_2O_3 Refractory Corrosion in Oxidizing Melter Feeds: Relevance to Nuclear and Hazardous Waste Vitrification,” WSRC-MS-97-00856, Revision 0 (1997).
9. P. Hrma, J.D. Vienna, M. Mika, J.V. Crum, G.F. Piepel, “Liquidus Temperature Data for DWPF Glass,” U.S. DOE Report PNNL-11790, Pacific Northwest National Laboratory, Richland, WA (May, 1999).
10. T. B. Edwards, “A Statistically Designed Sampling Plan for Investigating Liquidus Temperature Versus Glass Composition (U),” Inter-Office Memorandum, SRT-SCS-97-0022, Westinghouse Savannah River Company, Aiken, South Carolina, 1997.

[†] DRAFT Cost Analysis by Tony Robinson, BDM International. Attachment to Tanks Focus Area Technical Response 98059, 1997. This cost analysis was based upon an increase of 2 kg of additional sludge being immobilized per 100 kg of waste glass, which translated into 400 fewer canisters over the lifetime of DWPF. The potential cost savings were bracketed by assuming, on the low end, that emplacement costs were $250K per canister translating into $100MM and, on the high end, reducing the HLW operations budget (which was $400MM in 1997) would result in a cost savings of over $533MM.

11. K. Yagi, "Liquidus Data on the System Acmite-Nepheline-Diopside at 1 Atmosphere," Carnegie Institute of Washington Year Book (C.I.W.Y.B.) 62, Annual Report of the Director of the Geophysical Laboratory, Carnegie Institution of Washington, Washington, DC, 133-134 (1963).
12. M.C. Gilbert, "High pressure stability of acmite," Am. J. Sci., **267-A**, 145-149 (1969).
13. I. N. Levine. **Physical Chemistry**, 2nd Ed., McGraw-Hill Book Company, New York, 1983.
14. **Annual Book of ASTM Standards, Section 15: General Products and Chemical Specialties**, Vol. 15.02, Standard C162-99, ASTM, West Conshohocken, PA, 2001.
15. C. W. Burnham, "The nature of multicomponent aluminosilicate melts," **Phys. Chem. Of the Earth**, **13&14**, 191-227 (1981).
16. A.J.G. Ellison and A. Navrotsky, "Thermochemistry and Structure of Model Waste Glass Compositions," **Scientific Basis for Nuclear Waste Management**, **XIII**, V.M. Oversby and P.W. Brown (Eds.) Materials Research Society, Pittsburgh, PA, 193-207 (1990).
17. E. W. Baumann. "Colorimetric Determination of Iron (II) and Iron (III) in Glass," **Analyst**, Vol. 117, 913-916 (1992).
18. Ramsey, W.G. and Schumacher, R.F. "Effects of Formate and Nitrate on Waste Glass Redox at High Copper Concentration," WSRC-TR-92-242, October 23, 1992.
19. E.T. Turkdogan, "Physicochemical Properties of Molten Slags and Glasses," **The Metals Society**, London, 516 pp. (1983).
20. A.K Varshneya, **Fundamentals of Inorganic Glasses**, Academic Press, Inc., New York, 570 pp. (1994).
21. Richet, P. and Bottinga, Y. "Glass transitions and thermodynamic properties of amorphous SiO_2, $NaAlSi_nO_{2n+2}$, and $KAlSi_3O_8$," **Geochim. Cosmochim. Acta**, **48**, 453-470 (1984).
22. **Annual Book of ASTM Standards, Section 15: General Products and Chemical Specialties**, Vol. 15.02, Standard C829-81 (reapproved in 2000), ASTM, West Conshohocken, PA, 2001.
23. C.M. Jantzen, "Relationship of Glass Composition to Glass Viscosity, Resistivity, Liquidus Temperature, and Durability: First Principles Process-Product Models for Vitrification of Nuclear Waste," **Nuclear Waste Management IV**, G.G. Wicks, D.F. Bickford, and L.R. Bunnell (Eds.), Ceramic Transactions, Vol. 23, American Ceramic Society, Westerville, OH, 37-51 (1991).
24. SAS Institute, Inc. **JMP® Statistics and Graphics Guide: JMP Version 4**, SAS Institute, In., Cary, NC, 2000.
25. **Annual Book of ASTM Standards, Section 12: Nuclear, Solar, and Geothermal Energy**, Vol. 12.01, Standard C1174, ASTM, West Conshohocken, PA, 2000.
26. M. Muhlbauer, " Physical Properties of Glass Based on Chemical Composition," **Sklar. Keram**. **30** [8], 216-225 (1988) – translation DP-TR-112.
27. P. Hrma, J. D. Vienna, J. V. Crum, G. F. Piepel, and M. Mika. "Liquidus Temperature of High-Level Waste Borosilicate Glasses with Spinel Primary Phase," U.S. DOE Report PNNL-SA-32484, Pacific Northwest National Laboratory, Richland, WA (1999).
28. Scheffé, H. **The Analysis of Variance**, John Wiley & Sons, New York, NY, 1959.
29. D.F. Bickford and C.M. Jantzen, "Devitrification of Defense Nuclear Waste Glasses: Role of Melt Insolubles," **J. Non-Cryst. Solids**, **84**, 299-307 (1986).
30. D.A. Duke, J.F. McDowell, and B.R. Karstetter, "Crystallization and Chemical Strengthening of Nepheline Glass-Ceramics," **J. Am. Ceram. Soc.**, **50**, 67-75 (1967).
31. A.D. Cozzi, D.K. Peeler, and C.M. Jantzen, "Scoping Study to Evaluate Liquidus Temperature Measurements Performed by PNNL and CELS," U.S. DOE Report WSRC-RP-97-249, Westinghouse Savannah River Co., Aiken, SC (1999).

32. I. Joseph, A. Mathur, C. Capozzi, J. Shegal, D. Butts, D.McPherson, L.D. Pye, and L. Eisenstatt. "Crystallization Behavior of a Fully Simulated West Valley Borosilicate Glass," **Waste Management 88**, pp. 0487-0491 (1988).

33. D.S. Kim, P. Hrma, D. E. Smith, and M.J. Schweiger, "Crystallization in Simulated Glasses from Hanford High-Level Nuclear Waste Composition Range," **Environmental and Waste Management Issues in the Ceramic Industry**, G.B. Mellinger (Ed.), Am. Ceram. Soc., Westerville, OH 179-189 (1990).

34. P.R. Hrma, G.F. Piepel, M.J. Schweiger, D. E. Smith, D.S. Kim, P. E. Redgate, J.D. Vienna, C.A. LoPresti, D.B. Simpson, D.K. Peeler, and M.H. Langowski, "Property/Composition Relationships for Handford High-Level Waste Glasses Melting at 1150C," U.S. DOE Report PNL-10359, Vol. 1, Pacific Northwest Laboratory, Richland, WA (December 1994).

35. R.L. Schulz, K.G. Brown and C.M. Jantzen, "Technical Report on the Impact of MgO on DWPF Glass Liquidus Temperature and Durability," WSRC-RP-2000-00419, Revision 0, June 26, 2000.

36. H. H. Elder, "Position Paper on Sludge Batch 2 Qualification Strategy and Simulant Composition," HLW-SRT-2000-00128, High Level Waste Salt Disposition Systems Engineering Team, May 2000.

37. A.D. Cozzi, D.K. Peeler, and C.M. Jantzen, "Scoping Study to Evaluate Liquidus Temperature Measurements Performed by PNNL and CELS," U.S. DOE Report WSRC-RP-97-249, Westinghouse Savannah River Co., Aiken, SC (1999).

13. APPENDIX: SOLUBILITY SOLUTION TO LIQUIDUS TEMPERATURE PREDICTION

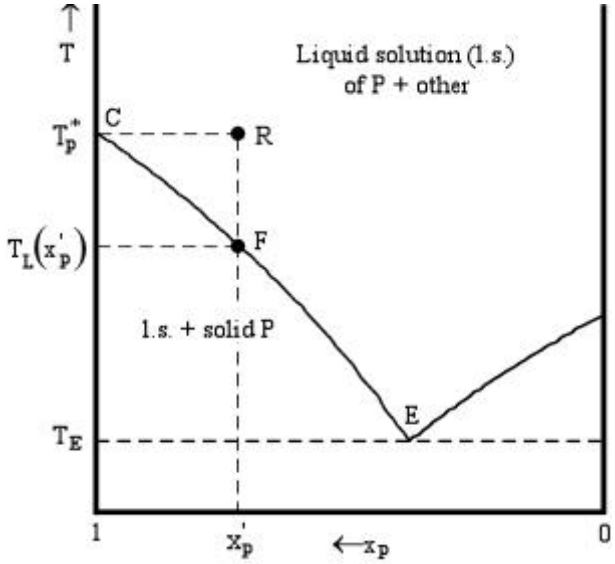

Figure 13-1. Solid-liquid phase diagram for complete liquid miscibility and solid immiscibility and ideal behavior. Only line CE is of interest as it describes the equilibrium between liquid (or melt) and crystallization of the primary phase (P or pyroxene) and, thus, the liquidus temperature as a function of composition (i.e., addition of the solute or substituted nepheline). Other characteristics of the phase diagram are immaterial for this discussion. This is a reprint of Figure 3.

As illustrated in Figure 13-1, the liquidus temperature represents the equilibrium between liquid and the primary phase, P, controlling the onset of crystallization as described by point F [14]. This condition implies that the chemical potentials, μ_P, of the pure crystalline (or solid) phase, P, and of P in the liquid (or melt) must be equal. At a given, constant pressure and liquidus temperature, T_L, this means that the potentials are related by [13]:

Equation 13-1
$$\mu^*_{P(s)}(T_L) = \mu^*_{P(l)}(T_L) + RT_L \ln\{a(P_{(l)})\}$$

where μ is the appropriate chemical potential, $a(P_{(l)})$ represents the activity of P in the liquid (or melt) phase, R is the appropriate gas constant, and the asterisk (*) indicates a pure substance. Rearranging this expression provides:

Equation 13-2
$$\mu^*_{P(l)}(T_L) - \mu^*_{P(s)}(T_L) = -RT_L \ln\{a(P_{(l)})\}.$$

Furthermore, the chemical potential for a pure substance is merely its Gibbs free energy $\overline{G}$, or:

Equation 13-3
$$\mu^*_{P(l)}(T_L) - \mu^*_{P(s)}(T_L) = \Delta\overline{G}_{fus,P}(T_L)$$

where $\Delta\overline{G}_{fus,P}(T_L)$ is the free energy of fusion for P at the liquidus temperature, T_L. Thus Equation 13-2 can now be written as:

Equation 13-4
$$\Delta\overline{G}_{fus,P}(T_L) = -RT_L \ln\{a(P_{(l)})\}.$$

The free energy of fusion can also be expressed in terms of the enthalpy, $\overline{H}$, and entropy, $\overline{S}$, of P [13]:

Equation 13-5 $$\Delta\overline{G}_{\mathrm{fus,P}}(T_L) = \Delta\overline{H}_{\mathrm{fus,P}}(T_L) - T_L\Delta\overline{S}_{\mathrm{fus,P}}(T_L).$$

Combining Equation 13-4 and Equation 13-5 provides a fundamental relationship between activity and liquidus temperature:

Equation 13-6 $$-RT_L \ln\left\{a\left(P_{(l)}\right)\right\} = \Delta\overline{H}_{\mathrm{fus,P}}(T_L) - T_L\Delta\overline{S}_{\mathrm{fus,P}}(T_L).$$

At T_L (which is below T_P^*), $P_{(l)}$ is a supercooled liquid. Thus the isothermal transformation from liquid to solid P at T_L is irreversible: $\Delta\overline{S} \neq \Delta\overline{H}/T$ and $\Delta\overline{G} \neq 0$ [13]. To find $\Delta\overline{G}_{\mathrm{fus,P}}(T_L)$, the following reversible process (i.e., $\Delta\overline{S} = 0$) can be used to convert pure, liquid P at T_L to pure, solid P at T_L:

$$P(l, T_L) \xrightarrow{1} P\left(l, T_P^*\right) \xrightarrow{2} P\left(s, T_P^*\right) \xrightarrow{3} P(s, T_L)$$

at constant pressure. Step 1 is the reversible heating of liquid P from T_L to T_P^* (i.e., the normal melting point of "pure" P). Step 2 is the reversible "freezing" of liquid P to solid P at T_P^*. Step 3 is the reversible cooling of solid P from T_P^* to T_L. Based upon Figure 13-1 for an ideal system, this process is equivalent to starting at point F, heating up the melt to T_P^* (at point R), crystallizing P at the melt temperature (still at point R), and then cooling the crystalline P back to T_L (as described by point F). For these steps, the corresponding changes in enthalpies and entropies are:

Equation 13-7

$$\Delta\overline{H}_1 = \int_{T_L}^{T_P^*} \overline{C}_{\mathrm{p,P}(l)}\mathrm{d}T = -\int_{T_P^*}^{T_L} \overline{C}_{\mathrm{p,P}(l)}\mathrm{d}T, \qquad \Delta\overline{S}_1 = \int_{T_L}^{T_P^*} \overline{C}_{\mathrm{p,P}(l)}\frac{\mathrm{d}T}{T} = -\int_{T_P^*}^{T_L} \overline{C}_{\mathrm{p,P}(l)}\frac{\mathrm{d}T}{T},$$

$$\Delta\overline{H}_2 = \Delta\overline{H}_{\mathrm{fus,P}}\left(T_P^*\right) \qquad \Delta\overline{S}_2 = \frac{\Delta\overline{H}_{\mathrm{fus,P}}\left(T_P^*\right)}{T_P^*}$$

$$\Delta\overline{H}_3 = \int_{T_P^*}^{T_L} \overline{C}_{\mathrm{p,P}(s)}\mathrm{d}T, \qquad \Delta\overline{S}_3 = \int_{T_P^*}^{T_L} C_{\mathrm{p,P}(s)}\frac{\mathrm{d}T}{T},$$

where $\overline{C}_p$ is the appropriate constant pressure heat capacity for P. Summing the changes for these three steps provides $\Delta\overline{H}$ and $\Delta\overline{S}$ for the transformation of liquid P at T_L to solid P at T_L:

Equation 13-8

$$\Delta\overline{H}_{\mathrm{fus,P}}(T_L) = \Delta\overline{H}_{\mathrm{fus,P}}\left(T_P^*\right) + \int_{T_P^*}^{T_L} \Delta\overline{C}_{\mathrm{p,P}}\mathrm{d}T$$

$$\Delta\overline{S}_{\mathrm{fus,P}}(T_L) = \frac{\Delta\overline{H}_{\mathrm{fus,P}}\left(T_P^*\right)}{T_P^*} + \int_{T_P^*}^{T_L} \Delta\overline{C}_{\mathrm{p,P}}\frac{\mathrm{d}T}{T}$$

where $\Delta\overline{C}_{\mathrm{p,P}} \equiv \overline{C}_{\mathrm{p,P}(s)} - \overline{C}_{\mathrm{p,P}(l)}$.

Substitution of these expressions into Equation 13-6 provides:

Equation 13-9 $$-R\ln\left\{a\left(P_{(l)}\right)\right\}=\Delta\overline{H}_{fus,P}\left(T_P^*\right)\left(\frac{1}{T_L}-\frac{1}{T_P^*}\right)+\frac{1}{T_L}\int_{T_P^*}^{T_L}\Delta\overline{C}_{p,P}\left(1-\frac{T_L}{T}\right)dT\,.$$

It is usually an excellent approximation to take $\Delta\overline{C}_p$ as independent of temperature and to evaluate it at the melting point of pure P [13]. Upon integration, this provides the following expression:

Equation 13-10 $$-R\ln\left\{a\left(P_{(l)}\right)\right\}\approx\Delta\overline{H}_{fus,P}\left(T_P^*\right)\left(\frac{1}{T_L}-\frac{1}{T_P^*}\right)+\Delta\overline{C}_{p,P}\left(T_P^*\right)\left[1-\frac{T_P^*}{T_L}-\ln\left(\frac{T_L}{T_P^*}\right)\right].$$

In general, it is also often reasonable to assume that $\Delta\overline{C}_{p,P} << \Delta\overline{H}_{fus,P}\left(T_P^*\right)$ [13]. Imposing this assumption on Equation 13-10 results in the following relationship between the activity of P in the liquid (or melt) phase and the reciprocal of the liquidus temperature:

Equation 13-11 $$-R\ln\left\{a\left(P_{(l)}\right)\right\}\approx\Delta\overline{H}_{fus,P}\left(T_P^*\right)\left(\frac{1}{T_L}-\frac{1}{T_P^*}\right).$$

A relationship very similar to Equation 13-11 is often used to estimate the curve CE on phase diagrams such as that found in Figure 13-1 describing the relationship between liquidus temperature and composition. For these ideal, binary systems, the molar concentration of P is substituted for the activity of P in Equation 13-11. It should be noted that if any of the above assumptions are not valid for the glass compositions under consideration, then the model developed would likely have significant prediction biases evident in the validation data. The validation data appear to confirm that these assumptions were appropriate for the composition region under consideration.

14. APPENDIX: LIQUIDUS TEMPERATURE AND COMPOSITION MEASUREMENTS

Table XXI. Liquidus Temperature Data for SRTC Glasses Melted at 1150°C*

Sample ID	Melted	T_L Meas.	Air T_L (°C)	Internal T_L (°C)	Platinum T_L (°C)	T_L Method	Reference
AH 131AL	1988	1985	---	863	---	Gradient	SS**
AH 131AL	1988	1988	---	Broke	---	Gradient	CELS-022
AH 131AL	1992	1993	860	835	885	Gradient	CELS-044
AH 131AV	1985	1985	1044	990	1027	Gradient	CELS-009
AH 131AV	1988	1988	---	Broke	---	Gradient	CELS-022
AH 131AV	1992	1993	995	995	1015	Gradient	CELS-044
AH 131 FE-RED	1988	1988	1048	996	1099	Gradient	CELS-022
AH 131 FE-RED	1992	1993	1085	1075	1105	Gradient	CELS-044
AH 131 FE-RED	1992	1996	1060	1035	1090	Gradient	CELS-076
AH 131 FE-RED-A	1992	1996	---	1109	---	Isotherm.	PNNL [37]
AH 131 FE-RED-B	1992	1996	---	1107	---	Isotherm.	PNNL [37]
AH 131 FE-OX	1996	1997	1040	1035	1040	Gradient	CELS-068
AH 165AL	1985	1985	882	863	933	Gradient	CELS-009
AH 165AL	1988	1988	972	946	975	Gradient	CELS-022
AH 165AL	1992	1993	905	840	905	Gradient	CELS-044
AH 165AV	1985	1985	1069	917	923	Gradient	CELS-009
AH 165AV-REV.	1988	1988	1041	1006	978	Gradient	CELS Letter (5-3-89)
AH 165AV	1992	1993	1000	1000	970	Gradient	CELS-044
AH 165FE-RED	1985	1985	1110	1102	1125	Gradient	CELS-009
AH 165FE-RED	1988	1988	940	920	927	Gradient	CELS-022
AH 165FE-RED	1992	1993	1105	1085	1100	Gradient	CELS-044
AH 165 FE	1992	1996	1070	1015	1095	Gradient	CELS-076
AH 165 FE-RED-A	1992	1996	---	1086	---	Isotherm.	PNNL [37]
AH 165 FE-RED-B	1992	1996	---	1113	---	Isotherm.	PNNL [37]
AH 165FE-OX	1996	1997	1140	1135	1120	Gradient	CELS-068
AH 168AL	1988	1988	944	846	897	Gradient	CELS-022
AH 168AL	1992	1993	695	720	715	Gradient	CELS-044
AH 168AV	1985	1985	1067	1014	1003	Gradient	CELS-009
AH 168AV	1988	1988	1000	925	972	Gradient	CELS-022
AH 168AV	1992	1993	990	990	980	Gradient	CELS-044
AH 168AV	1992	1996	1065	980	1015	Gradient	CELS-076
AH 168AV-A	1992	1996	---	967	---	Isotherm.	PNNL [37]
AH 168AV-B	1992	1996	---	971	---	Isotherm.	PNNL [37]
AH 168FE-RED	1988	1988	1049	1022	1036	Gradient	CELS-022
AH 168FE-RED	1992	1992	1090	1085	1110	Gradient	CELS-044
AH 168FE-RED	1992	1996	1025	900	1015	Gradient	CELS-076
AH 168 FE-OX	1996	1997	1145	1130	1110	Gradient	CELS-068
AH 200AL	1988	1988	1035	929	951	Gradient	CELS-022
AH 200AL	1992	1992	995	845	900	Gradient	CELS-044

* Glasses in the shaded rows are excluded from Model Data; italicized sample identifiers indicate glasses used in the original, DWPF liquidus temperature model. Three liquidus temperature measurements were routinely provided by CELS: those at the air-glass and platinum glass interfaces as well as the internal or bulk glass.

** Measured by Sharpe-Shurtz using the ASTM gradient furnace method.

Table XXI. Liquidus Temperature Data for SRTC Glasses Melted at 1150°C*

Sample ID	Melted	T_L Meas.	Air T_L (°C)	Internal T_L (°C)	Platinum T_L (°C)	T_L Method	T_L Reference
AH 200AV(AH-8)	1985	1985	1012	996	1036	Gradient	CELS-009
AH 200AV	1988	1988	1041	997	1056	Gradient	CELS-022
AH 200AV	1992	1993	1010	985	1000	Gradient	CELS-044
AH 200FE-RED	1988	1988	1140	1126	1188	Gradient	CELS-022
AH 200FE-RED	1992	1992	1070	1065	1080	Gradient	CELS-044
AH 200FE	1992	1996	1100	1070	1135	Gradient	CELS-076
AH 200FE-RED-A	1992	1996	---	1113	---	Isotherm.	PNNL [37]
AH 200FE-RED-B	1992	1996	---	1062	---	Isotherm.	PNNL [37]
AH 200FE-OX	1996	1997	900	895	920	Gradient	CELS-068
AH 202AL	1988	1988	1001	959	978	Gradient	CELS-022
AH 202AL	1992	1992	1035	965	930	Gradient	CELS-044
AH 202AV (AH-10)	1985	1985	996	965	1065	Gradient	CELS-009
AH 202AV	1988	1988	---	967	---	Gradient	CELS-022
AH 202AV	1992	1992	1015	1010	1010	Gradient	CELS-044
AH 202FE-RED	1988	1988	1130	1123	1093	Gradient	CELS-022
AH 202FE-RED	1992	1992	1125	1110	1135	Gradient	CELS-044
AH 202FE	1992	1996	1175	1160	1165	Gradient	CELS-076
AH 202FE-RED-A	1992	1996	---	1118	---	Isotherm.	PNNL [37]
AH 202FE-RED-B	1992	1996	---	1127	---	Isotherm.	PNNL [37]
AH 202FE-OX	1996	1997	1135	1100	1130	Gradient	CELS-068
AH-5-1985#	1985	1985	1037	991	973	Gradient	CELS-009
AH-9-1985#	1985	1985	---	1000	---	Gradient	SS
AH-9-1985#	1985	1985	1080	778	773	Gradient	CELS-009
AH-13 –1985#	1985	1985	1151	1096	1135	Gradient	CELS-009
AH-16-1985#	1985	1985	1111	1073	1111	Gradient	CELS-009
DWPF STARTUP FRIT (10/26/87)	1987	1988	1102	1066	1028	Gradient	CELS-024
DWPF STARTUP FRIT (10/28/87)	1987	1988	1084	1062	1059	Gradient	CELS-024
DWPF STARTUP FRIT (10/27/87)	1987	1988	987	997	998	Gradient	CELS Letter (5-3-89)
DWPF STARTUP FRIT (10/27/87)	1987	1988	1001	1012	1014	Gradient	CELS-024
Frit 165 (Nominal)	1984	1984	726	732	733	Gradient	CELS-001
Carter's 165 Frit	1988	1988	904	909	913	Gradient	CELS Letter (5-3-89)

* Glasses in the shaded rows are excluded from Model Data; italicized sample identifiers indicate glasses used in the original, DWPF liquidus temperature model.

Table XXII. Mass Compositions (on a 100g glass basis) for SRTC Glasses Melted at 1150°C[†]

Sample ID	Melted	Lab	Reps	Ref.[††]	Al_2O_3	B_2O_3	CaO	Cr_2O_3	FeO	Fe_2O_3	K_2O	Li_2O	MgO	MnO	Na_2O	NiO	SiO_2	TiO_2	Others
AH 131AL	1988	CELS	4	CELS-158	14.05	11.35	0.39	0.002	0.13	3.99	0.05	4.19	1.42	2.69	14.90	0.61	44.60	0.77	0.75
AH 131AL	1988	CELS	2	CELS-158	14.05	11.35	0.39	0.002	0.13	3.99	0.05	4.19	1.42	2.69	14.90	0.61	44.60	0.77	0.75
AH 131AL	1992	CELS	4	CELS-044	13.50	10.90	0.38	0	0.09	4.58	0.00	4.09	1.38	2.51	14.10	0.63	46.40	0.72	0.70
AH 131AV	1985	CELS	6	CELS-025	7.18	10.88	0.74	0.074	0.27	11.40	0.04	3.88	1.28	0.82	14.30	1.08	45.20	0.70	0.38
AH 131AV	1988	CELS	2	CELS-158	4.29	7.73	0.78	0.002	0.26	11.21	0.05	4.41	0.66	2.79	10.35	1.02	54.65	0.06	1.29
AH 131AV	1992	CELS	4	CELS-044	4.39	7.60	0.76	0	0.29	11.57	0.00	4.25	0.67	2.59	9.86	1.04	54.99	0.06	0.88
AH 131 FE-RED	1988	CELS	2	CELS-158	1.02	7.52	1.12	0.007	6.17	11.69	0.05	4.23	0.67	1.09	11.10	2.92	51.05	0.06	1.24
AH 131 FE-RED	1992	CELS	4	CELS-044	2.25	7.33	1.01	0	5.86	11.09	0.00	4.09	0.66	0.93	10.90	2.56	51.40	0.05	0.87
AH 131 FE-RED	1992	CELS	4	CELS-044	2.25	7.33	1.01	0	5.86	11.09	0.00	4.09	0.66	0.93	10.90	2.56	51.40	0.05	0.87
AH 131 FE-RED-A	1992	CELS	4	CELS-044	2.25	7.33	1.01	0	5.86	11.09	0.00	4.09	0.66	0.93	10.90	2.56	51.40	0.05	0.87
AH 131 FE-RED-B	1992	CELS	4	CELS-044	2.25	7.33	1.01	0	5.86	11.09	0.00	4.09	0.66	0.93	10.90	2.56	51.40	0.05	0.87
AH 131 FE-OX	1996	CELS	4	CELS-068	3.61	14.00	1.39	0	2.15	18.51	0.07	4.51	1.39	1.10	15.40	0.04	35.50	0.76	0.92
AH 165AL	1985	CELS	1	CELS-158	13.30	7.57	0.52	0	0.04	4.12	0.05	4.28	0.67	2.75	11.10	0.57	52.70	0.06	1.27
AH 165AL	1988	CELS	1	CELS-158	13.30	7.57	0.52	0	0.04	4.12	0.05	4.28	0.67	2.75	11.10	0.57	52.70	0.06	1.27
AH 165AL	1992	CELS	4	CELS-044	13.40	7.34	0.51	0	0.12	4.70	0.00	4.20	0.66	2.62	10.60	0.67	53.60	0.00	0.79
AH 165AV	1985	CELS	1	CELS-025	5.34	7.33	0.69	0.052	0.20	11.88	0.06	5.11	0.73	2.78	10.30	1.07	53.10	0.17	0.74
AH 165AV-REV.	1988	CELS	2	CELS-025 CELS-158	5.08	7.27	0.88	0.027	0.20	11.78	0.09	5.09	0.69	2.76	10.23	1.02	53.27	0.11	0.83
AH 165AV	1992	CELS	4	CELS-044	5.17	6.57	1.04	0	0.19	11.38	0.00	5.02	0.66	2.57	9.96	1.01	55.29	0.00	0.76
AH 165FE-RED	1985	CELS	1	CELS-158	1.28	7.48	1.49	0.01	6.65	9.71	0.03	4.18	0.66	1.13	11.20	3.05	51.70	0.06	1.26
AH 165FE-RED	1988	CELS	1	CELS-158	1.28	7.48	1.49	0.01	6.65	9.71	0.03	4.18	0.66	1.13	11.20	3.05	51.70	0.06	1.26
AH 165FE-RED	1992	CELS	4	CELS-044	1.42	7.28	1.40	0	5.46	10.93	0.00	4.05	0.65	1.07	10.70	2.97	52.00	0.00	0.85
AH 165 FE	1992	CELS	4	CELS-044	1.42	7.28	1.40	0	5.46	10.93	0.00	4.05	0.65	1.07	10.70	2.97	52.00	0.00	0.85
AH 165 FE-RED-A	1992	CELS	4	CELS-044	1.42	7.28	1.40	0	5.46	10.93	0.00	4.05	0.65	1.07	10.70	2.97	52.00	0.00	0.85
AH 165 FE-RED-B	1992	CELS	4	CELS-044	1.42	7.28	1.40	0	5.46	10.93	0.00	4.05	0.65	1.07	10.70	2.97	52.00	0.00	0.85
AH 165FE-OX	1996	CELS	4	CELS-068	1.45	7.36	1.42	0	5.99	10.54	0.03	4.27	0.64	1.01	11.20	2.58	49.60	0.00	0.88
AH 168AL	1988	SRTC	1	SRTC/ADS	14.16	12.11	0.44	0.001	0.02	3.43	0.23	4.24	0.71	2.66	10.42	0.53	47.66	0.05	0.68
AH 168AL	1992	CELS	4	CELS-044	6.72	13.70	0.14	0	0.03	2.43	0.00	5.34	0.89	1.09	11.80	0.33	56.40	0.00	0.87
AH 168AV	1985	CELS	1	CELS-158	5.31	12.65	0.70	0.002	0.63	10.90	0.05	4.28	0.73	2.72	10.30	0.98	50.40	0.06	0.79
AH 168AV	1988	CELS	1	CELS-158	5.31	12.65	0.70	0.002	0.63	10.90	0.05	4.28	0.73	2.72	10.30	0.98	50.40	0.06	0.79
AH 168AV	1992	CELS	4	CELS-044	5.58	10.60	0.68	0	0.61	10.51	0.00	4.24	0.74	2.64	10.10	1.02	51.60	0.00	0.69
AH 168AV	1992	CELS	4	CELS-044	5.58	10.60	0.68	0	0.61	10.51	0.00	4.24	0.74	2.64	10.10	1.02	51.60	0.00	0.69
AH 168AV-A	1992	CELS	1	CELS-044	5.31	12.65	0.70	0.002	0.63	10.90	0.05	4.28	0.73	2.72	10.30	0.98	50.40	0.06	0.79
AH 168AV-B	1992	CELS	1	CELS-044	5.31	12.65	0.70	0.002	0.63	10.90	0.05	4.28	0.73	2.72	10.30	0.98	50.40	0.06	0.79
AH 168FE-RED	1988	SRTC	1	SRTC/ADS	1.44	11.73	1.05	0.014	5.20	7.85	0.06	4.17	0.71	0.74	11.15	2.77	53.05	0.04	0.70
AH 168FE-RED	1992	CELS	4	CELS-044	2.47	11.40	1.35	0	6.22	9.39	0.00	4.12	0.71	0.98	10.80	2.82	48.30	0.00	0.67

[†] Glasses in the shaded rows are excluded from Model Data; italicized rows indicate glasses used in the original, DWPF liquidus temperature model. Others include those oxides present in the glass that are not listed in the table (e.g., BaO, Ce_2O_3, Cs_2O, etc.).

[††] The SRTC/ADS data are from reports 200016931, 200016836, 200016934, and 200016838.

Table XXII. Mass Compositions (on a 100g glass basis) for SRTC Glasses Melted at 1150°C[††]

Sample ID	Melted	Lab	Reps	Ref.	Al_2O_3	B_2O_3	CaO	Cr_2O_3	FeO	Fe_2O_3	K_2O	Li_2O	MgO	MnO	Na_2O	NiO	SiO_2	TiO_2	Others
AH 168FE-RED	1992	CELS	4	CELS-044	2.47	11.40	1.35	0	6.22	9.39	0.00	4.12	0.71	1.03	10.80	2.82	48.30	0.00	0.67
AH 168FE-OX	1996	CELS	4	CELS-068	3.29	12.00	1.29	0	0.38	16.98	0.03	4.00	0.68	0.96	13.80	2.72	42.50	0.00	0.71
AH 200AL	1988	CELS	1	CELS-158	13.85	10.30	0.56	0.002	0.02	3.95	3.29	2.58	1.25	2.60	10.90	0.55	47.70	1.76	0.04
AH 200AL	1992	CELS	4	CELS-044	13.40	10.20	0.54	0	0.06	4.40	3.12	2.65	1.25	2.49	10.60	0.61	48.40	1.70	0.03
AH 200AV(AH-8)	1985	CELS	4	CELS-038	5.88	10.10	0.69	0.018	0.29	11.28	3.08	3.17	1.20	2.68	9.76	0.97	49.00	1.32	0.09
AH 200AV	1988	CELS	6	CELS-158	5.16	10.24	0.88	0.005	0.08	11.21	3.18	2.71	1.27	2.75	10.10	1.00	49.22	1.58	0.06
AH 200AV	1992	CELS	4	CELS-044	5.14	10.30	0.63	0	0.08	11.81	3.18	2.68	1.22	2.55	9.77	1.02	49.50	1.41	0.02
AH 200FE-RED	1988	CELS	1	CELS-158	1.39	10.35	0.97	0.008	6.01	9.92	3.31	2.49	1.27	1.03	11.00	2.74	47.40	1.85	0.05
AH 200FE-RED	1992	CELS	4	CELS-044	2.07	10.10	0.92	0	5.90	9.84	3.15	2.59	1.21	0.95	10.60	2.57	47.40	1.78	0.02
AH 200FE	1992	CELS	4	CELS-044	2.07	10.10	0.92	0	5.90	9.84	3.15	2.59	1.21	0.95	10.60	2.57	47.40	1.78	0.02
AH 200FE-RED-A	1992	CELS	4	CELS-044	2.07	10.10	0.92	0	5.90	9.84	3.15	2.59	1.21	0.95	10.60	2.57	47.40	1.78	0.02
AH 200FE-RED-B	1992	CELS	4	CELS-044	2.07	10.10	0.92	0	5.90	9.84	3.15	2.59	1.21	0.95	10.60	2.57	47.40	1.78	0.02
AH 200FE-OX	1996	CELS	4	CELS-068	1.35	9.92	1.53	0	1.64	14.97	3.19	2.58	1.25	0.95	11.00	2.81	46.50	1.67	0.02
AH 202AL	1988	CELS	1	CELS-158	13.70	7.53	0.40	0.004	0.07	3.81	3.45	4.28	1.30	2.64	7.56	0.56	52.15	1.77	0.06
AH 202AL	1992	CELS	4	CELS-044	13.90	7.42	0.41	0	0.19	4.19	3.32	4.18	1.28	2.51	7.34	0.62	52.40	1.71	0.03
AH 202AV (AH-10)	1985	CELS	4	CELS-038	5.14	7.59	0.68	0.011	0.14	11.14	3.09	4.44	1.11	2.67	6.83	0.96	54.20	1.30	0.11
AH 202AV	1988	CELS	2	CELS-158	4.98	7.55	0.72	0.003	0.08	11.66	3.45	4.37	1.31	2.67	6.75	0.96	53.30	1.41	0.06
AH 202AV	1992	CELS	4	CELS-044	4.96	7.44	0.72	0	0.14	11.75	3.33	4.27	1.30	2.59	6.55	1.00	54.10	1.37	0.03
AH 202FE-RED	1988	CELS	2	CELS-158	1.38	7.32	1.01	0.008	6.88	9.86	3.47	4.20	1.31	1.04	7.73	2.87	51.00	1.84	0.08
AH 202FE-RED	1992	CELS	4	CELS-044	1.36	7.08	0.96	0	6.90	8.93	3.28	4.27	1.26	0.95	7.62	2.73	52.50	1.72	0.02
AH 202FE	1992	CELS	4	CELS-044	1.36	7.08	0.96	0	6.90	8.93	3.28	4.27	1.26	0.95	7.62	2.73	52.50	1.72	0.02
AH 202FE-RED-A	1992	CELS	4	CELS-044	1.36	7.08	0.96	0	6.90	8.93	3.28	4.27	1.26	0.95	7.62	2.73	52.50	1.72	0.02
AH 202FE-RED-B	1992	CELS	4	CELS-044	1.36	7.08	0.96	0	6.90	8.93	3.28	4.27	1.26	0.95	7.62	2.73	52.50	1.72	0.02
AH 202FE-OX	1996	CELS	4	CELS-068	0.99	7.34	1.36	0	0.62	15.31	3.26	4.36	1.31	0.96	7.77	2.66	50.10	1.75	0.02
AH-5-1985#	1985	CELS	4	CELS-038	5.48	6.95	0.66	0.002	0.19	11.19	3.16	3.77	0.60	2.64	9.24	0.96	53.08	1.31	0.01
AH-9-1985#	1985	CELS	4	CELS-038	6.04	8.75	0.69	0.013	0.16	11.43	3.13	3.47	0.58	2.64	9.20	0.97	50.88	1.33	0.11
AH-9-1985#	1985	CELS	4	CELS-038	6.04	8.75	0.69	0.013	0.16	11.43	3.13	3.47	0.58	2.64	9.20	0.97	50.88	1.33	0.11
AH-13 –1985#	1985	CELS	4	CELS-038	6.48	6.41	1.25	0.011	0.06	13.53	3.06	3.32	0.49	3.25	8.80	1.14	49.00	1.29	0.13
AH-16-1985#	1985	CELS	4	CELS-038	6.36	7.20	1.26	0.077	0.19	13.19	3.06	4.06	1.00	3.22	6.54	1.10	50.20	1.30	0.11
DWPF SF (10/26/87)	1987	CELS	6	CELS-025	4.59	8.49	1.45	0.091	0.19	13.89	2.68	3.22	0.86	1.93	11.50	1.10	48.10	1.16	0.26
DWPF SF (10/28/87)	1987	CELS	6	CELS-025	4.67	8.66	1.44	0.096	0.19	14.00	2.69	3.32	0.81	1.89	11.60	1.11	47.60	1.21	0.15
DWPF SF (10/27/87)	1987	CELS	6	CELS-025	4.53	8.37	1.51	0.090	0.19	14.08	2.74	3.21	0.86	1.97	11.50	1.11	48.00	1.16	0.23
DWPF SF (10/27/87)	1987	CELS	6	CELS-025	4.53	8.37	1.51	0.090	0.19	14.08	2.74	3.21	0.86	1.97	11.50	1.11	48.00	1.16	0.23
Frit 165 (Nominal)	1984	CELS	---	CELS-001	0.00	8.49	0.00	0	0	0.00	0.00	6.86	0.96	0.00	12.80	0.00	70.08	0.00	0.80
Carter's 165 Frit	1988	CELS	6	CELS-025	4.62	6.84	1.58	0	0.16	11.43	0.13	4.94	0.75	1.96	11.20	0.84	54.40	0.23	0.83

[†] Glasses in the shaded rows are excluded from Model Data; italicized rows indicate glasses used in the original, DWPF liquidus temperature model. Others include those oxides present in the glass that are not listed in the table (e.g., BaO, Ce_2O_3, Cs_2O, etc.).

Table XXIII. PNNL Liquidus Temperature Measurements and SRTC-ML Compositions for the T_L Design Study Glasses[†]

Sample ID	T_{M2}(°C)	T_L(°C)	Phase(s)[††]	Al_2O_3	B_2O_3	CaO	Cr_2O_3	FeO	Fe_2O_3	K_2O	Li_2O	MgO	MnO	Na_2O	NiO	SiO_2	TiO_2	U_3O_8
SG01	1107	1124	S	2.50	10.23	1.98	0.09	0.19	13.95	3.79	5.89	0.49	0.97	6.22	2.13	42.71	0.65	4.48
SG02	1250	775	R, C	2.56	5.11	1.93	0.02	0.08	5.89	3.77	5.89	2.35	3.03	11.00	0.06	57.79	0.15	0.00
	1250	755	C															
SG03	1250	1164	S	3.95	9.42	1.52	0.24	0.16	11.62	2.07	3.41	1.88	2.41	9.90	1.56	46.64	0.28	3.52
SG04[‡]	1300	1261	S	8.28	4.89	0.32	0.08	0.20	14.50	1.49	5.99	2.58	0.96	6.17	2.06	51.75	0.16	0.26
SG05	1300	1084	S	5.60	7.73	1.15	0.20	0.14	10.49	2.67	4.44	1.56	1.96	8.48	1.10	52.27	0.40	2.51
SG05B	1284	1082	S	5.56	7.84	1.14	0.19	0.14	10.21	2.51	4.02	1.43	1.97	8.57	1.08	51.07	0.42	2.39
SG06	1322	911	R,S	7.90	5.01	2.00	0.09	0.19	14.06	3.77	2.97	0.50	0.98	10.95	0.05	47.93	0.65	0.26
	1322	931	R,S															
SG07	1294	950	S	8.11	10.62	0.31	0.29	0.04	5.77	3.64	5.43	2.29	2.91	6.03	0.06	53.29	0.17	0.26
SG08	1330	1114	R, S	4.12	6.50	1.57	0.14	0.17	12.34	3.21	3.44	2.06	2.43	7.54	0.56	54.26	0.28	1.54
SG09	1200	1173	S	8.21	10.11	2.01	0.28	0.20	14.62	1.51	5.78	0.52	0.98	6.30	0.05	43.96	0.16	4.81
SG10	1275	1098	R, S	4.03	6.65	0.75	0.25	0.11	8.12	3.22	5.25	2.03	2.45	7.47	1.61	54.17	0.28	3.62
SG11	1264	895	R, S	3.86	9.48	0.76	0.14	0.11	8.00	2.10	5.11	1.94	1.48	9.72	0.57	53.48	0.29	1.54
SG12	1384	1030	R, S	2.59	5.01	0.32	0.28	0.13	14.53	1.50	3.04	2.48	0.97	11.14	0.04	56.35	0.16	0.27
SG13	1400	1063	R, S	2.56	9.75	0.32	0.28	0.29	8.13	1.48	5.87	0.50	2.88	5.99	2.14	56.71	0.16	0.27
SG14	1160	951	S	2.66	11.00	0.31	0.09	0.14	14.93	3.73	2.74	2.60	2.93	11.28	0.05	43.34	0.17	5.14
SG15	1285	935	R, C	2.53	10.13	1.94	0.09	0.08	5.80	1.51	5.97	2.48	0.94	6.10	2.06	55.91	0.64	0.72
SG16	1250	995	R, S	6.93	6.33	1.57	0.14	0.11	8.28	2.06	5.18	2.01	2.38	9.87	0.56	50.08	0.52	3.67
SG17	1160	1075	S	3.97	7.92	1.59	0.14	0.17	12.19	3.23	5.32	0.98	1.45	9.98	1.59	45.72	0.53	3.58
SG18	1142	859[‡‡]	S	2.52	10.43	0.33	0.28	0.08	14.27	1.50	5.90	0.47	2.84	10.85	0.04	46.78	0.64	0.27
SG18B	1142	869[‡‡]	R, S	2.67	10.28	0.32	0.28	0.08	14.61	1.46	5.89	0.49	2.87	10.89	0.04	47.77	0.64	0.27
SG19	1140	929	S	6.59	10.31	0.31	0.28	0.08	5.72	3.72	5.91	0.49	0.95	10.90	2.15	44.38	0.18	4.65
SG20	1240	799	R, S, C	8.34	4.97	1.95	0.10	0.08	6.03	1.52	5.90	2.56	0.99	11.05	0.06	51.51	0.64	4.98
SG21	1284	987	R, S	3.97	8.93	1.59	0.24	0.11	7.77	2.04	5.17	0.97	2.31	7.23	1.60	53.43	0.52	1.58
SG22	1246	1145	S	6.94	6.54	1.53	0.25	0.17	12.57	2.10	5.19	1.01	1.46	9.84	1.58	50.01	0.28	1.61
SG23	1304	1069	R, S	4.27	6.52	1.58	0.25	0.11	7.87	3.14	3.39	1.88	1.48	9.93	1.58	53.45	0.54	1.49
SG24	1345	995	R, C	2.64	5.16	0.31	0.11	0.16	11.68	1.50	5.83	0.52	1.00	6.08	0.06	58.50	0.66	4.73
SG25[‡]	1333	1310	S	7.91	11.54	0.35	0.09	0.19	14.21	3.66	2.72	2.37	0.99	6.59	2.06	47.05	0.17	0.26
	1333	1309	S															

[†] Glasses in the shaded rows are excluded from Model Data.

[††] The primary phases identified by PNNL for these glasses were spinel (S) and clinopyroxene (C); the presence of RuO_2 needles is indicated by R.

[‡] Water quenched instead of quenched in air.

[‡‡] Glasses SG18 and SG18B (which was referred to as SG52 by PNNL [9]) were measured for liquidus temperature additional times after using different preparation methods and furnaces. The additional values were 883, 879, 891, 883, 887, and 882°C for glass SG18 and 883, 882, 883, and 891°C for glass SG18B (or SG52) [9].

Table XXIII. PNNL Liquidus Temperature Measurements and SRTC-ML Compositions for the T_L Design Study Glasses[†]

Sample ID	T_{M2}(°C)	T_L(°C)	Phase(s)[††]	Al_2O_3	B_2O_3	CaO	Cr_2O_3	FeO	Fe_2O_3	K_2O	Li_2O	MgO	MnO	Na_2O	NiO	SiO_2	TiO_2	U_3O_8
SG26	1304	1071	S	4.07	6.69	0.77	0.24	0.17	12.35	2.07	3.75	1.00	1.46	10.07	0.58	52.27	0.52	3.66
SG27	1218	1086	S	6.95	9.43	1.53	0.25	0.15	10.91	3.25	5.11	1.98	1.48	7.44	0.58	47.15	0.29	3.62
SG28	1150	833	R, C	2.58	10.54	1.95	0.09	0.20	14.51	1.52	5.95	0.49	0.95	11.23	0.05	49.48	0.16	0.26
SG29	1280	811	S	8.14	5.15	0.32	0.10	0.08	5.76	1.54	6.16	0.48	2.91	11.20	0.05	51.42	0.65	4.65
SG30	1157	1030	S	8.03	5.09	1.92	0.10	0.08	5.81	3.67	5.37	2.37	2.85	10.90	2.06	44.10	0.18	4.50
SG31	1149	1081	S	8.36	11.10	2.00	0.09	0.08	15.09	3.70	5.34	2.65	2.93	6.23	0.06	43.11	0.65	0.26
SG32[‡]	1250	1132	S	8.21	10.58	0.32	0.10	0.31	14.54	1.51	5.97	0.49	0.97	10.94	2.08	42.96	0.63	0.27
SG33	1145	943	S	8.36	10.43	1.95	0.28	0.13	6.04	3.77	5.91	0.52	2.86	10.62	2.11	47.55	0.61	0.26
SG34[‡]	1320	1282	S	8.33	9.61	1.96	0.27	0.20	14.41	1.50	2.99	2.52	2.85	6.35	0.05	42.05	0.64	4.76
SG35[‡]	1200	1231	S	8.12	5.31	0.32	0.28	0.19	13.66	3.67	6.06	2.38	2.89	10.95	2.13	41.80	0.65	0.26
SG36	1265	813	R, C	2.53	10.41	1.99	0.27	0.08	5.59	3.74	2.97	0.48	0.97	10.96	0.05	51.42	0.17	4.43
SG37	1268	944	R, S	2.63	10.29	1.96	0.30	0.11	5.67	3.83	5.88	2.40	0.98	6.04	0.32	58.23	0.66	0.26
	1268	945	R, S															
SG38	1151	897	S	2.67	11.13	0.32	0.09	0.20	14.50	3.71	2.71	2.57	2.97	11.28	0.06	43.29	0.65	5.07
SG39	1322	1164	S	2.61	5.44	1.96	0.28	0.22	14.13	1.48	3.01	0.50	2.87	11.16	2.12	52.23	0.64	0.26
SG40	1300	1173	S	8.20	10.80	0.31	0.29	0.08	5.86	1.44	2.65	2.39	0.97	10.96	2.08	46.93	0.66	4.71
SG41[‡]	1300	1304	S	8.10	11.12	1.98	0.08	0.20	14.32	1.61	2.75	0.52	2.94	6.52	2.02	42.42	0.18	4.90
SG42	1160	990	S	4.55	9.15	0.74	0.23	0.16	12.04	3.23	5.10	1.94	2.41	9.78	0.57	45.99	0.54	1.58
SG43	1317	924	S	6.77	8.80	0.73	0.15	0.11	7.95	3.23	3.77	0.98	2.45	9.69	0.58	51.54	0.28	1.61
SG44[‡]	1330	1244	R, S	7.00	9.19	0.74	0.15	0.17	12.59	2.13	3.71	1.98	1.46	7.55	1.59	51.02	0.53	1.67
SG45	1317	936	R, S, C	2.61	10.56	1.96	0.10	0.08	5.72	1.53	2.96	2.43	2.94	10.80	2.14	55.89	0.17	0.26
SG46[‡]	1250	1247	S	2.65	5.22	0.31	0.28	0.20	14.59	3.88	5.85	2.49	0.99	6.46	2.10	49.20	0.64	4.90
SG47	1193	1144	S	2.67	5.03	1.97	0.28	0.20	14.73	1.52	5.83	2.48	1.00	11.08	2.06	45.57	0.18	5.00
SG48	1356	862	C	2.71	9.84	0.31	0.09	0.08	5.63	3.73	2.96	0.48	0.97	10.70	2.13	56.70	0.65	0.26
	1356	847	C															
SG49	1315	877	C	2.91	5.08	0.31	0.10	0.11	7.93	3.72	5.28	0.51	2.89	6.20	0.07	59.53	0.18	4.69
SG50[‡]	1320	1285	S	2.65	5.42	1.98	0.28	0.20	14.71	3.72	3.02	0.50	2.89	6.30	2.10	49.32	0.64	4.81
SG51	1326	1033	R, S	7.98	5.22	1.95	0.28	0.20	14.64	3.72	2.99	0.50	0.96	10.90	0.05	48.89	0.16	0.26

[†] Glasses in the shaded rows are excluded from Model Data.

[††] The primary phases identified by PNNL for these glasses were spinel (S) and clinopyroxene (C); the presence of RuO_2 needles is indicated by R.

[‡] Water quenched instead of quenched in air.

Table XXIV. Average Corrected Compositions Results for the SG1 Study Glasses

Sample ID	Al_2O_3	B_2O_3	CaO	Cr_2O_3	Fe_2O_3	Li_2O	MgO	MnO	Na_2O	NiO	RuO_2	SiO_2	ZrO_2
SG06	7.78	5.16	1.98	0.108	14.58	2.94	0.486	0.983	11.26	0.138	0.0398	50.22	0.0015
SG06-PNNL-1	7.94	5.14	2.02	0.108	14.69	3.00	0.481	0.978	11.20	0.145	0.0414	50.40	0.0015
SG06-PNNL-2	7.91	4.85	1.91	0.113	14.86	2.89	0.513	0.971	10.87	0.164	0.0492	51.01	0.0015
SG06-SRTC-1	8.02	4.83	2.00	0.177	14.03	2.91	0.448	0.982	11.23	0.124	0.0479	50.81	0.0066
SG06-SRTC-2	8.01	4.76	2.00	0.112	14.13	2.90	0.480	0.983	11.19	0.143	0.0379	50.50	0.0469
SG12	2.49	5.14	0.303	0.337	14.86	2.89	2.47	0.977	10.18	0.177	0.0993	57.18	0.0015
SG12-PNNL-1	2.50	4.99	0.312	0.323	14.93	2.93	2.50	1.00	10.23	0.171	0.0931	57.41	0.0033
SG12-PNNL-2	2.54	4.87	0.308	0.339	14.56	2.88	2.35	0.991	10.88	0.153	0.0900	57.09	0.0026
SG12-SRTC-1	2.60	4.96	0.308	0.330	13.29	2.96	2.41	1.02	10.21	0.170	0.1089	58.40	0.0092
SG12-SRTC-2	2.61	5.03	0.311	0.325	13.51	2.96	2.38	1.03	11.20	0.154	0.0960	58.55	0.0015
SG13	2.54	10.67	0.303	0.367	8.57	5.92	0.478	3.03	5.89	1.80	0.0939	57.98	0.0151
SG13-PNNL-1	2.54	9.91	0.306	0.337	8.54	5.79	0.472	3.04	6.14	1.86	0.1122	58.87	0.0043
SG13-PNNL-2	2.54	9.82	0.304	0.338	8.78	5.86	0.478	3.07	5.91	1.88	0.1022	59.19	0.0157
SG13-SRTC-1	2.56	9.71	0.314	0.329	8.38	5.79	0.499	3.00	5.94	1.86	0.1017	59.87	0.0015
SG13-SRTC-2	2.57	9.78	0.290	0.319	8.49	5.85	0.454	3.10	5.95	1.77	0.0941	58.55	0.0075
SG45	2.51	10.27	2.04	0.116	5.90	2.88	2.41	2.98	10.83	1.81	0.0356	55.49	0.0045
SG45-PNNL-1	2.54	9.74	1.98	0.095	6.01	2.86	2.40	3.01	10.81	1.81	0.0345	54.74	0.0087
SG45-PNNL-2	2.56	9.78	1.99	0.119	5.82	2.89	2.45	3.00	10.67	1.79	0.0411	55.49	0.0015
SG45-SRTC-1	2.81	9.74	1.99	0.108	5.91	2.93	2.36	3.15	10.95	1.81	0.0393	56.29	0.0069
SG45-SRTC-2	2.56	9.69	1.93	0.113	5.65	2.89	2.39	3.03	10.39	1.83	0.0537	56.07	0.0067
SP-1	7.93	7.02	1.02	0.230	12.40	2.92	0.567	0.354	15.85	0.531	0.0615	45.63	1.90
SP-1	7.95	7.08	0.975	0.241	12.43	2.93	0.573	0.355	16.39	0.535	0.0567	45.64	2.03

Table XXV. Measured Composition Results for the SG06 Glasses Produced for the SG1 Study*

Sample ID	Al	Ca	Cr	Fe	K	Mg	Mn	Ni	Ru	Ti	Na	B	Li	Si
PNNL-1	4.32	1.51	0.083	11.2	2.95	0.319	0.853	0.065	0.027	0.374	8.55	1.63	1.34	23.8
PNNL-1	4.09	1.44	0.077	10.6	2.78	0.297	0.787	0.05	0.027	0.355	8.27	1.57	1.34	24
PNNL-1	4.28	1.51	0.08	11	2.88	0.323	0.829	0.045	0.028	0.376	8.52	1.54	1.33	23.4
PNNL-1	4.2	1.48	0.236	10.9	2.87	0.312	0.813	0.043	0.031	0.367	8.34	1.58	1.35	23.9
PNNL-1	4.2	1.48	0.078	10.9	2.85	0.311	0.809	0.049	0.025	0.364	8.2	1.54	1.34	23.5
PNNL-1	4.09	1.45	0.128	10.6	2.77	0.309	0.789	0.046	0.031	0.357	8.16	1.57	1.34	23.8
PNNL-1	4.22	1.48	0.081	10.8	2.85	0.315	0.814	0.045	0.025	0.367	8.75	1.54	1.32	23
PNNL-1	4.29	1.48	0.08	10.8	2.87	0.31	0.803	0.056	0.027	0.365	8.49	1.54	1.32	23.6
PNNL-2	4.12	1.46	0.086	10.8	2.79	0.304	0.797	0.047	0.025	0.359	8.29	1.58	1.37	23.9
PNNL-2	4.1	1.45	0.077	10.8	2.79	0.303	0.793	0.049	0.026	0.36	8.18	1.54	1.33	23.4
PNNL-2	4.17	1.5	0.082	10.5	2.81	0.292	0.777	0.045	0.027	0.353	8.14	1.56	1.35	24.5
PNNL-2	4.21	1.5	0.083	11	2.84	0.318	0.817	0.046	0.025	0.365	8.45	1.58	1.35	23.7
PNNL-2	4.25	1.52	0.082	11.1	2.89	0.309	0.812	0.06	0.027	0.367	8.39	1.53	1.31	23
PNNL-2	4.18	1.48	0.097	10.8	2.84	0.305	0.803	0.046	0.028	0.363	8.45	1.54	1.33	23.5
PNNL-2	4.21	1.48	0.085	10.8	2.87	0.303	0.807	0.044	0.027	0.363	8.29	1.56	1.34	23.8
PNNL-2	4.18	1.48	0.08	10.9	2.87	0.303	0.8	0.044	0.027	0.359	8.43	1.52	1.3	23.8
SRTC-1	4.28	1.51	0.09	10.5	2.89	0.299	0.829	0.043	0.029	0.375	8.54	1.59	1.39	24.3
SRTC-1	4.16	1.46	0.111	10.3	2.81	0.301	0.801	0.045	0.03	0.367	8.19	1.53	1.34	23.6
SRTC-1	4.32	1.6	0.08	10.6	2.9	0.3	0.824	0.042	0.028	0.371	8.51	1.54	1.35	23.6
SRTC-1	4.34	1.53	0.079	10.7	2.93	0.304	0.837	0.046	0.03	0.379	8.54	1.56	1.36	23.5
SRTC-1	4.23	1.48	0.079	10.5	2.84	0.301	0.821	0.044	0.028	0.371	8.43	1.55	1.35	24
SRTC-1	4.23	1.48	0.08	10.3	2.86	0.297	0.806	0.042	0.027	0.369	8.28	1.56	1.36	24
SRTC-1	4.23	1.48	0.078	10.3	2.86	0.291	0.807	0.041	0.023	0.367	8.22	1.56	1.35	23.6
SRTC-1	4.26	1.49	0.077	10.3	2.93	0.293	0.803	0.043	0.027	0.368	8.57	1.55	1.37	23.8
SRTC-2	4.25	1.48	0.09	10.2	2.94	0.3	0.801	0.041	0.03	0.365	8.57	1.56	1.37	23.9
SRTC-2	4.19	1.48	0.077	10.5	2.83	0.313	0.814	0.043	0.03	0.37	8.27	1.57	1.34	23.4
SRTC-2	4.27	1.48	0.089	10.3	2.89	0.308	0.807	0.043	0.029	0.369	8.24	1.54	1.37	23.8
SRTC-2	4.32	1.51	0.129	10.6	2.95	0.313	0.828	0.043	0.027	0.376	8.39	1.59	1.36	24.3
SRTC-2	4.32	1.49	0.089	10.4	2.87	0.314	0.828	0.043	0.03	0.373	8.5	1.49	1.32	23.1
SRTC-2	4.06	1.43	0.076	10.1	2.76	0.301	0.783	0.042	0.031	0.359	8.03	1.5	1.34	23.7
SRTC-2	4.26	1.5	0.104	10.4	2.87	0.313	0.822	0.044	0.027	0.37	8.59	1.53	1.34	23.5
SRTC-2	4.32	1.54	0.09	10.5	2.9	0.314	0.83	0.079	0.023	0.371	8.69	1.53	1.36	23.8

* Standard glasses were run (and the data are available upon request) but are not shown because these data are only for glass to glass comparison purposes.

Table XXVI. Measured Composition Results for the SG13 Glasses Produced for the SG1 Study*

Sample ID	Al	Ca	Cr	Fe	K	Mg	Mn	Na	Ni	Ru	Si	Ti	B	Li
PNNL-1	1.29	0.134	0.196	5.91	1.41	0.26	2.16	4.43	1.56	0.06	27.2	0.085	3.1386	2.7632
PNNL-1	1.23	0.121	0.201	5	1.26	0.26	2.16	4.25	1.59	0.0572	27.5	0.086	2.9567	2.6711
PNNL-1	1.26	0.12	0.21	6.01	1.33	0.264	2.2	4.42	1.59	0.0556	27.6	0.0891	3.1488	2.7929
PNNL-1	1.26	0.133	0.195	5.94	1.29	0.265	2.23	4.31	1.59	0.0578	27.5	0.0937	3.0299	2.7444
PNNL-1	1.23	0.154	0.202	5.91	1.29	0.258	2.15	4.29	1.59	0.0575	27	0.0898	3.0066	2.7161
PNNL-1	1.36	0.165	0.21	6.13	1.44	0.275	2.24	4.44	1.69	0.0539	27.7	0.0976	3.0748	2.71
PNNL-1	1.25	0.158	0.202	5.98	1.3	0.269	2.24	5.03	1.6	0.0587	27.4	0.112	2.9009	2.7099
PNNL-1	1.33	0.169	0.193	5.94	1.29	0.264	2.18	4.48	1.58	0.057	27.3	0.0877	3.0983	2.7309
PNNL-2	1.25	0.133	0.201	6	1.27	0.268	2.24	4.28	1.57	0.058	27.3	0.0881	2.8917	2.6436
PNNL-2	1.24	0.191	0.202	6.1	1.28	0.271	2.19	4.42	1.6	0.0588	27.5	0.0945	3.0907	2.702
PNNL-2	1.27	0.147	0.206	6.01	1.32	0.286	2.2	4.38	1.58	0.0582	27.4	0.122	2.9238	2.645
PNNL-2	1.25	0.151	0.208	6.1	1.38	0.265	2.18	4.57	1.56	0.0586	27.3	0.118	3.0315	2.7499
PNNL-2	1.25	0.122	0.208	6	1.28	0.276	2.23	4.35	1.59	0.0597	27.4	0.0913	3.468	3.0785
PNNL-2	1.26	0.17	0.202	6.06	1.32	0.293	2.19	4.5	1.6	0.0587	27.6	0.131	3.0549	2.685
PNNL-2	1.25	0.183	0.201	6.09	1.31	0.283	2.19	4.56	1.58	0.0585	27.1	0.13	3.065	2.6576
PNNL-2	1.27	0.17	0.191	6.11	1.3	0.283	2.2	4.37	1.57	0.0556	27.4	0.114	2.9429	2.6124
SRTC-1	1.25	0.123	0.198	6.03	1.3	0.282	2.22	4.38	1.61	0.0606	27.6	0.0883	3.0347	2.732
SRTC-1	1.3	0.164	0.195	5.92	1.43	0.286	2.21	4.48	1.58	0.0593	27.7	0.103	3.0074	2.6929
SRTC-1	1.28	0.114	0.194	5.94	1.34	0.283	2.23	4.33	1.61	0.058	27.8	0.0914	3.5609	3.3319
SRTC-1	1.24	0.134	0.2	5.88	1.28	0.27	2.2	4.43	1.57	0.0568	27.3	0.0914	3.1544	2.8058
SRTC-1	1.25	0.21	0.202	5.91	1.32	0.276	2.19	4.34	1.61	0.0597	27.5	0.0923	3.1442	2.8014
SRTC-1	1.26	0.146	0.189	5.93	1.32	0.284	2.24	4.4	1.59	0.056	27.8	0.092	2.9227	2.7274
SRTC-1	1.24	0.117	0.196	5.82	1.27	0.276	2.2	4.33	1.59	0.0579	27.3	0.0945	3.0221	2.7271
SRTC-1	1.25	0.168	0.189	6.04	1.32	0.273	2.23	4.4	1.59	0.057	27.6	0.0906	2.9889	2.7012
SRTC-2	1.24	0.117	0.2	5.9	1.27	0.27	2.23	4.34	1.58	0.0587	27.3	0.0874	3.0906	2.7751
SRTC-2	1.3	0.141	0.212	5.95	1.36	0.275	2.21	4.61	1.61	0.0561	27.8	0.114	2.9914	2.7556
SRTC-2	1.28	0.135	0.196	6.05	1.32	0.272	2.22	4.56	1.58	0.0596	27.9	0.0936	3.0663	2.7532
SRTC-2	1.26	0.142	0.194	5.93	1.3	0.271	2.22	4.59	1.6	0.058	27.5	0.0957	2.9193	2.7474
SRTC-2	1.27	0.146	0.19	6.04	1.32	0.275	2.26	4.38	1.63	0.0567	27.9	0.0909	2.968	2.6978
SRTC-2	1.24	0.145	0.194	5.8	1.37	0.27	2.23	4.81	1.58	0.0576	27.4	0.104	3.5358	3.2138
SRTC-2	1.25	0.132	0.339	5.82	1.26	0.273	2.21	4.41	1.58	0.0576	27.1	0.101	3.2788	2.9029
SRTC-2	1.25	0.118	0.198	5.93	1.28	0.269	2.22	4.29	1.59	0.0584	27.2	0.0875	2.9558	2.7091

* Standard glasses were run (and the data are available upon request) but are not shown because these data are only for glass to glass comparison purposes.

Table XXVII. Initial MgO Study Glass Compositions in wt% to Examine the Effect of MgO on Crystallization

	WCP HM				**WCP PUREX**				**WCP BLEND**				**DWPF Startup Frit**			
Frit used	Frit 202				Frit 200				Frit 202				n/a			
Type	Target	Meas.	Target	Meas.	Target	Meas.	Target	Meas.	Target	Meas.	Target	Meas.	Target	Meas.	Target	Meas.
Al_2O_3	7.15	6.67	7.15	6.92	2.99	2.97	2.99	2.99	4.16	4.01	4.16	4.04	4.6	4.35	4.6	4.4
B_2O_3	7.03	7.05	7.145	6.99	10.33	10.13	10.790	10.79	8.05	8.02	8.353	7.68	8.51	8.63	8.731	8.13
BaO	0.11	0.09	0.11	0.07	0.2	0.17	0.2	0.2	0.18	0.15	0.18	0.15	0.1	0.04	0.1	0.06
CaO	1.01	0.98	1.01	0.99	1.09	1.07	1.09	1.09	1.03	1.01	1.03	1.01	1.47	1.43	1.47	1.49
Cr_2O_3	0.091	0.08	0.091	0.09	0.15	0.14	0.15	0.15	0.13	0.11	0.13	0.13	0.09	0.09	0.09	0.09
Cs_2O	0.06	--	0.06	--	0.06	--	0.06	--	0.08	--	0.08	--	0	--	0	--
CuO	0.25	0.25	0.25	0.24	0.42	0.4	0.42	0.42	0.44	0.42	0.44	0.43	0	0.01	0	0
Fe_2O_3	7.78	7.73	7.78	7.71	13.25	13.2	13.25	13.25	10.91	10.75	10.91	10.77	14.2	13.86	14.2	13.93
K_2O	2.21	2.42	2.21	2.36	3.41	3.63	3.41	3.41	3.68	3.9	3.68	3.91	2.7	2.89	2.7	2.89
Li_2O	4.62	4.66	4.62	4.62	3.22	3.16	3.22	3.22	4.44	4.48	4.44	4.35	3.25	3.23	3.25	3.25
MgO	1.49	1.47	0.0	0.01	1.41	1.37	0.0	0	1.41	1.39	0.0	0.01	0.84	0.81	0.0	0.01
MnO	1.75	1.74	1.75	1.76	1.69	1.68	1.69	1.69	1.67	1.65	1.67	1.67	1.93	1.85	1.93	1.9
MoO_3	0.22	0.18	0.22	0.18	0.08	0.06	0.08	0.08	0.15	0.12	0.15	0.1	0	0	0	0
Na_2O	8.56	8.44	8.905	8.75	12.62	12.44	12.864	12.86	9.13	8.73	9.410	8.98	11.53	11.09	11.688	10.91
Nd_2O_3	0.55	0.52	0.55	0.45	0.06	0.07	0.06	0.06	0.22	0.3	0.22	0.17	0	0.08	0	0.02
NiO	0.41	0.4	0.41	0.4	1.19	1.15	1.19	1.19	0.89	0.85	0.89	0.87	1.11	1.01	1.11	1.08
RuO_2	0.042	0.02	0.042	0.02	0.014	0.03	0.014	--	0.032	0.02	0.032	0.02	0	0.02	0	0.02
SiO_2	55.8	53.86	56.831	55.73	46.5	45.83	47.207	47.21	51.9	50.43	52.727	51.5	47.9	46.26	48.362	47.33
TiO_2	0.56	0.55	0.56	0.54	0.68	0.65	0.68	0.68	0.89	0.87	0.89	0.87	1.18	1.12	1.18	1.15
ZrO_2	0.33	0.35	0.33	0.31	0.045	0.06	0.045	0.05	0.14	0.18	0.14	0.14	0.11	0.18	0.11	0.13

15. APPENDIX: ANCILLARY LEAST-SQUARES RESULTS

Exhibit 1. Results of the JMP® Regression Analysis of $(1/T_L)$ versus f(composition) for the 50 SG Study Data. The dotted lines represent the 95% confidence curves about the fitted line.

Response 1/INT LIQ (K)
Whole Model
Actual by Predicted Plot

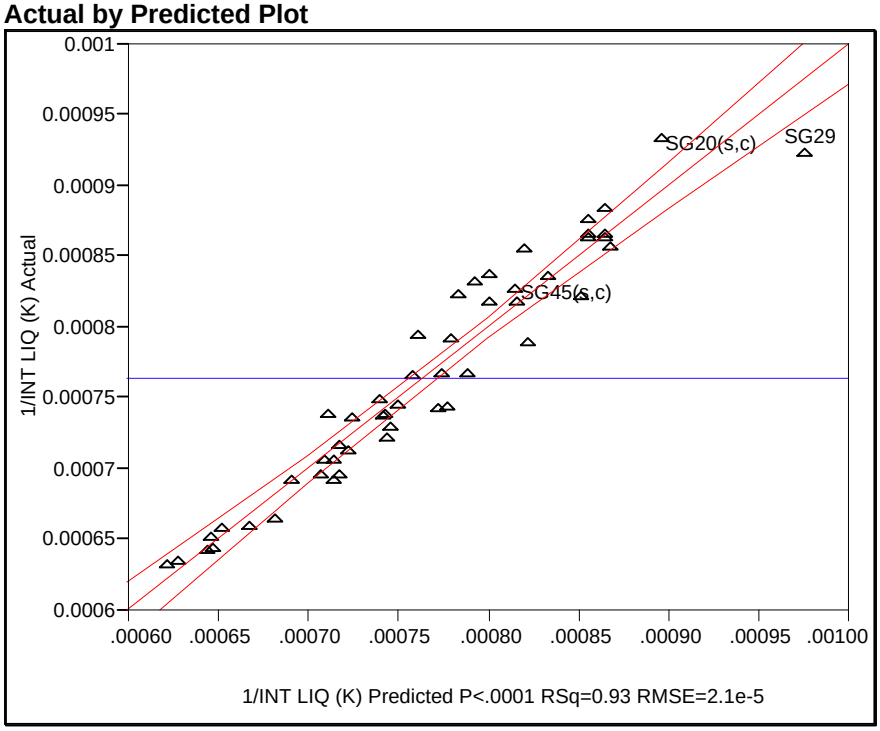

Summary of Fit

RSquare	0.9345847095
RSquare Adj	0.9303184949
Root Mean Square Error	0.000021271
Mean of Response	0.0007648561
Observations (or Sum Wgts)	50

Analysis of Variance

Source	DF	Sum of Squares	Mean Square	F Ratio
Model	3	2.97354e-7	9.9118e-8	219.0665
Error	46	2.0813e-8	4.525e-10	Prob > F
C. Total	49	3.18167e-7		<.0001

Lack Of Fit

Source	DF	Sum of Squares	Mean Square	F Ratio
Lack Of Fit	42	2.04543e-8	4.87e-10	5.4308
Pure Error	4	3.587e-10	8.967e-11	Prob > F
Total Error	46	2.0813e-8		0.0546
				Max RSq
				0.9989

Parameter Estimates

Term	Estimate	Std Error	t Ratio	Prob>|t|
Intercept	-0.0015001	0.000131	-11.46	<.0001
ln[SM2/D]	-0.00026	0.000037	-7.07	<.0001
ln[SM1/D]	-0.0005871	0.000027	-21.40	<.0001
ln[SMT/D]	-0.0001492	0.000015	-10.13	<.0001

Effect Tests

Source	Nparm	DF	Sum of Squares	F Ratio	Prob > F
ln[SM2/D]	1	1	2.26411e-8	50.0403	<.0001
ln[SM1/D]	1	1	2.07235e-7	458.0230	<.0001
ln[SMT/D]	1	1	4.64136e-8	102.5814	<.0001

Residual by Predicted Plot

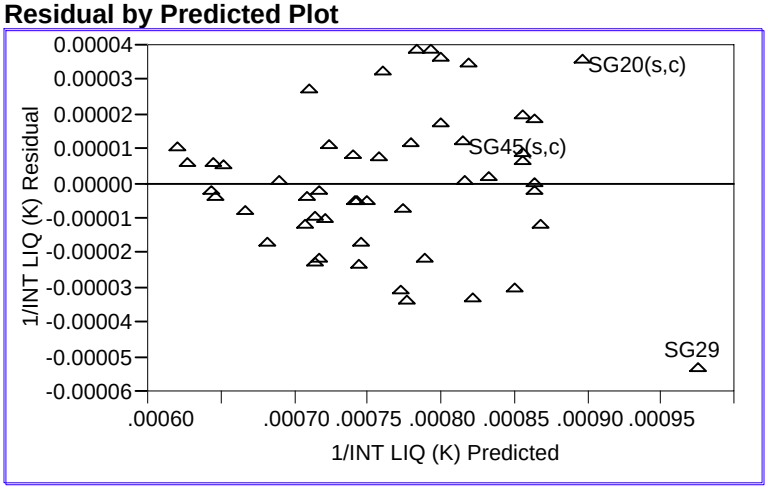

Exhibit 2. Results of the JMP® Regression Analysis of $(1/T_L)$ versus f(composition) for Model Data. The dotted lines represent the 95% confidence curves about the fitted line.

Response 1/INT LIQ (K)
Whole Model
Actual by Predicted Plot

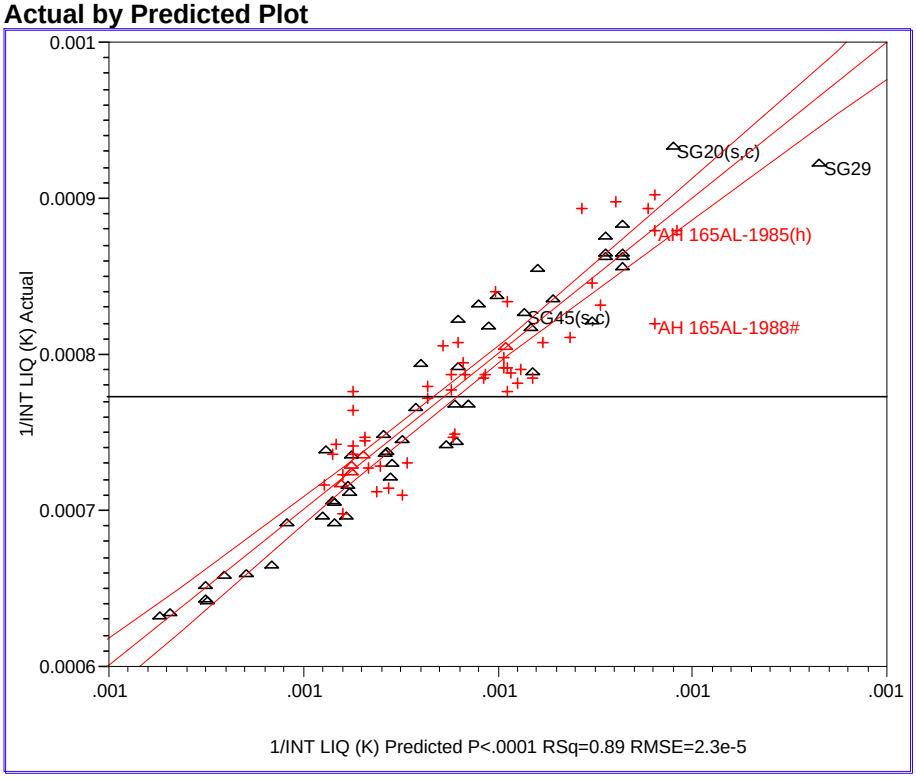

Summary of Fit

RSquare	0.89080782
RSquare Adj	0.88756449
Root Mean Square Error	0.00002278
Mean of Response	0.00077367
Observations (or Sum Wgts)	105

Analysis of Variance

Source	DF	Sum of Squares	Mean Square	F Ratio
Model	3	4.27412e-7	1.4247e-7	274.6582
Error	101	5.23907e-8	5.187e-10	Prob > F
C. Total	104	4.79803e-7		<.0001

Lack Of Fit

Source	DF	Sum of Squares	Mean Square	F Ratio
Lack Of Fit	84	4.59434e-8	5.469e-10	1.4422
Pure Error	17	6.44732e-9	3.793e-10	Prob > F
Total Error	101	5.23907e-8		0.1991
				Max RSq
				0.9866

Parameter Estimates

Term	Estimate	Std Error	t Ratio	Prob>|t|
Intercept	-0.001442	0.000108	-13.38	<.0001
ln[SM2/D]	-0.00026	0.000027	-9.76	<.0001
ln[SM1/D]	-0.000566	0.000023	-24.62	<.0001
ln[SMT/D]	-0.000153	0.000011	-14.43	<.0001

Effect Tests

Source	Nparm	DF	Sum of Squares	F Ratio	Prob > F
ln[SM2/D]	1	1	4.94018e-8	95.2379	<.0001
ln[SM1/D]	1	1	3.14343e-7	605.9982	<.0001
ln[SMT/D]	1	1	1.0802e-7	208.2437	<.0001

Residual by Predicted Plot

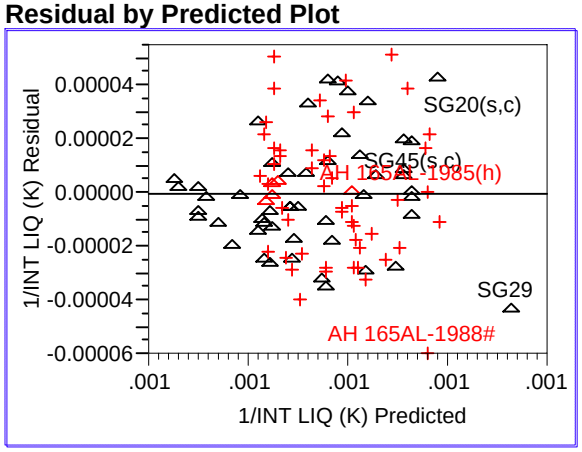

Exhibit 3. Pair-wise Correlations and Scatterplot Matrix for the Model Data Mass Oxide Compositions (These concentrations were normalized over the 13 oxides shown.)

Multivariate Correlations

	Al_2O_3	CaO	Cr_2O_3	Fe_2O_3	K_2O	Li_2O	MgO	MnO	Na_2O	NiO	SiO_2	TiO_2	ZrO_2
Al_2O_3	1.000	-0.196	-0.091	-0.736	-0.021	-0.006	0.086	0.350	0.079	-0.452	-0.151	0.001	-0.001
CaO	-0.196	1.000	0.118	0.206	0.114	-0.082	0.030	-0.216	-0.170	0.213	-0.129	-0.114	-0.073
Cr_2O_3	-0.091	0.118	1.000	-0.034	0.301	0.424	0.255	0.096	-0.133	-0.272	-0.017	-0.225	-0.538
Fe_2O_3	-0.736	0.206	-0.034	1.000	-0.030	-0.133	-0.163	-0.402	-0.063	0.397	-0.385	0.028	0.046
K_2O	-0.021	0.114	0.301	-0.030	1.000	-0.096	0.387	0.028	-0.448	-0.085	-0.190	0.585	-0.827
Li_2O	-0.006	-0.082	0.424	-0.133	-0.096	1.000	-0.061	0.067	-0.121	-0.154	0.049	-0.328	-0.040
MgO	0.086	0.030	0.255	-0.163	0.387	-0.061	1.000	-0.049	-0.208	-0.117	-0.060	0.040	-0.416
MnO	0.350	-0.216	0.096	-0.402	0.028	0.067	-0.049	1.000	-0.028	-0.556	0.063	-0.012	-0.087
Na_2O	0.079	-0.170	-0.133	-0.063	-0.448	-0.121	-0.208	-0.028	1.000	-0.038	-0.312	-0.179	0.341
NiO	-0.452	0.213	-0.272	0.397	-0.085	-0.154	-0.117	-0.556	-0.038	1.000	-0.069	0.029	0.222
SiO_2	-0.151	-0.129	-0.017	-0.385	-0.190	0.049	-0.060	0.063	-0.312	-0.069	1.000	-0.184	0.189
TiO_2	0.001	-0.114	-0.225	0.028	0.585	-0.328	0.040	-0.012	-0.179	0.029	-0.184	1.000	-0.537
ZrO_2	-0.001	-0.073	-0.538	0.046	-0.827	-0.040	-0.416	-0.087	0.341	0.222	0.189	-0.537	1.000

Scatterplot Matrix

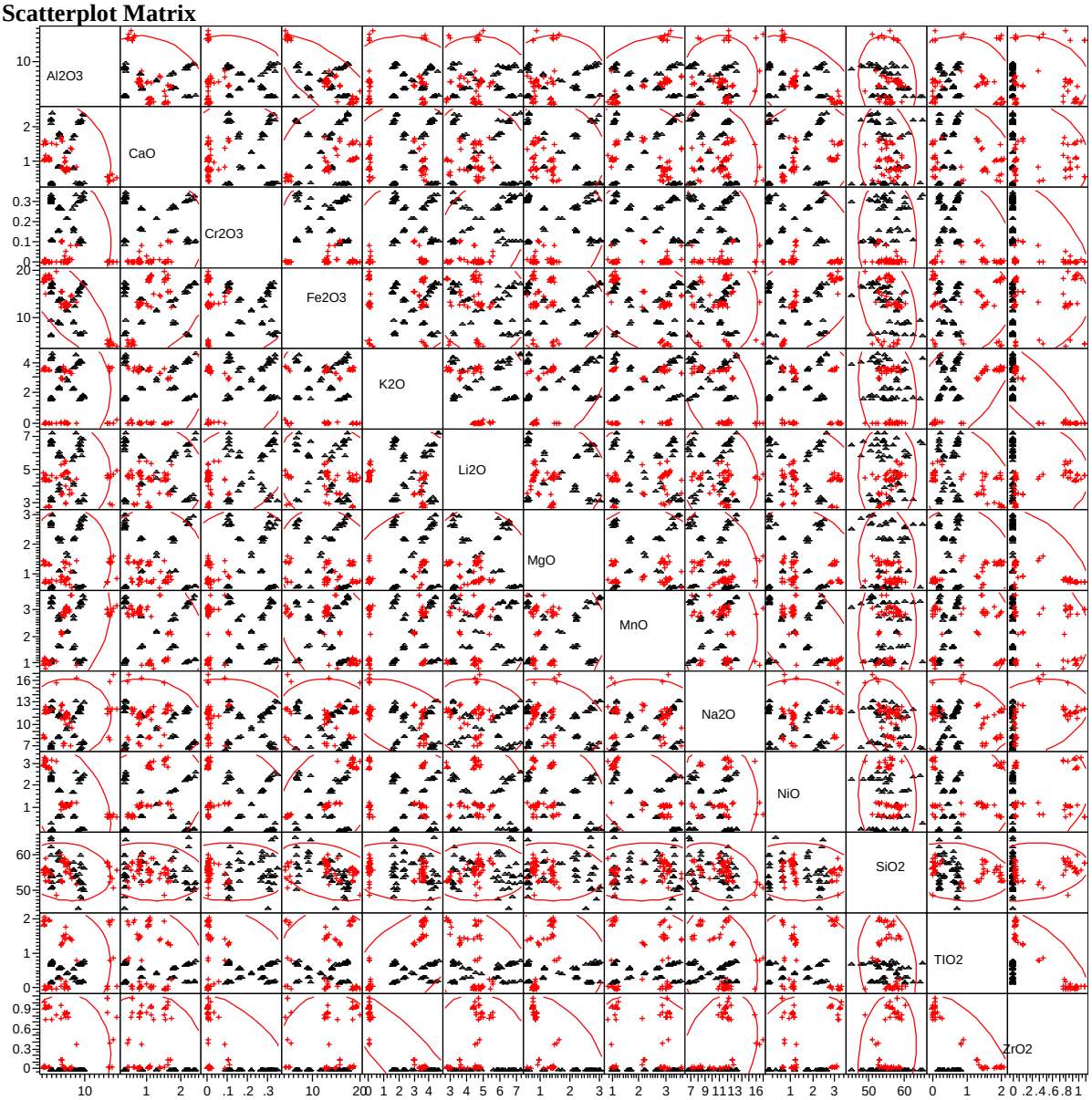

Exhibit 4. Summary of the Pyroxene Precursor Terms Used to Describe DWPF Liquidus Temperature

Model Data Correlations

	M_2	M_1	M_T
M_2	1.0000	0.4788	0.2427
M_1	0.4788	1.0000	0.6085
M_T	0.2427	0.6085	1.0000

Scatterplot Matrix

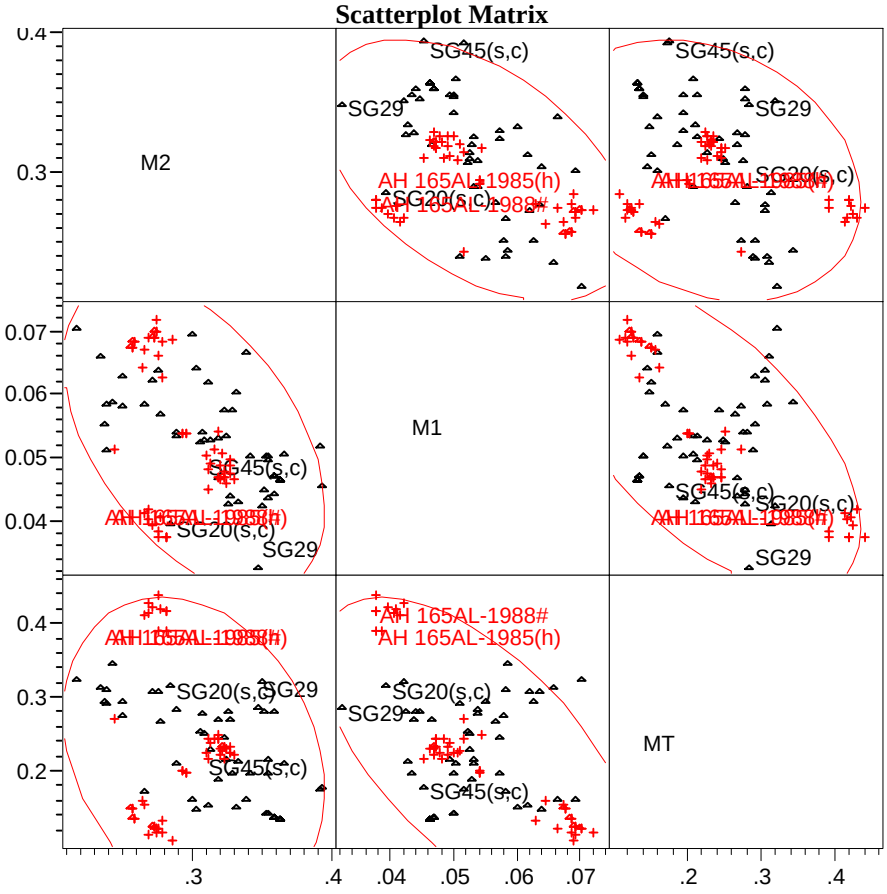

Exhibit 5. JMP® Results of the Least-Squares Fit of T_L(°C) versus 14 Normalized Mass Oxide Concentrations for the Model Data. (Note the ZrO2 concentration was excluded because 1) it was not included in the corresponding PNNL model and 2) it makes the resulting fit worse.) The dotted lines represent the 95% confidence curves about the individuals.

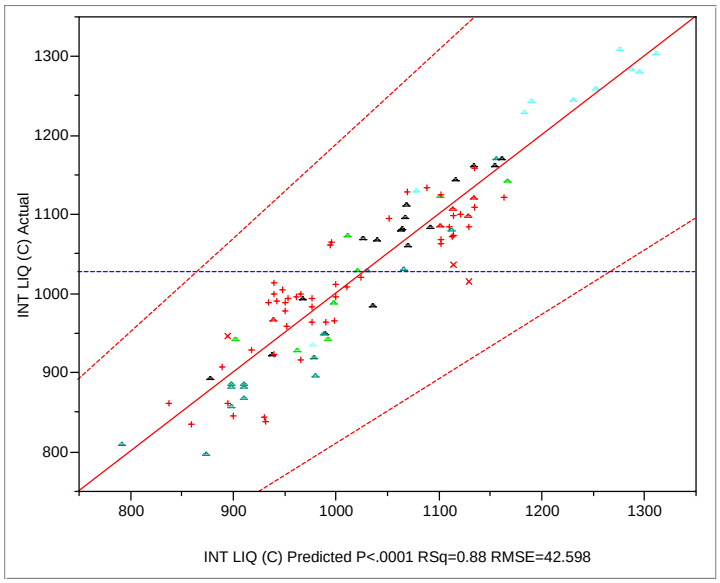

Summary of Fit

RSquare	0.880162
RSquare Adj	0.863042
Root Mean Square Error	42.59815
Mean of Response	1029.49
Observations (or Sum Wgts)	105

Analysis of Variance

Source	DF	Sum of Squares	Mean Square	F Ratio
Model	13	1212805.7	93292.7	51.4122
Error	91	165128.8	1814.6	Prob > F
C. Total	104	1377934.5		<.0001

Lack Of Fit

Source	DF	Sum of Squares	Mean Square	F Ratio
Lack Of Fit	74	148551.96	2007.46	2.0587
Pure Error	17	16576.83	975.11	Prob > F
Total Error	91	165128.80		0.0480
				Max RSq
				0.9880

Parameter Estimates

Term		Estimate	Std Error	t Ratio	Prob>|t|
Intercept	Zeroed	0	0	.	.
Al_2O_3		2646.702	169.7694	15.59	<.0001
B_2O_3		693.06207	196.9945	3.52	0.0007
CaO		1570.6161	834.6867	1.88	0.0631
Cr_2O_3		38552.43	5273.279	7.31	<.0001
Fe_2O_3		2798.6968	136.7714	20.46	<.0001
K_2O		-368.2044	529.9398	-0.69	0.4889
Li_2O		-1771.173	432.5635	-4.09	<.0001
MgO		3756.2064	720.1009	5.22	<.0001
MnO		1598.3022	624.1858	2.56	0.0121
Na_2O		-1447.964	220.5708	-6.56	<.0001
NiO		8578.4431	596.0225	14.39	<.0001
SiO_2		878.03312	70.92438	12.38	<.0001
TiO_2		737.75602	1146.202	0.64	0.5214
U_3O_8		1640.9942	312.5166	5.25	<.0001

Exhibit 6. JMP® Regression Results for $1/T_L(K)$ using the Model in Equation 16 versus other pertinent data: (a) WVNS, (b) PNNL SP, (c) PNNL SP-3, (d) PNNL SPx4, (e) PNNL SP-MC, (f) PNNL MS, (g) PNNL MISC, (h) PNNL US, (i) PNNL CVS-I and (j) PNNL CVS-II. All such data are provided in (k). The omitted SRTC data and the SG Study glasses exhibiting clinopyroxene at T_L are provided in (l). The glasses with phases other than spinel have a designation of "ca", "zr", "c", "o", or "pl" for $CaSiO_4$, $ZrSiO_4$, pyroxene (or clinopyroxene), orthopyroxene, or Plates, respectively. The dotted lines represent the 95% confidence curves about the regression line for the model (gray) data.

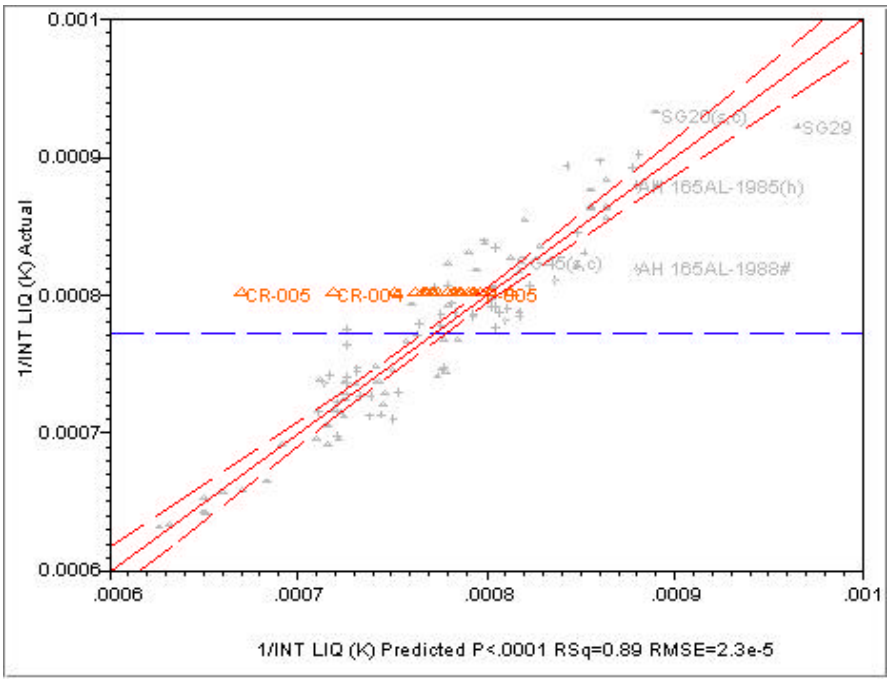

(a) WVNS (△)

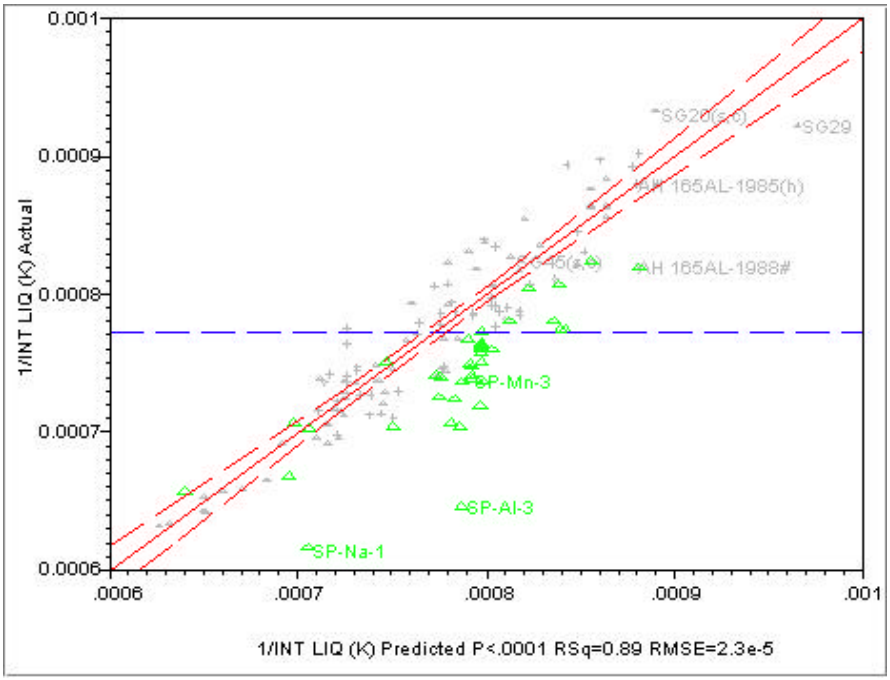

(b) PNNL SP (△)

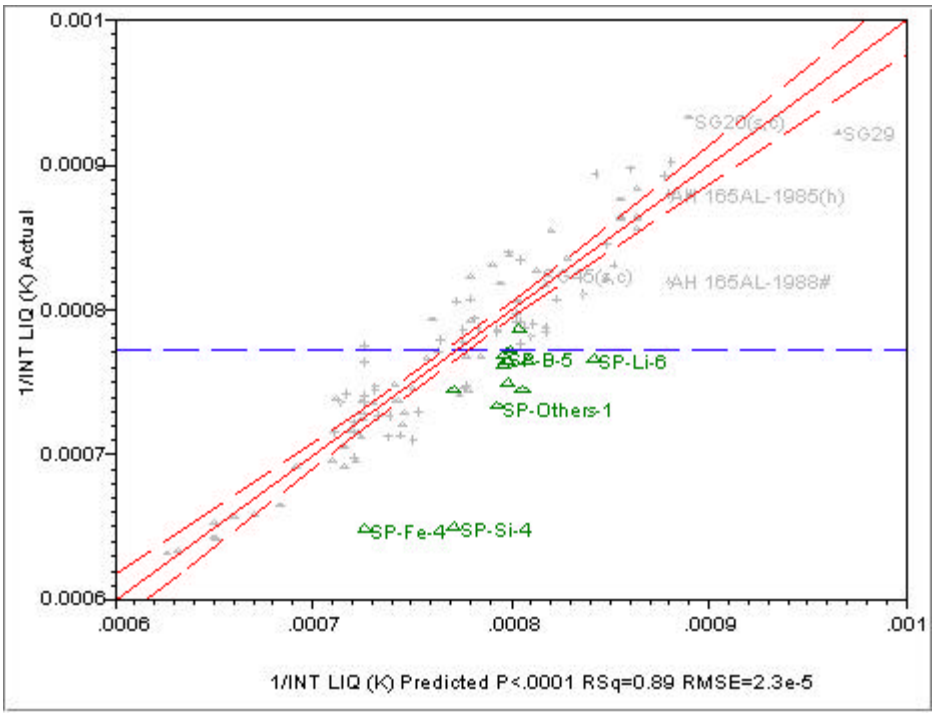

(c) PNNL SP-3 (△)

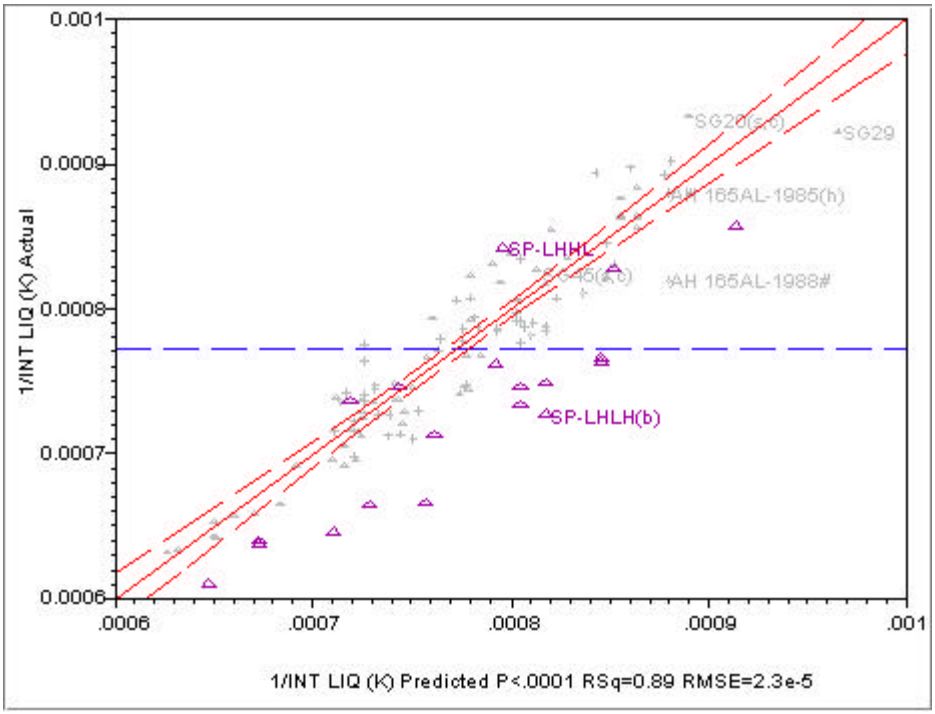

(d) PNNL SPx4 (△)

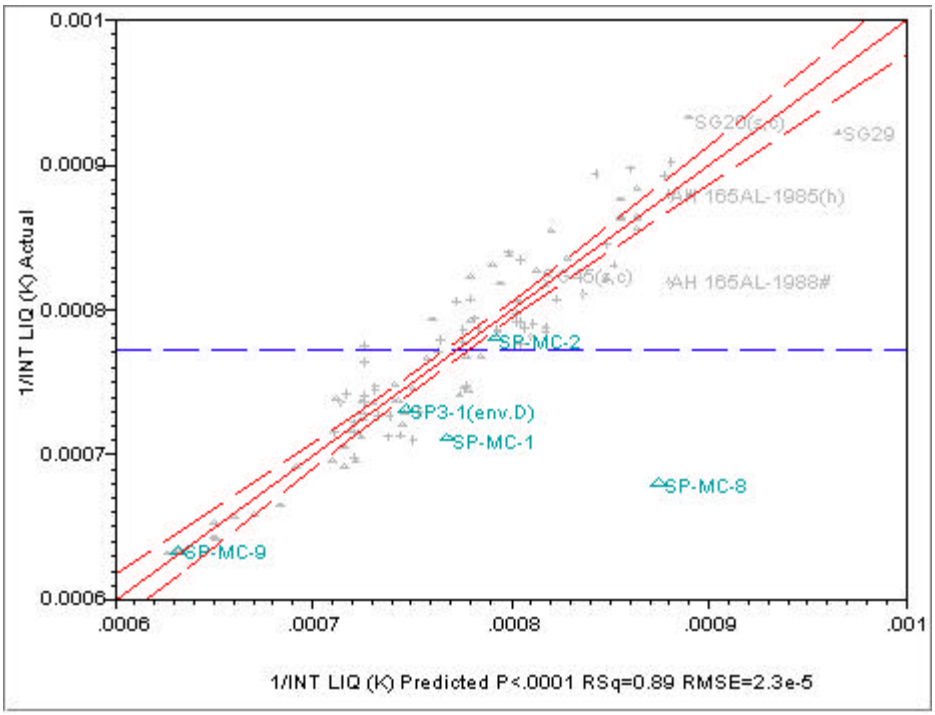

(e) PNNL SP-MC (△)

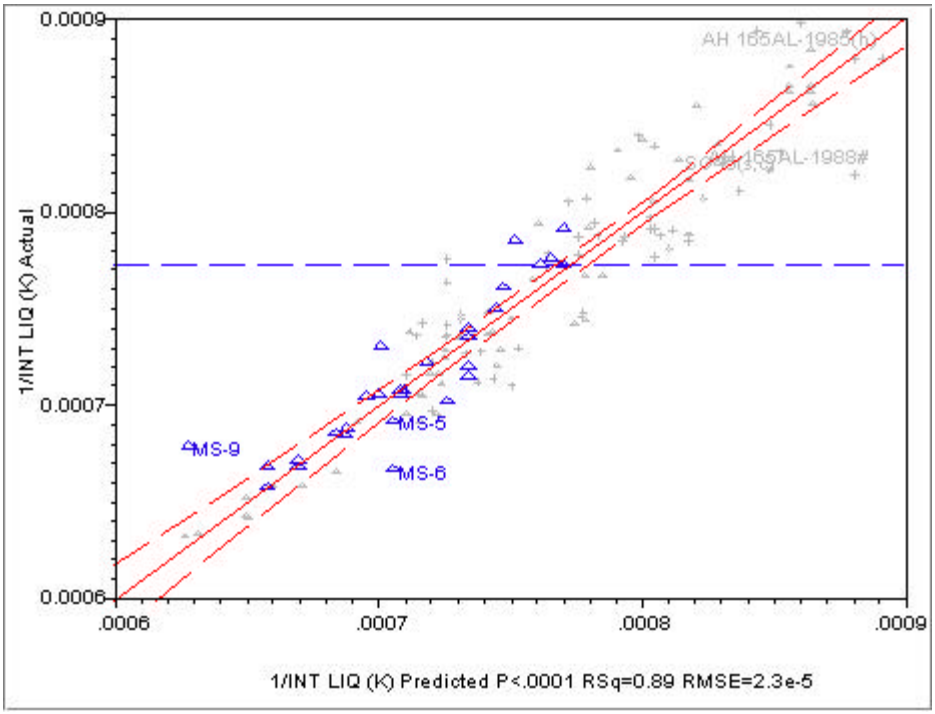

(f) PNNL MS (△)

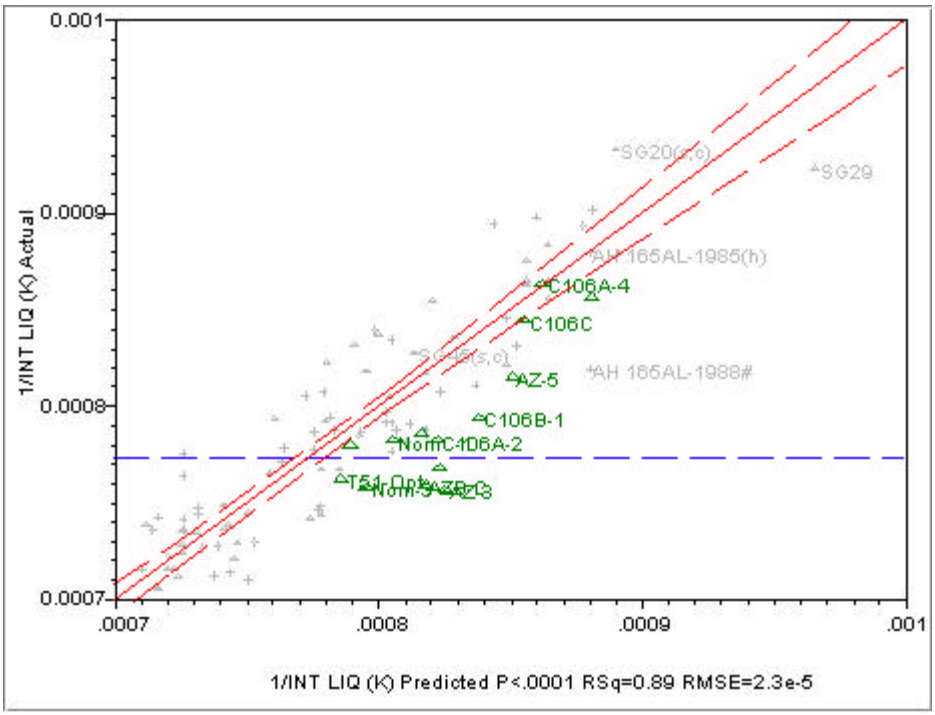

(g) PNNL MISC (△)

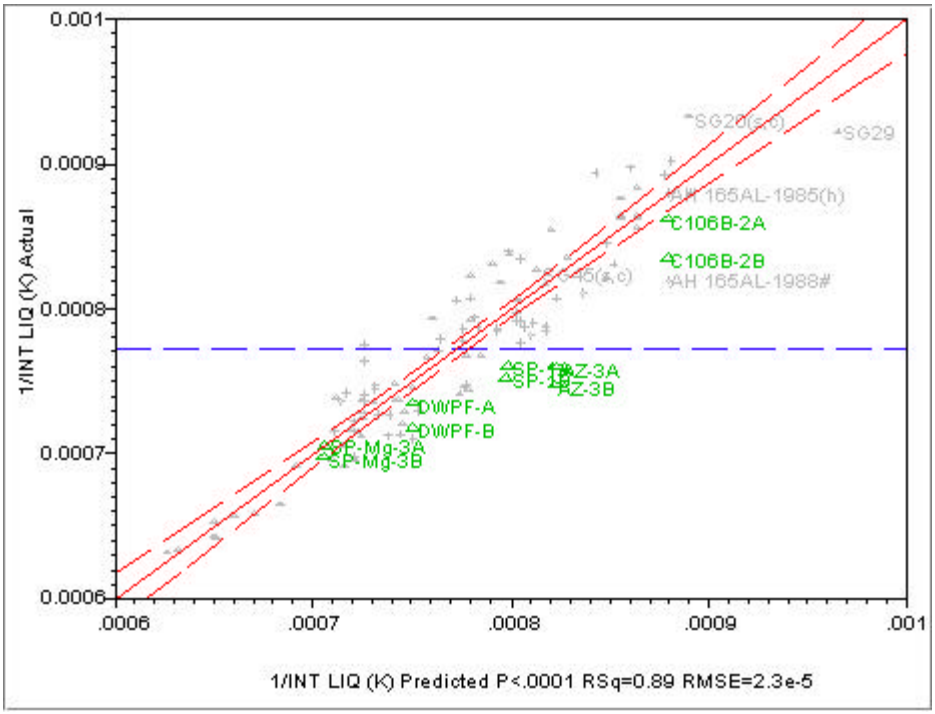

(h) PNNL US (△)

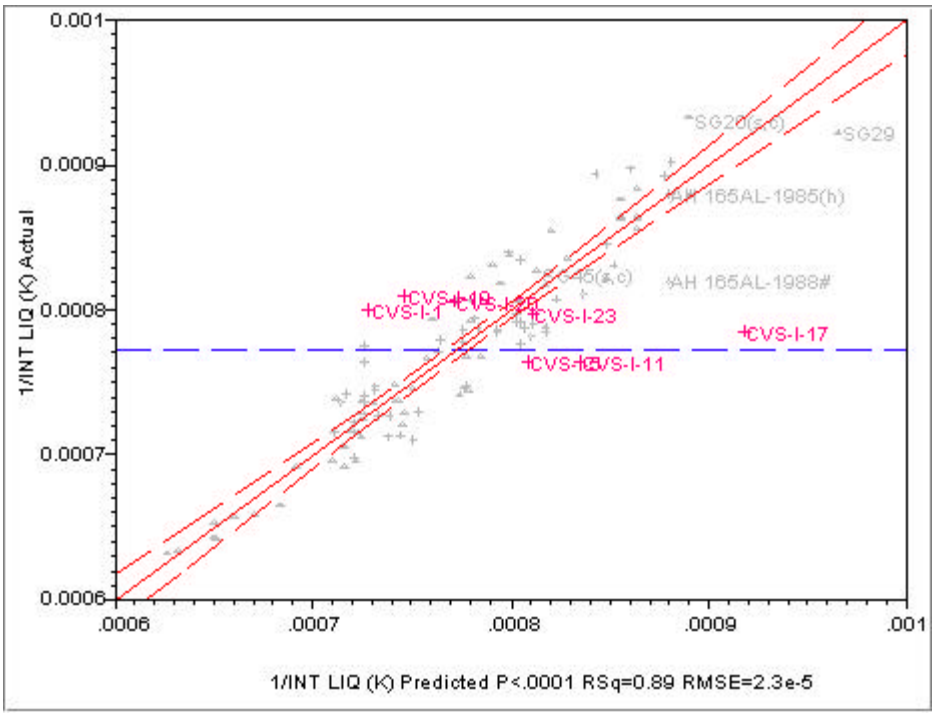

(i) PNNL CVS-I (+)

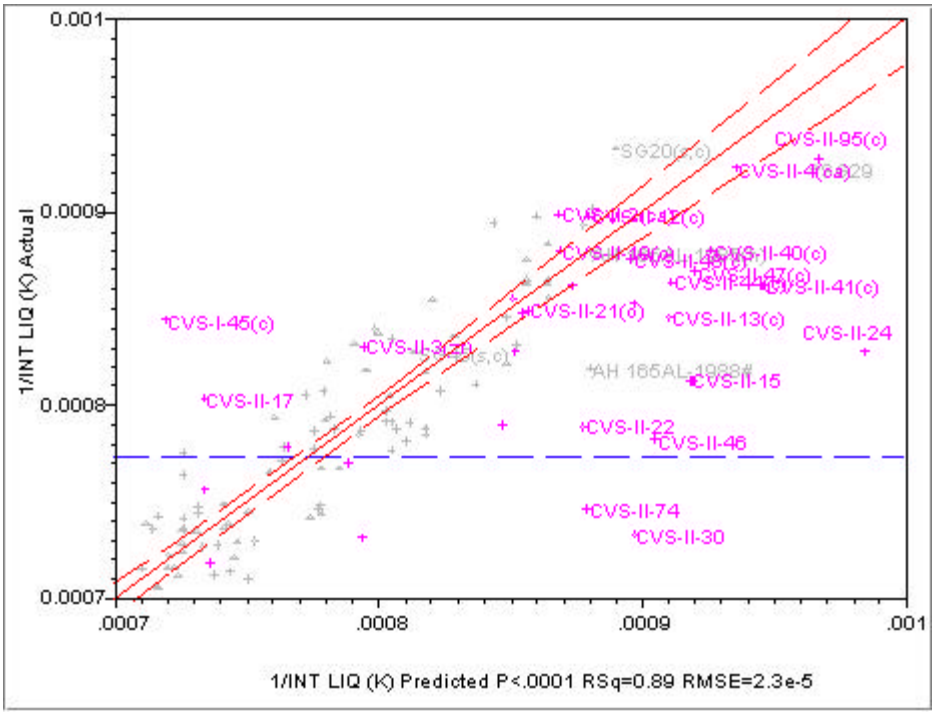

(j) PNNL CVS-II (+)

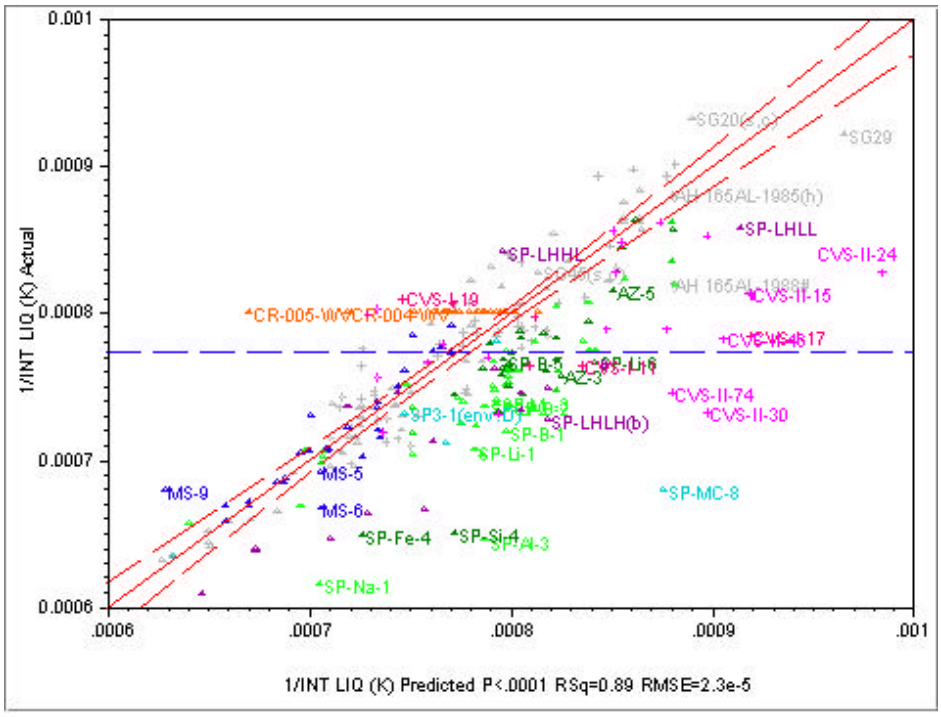

(k) All WVNS and PNNL Spinel Data

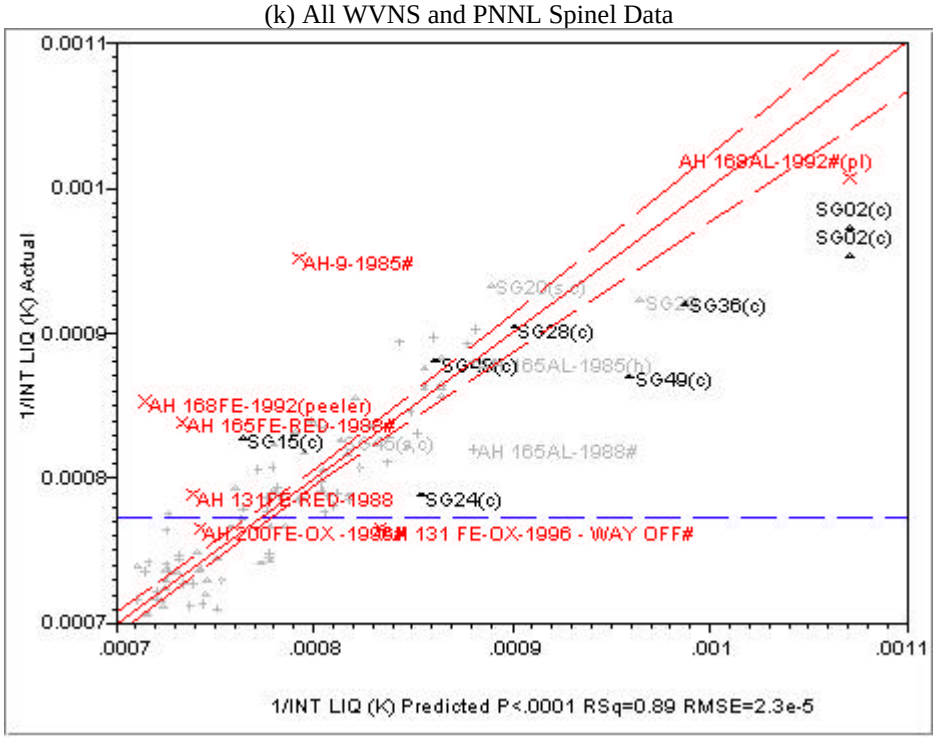

(l) Omitted SRTC (×) Data and SG Study Data (▲) Exhibiting Clinopyroxene at T_L

16. APPENDIX: MEASUREMENT VARIANCE ESTIMATION

The relationship between liquidus temperature and composition is related via Equation 17:

$$\left(\frac{1}{T_L}\right)_{pred} \approx \ln\left\{(M_2)^{a'}(M_1)^{b'}(M_T)^{c'}\right\} + d$$

where the terms representing the melt phase complexes are given by:

$$M_2 \equiv \frac{\Sigma_{M2}}{\Sigma}, \quad M_1 \equiv \frac{\Sigma_{M1}}{\Sigma}, \text{and} \quad M_T \equiv \frac{\Sigma_{MT}}{\Sigma}$$

where

$$\Sigma \equiv \Sigma_{M2} + \Sigma_{M1} + \Sigma_{MT} + \Sigma_{N1} + \Sigma_{T1}$$

and

$$\Sigma_{M2} \equiv \phi_{M2,NiO} z_{NiO} + \phi_{M2,MgO} z_{MgO} + \phi_{M2,MnO} z_{MnO} + \phi_{M2,CaO} z_{CaO} + \phi_{M2,K_2O} z_{K_2O} + \phi_{M2,Li_2O} z_{Li_2O} + \phi_{M2,Na_2O} z_{Na_2O}$$

$$\Sigma_{M1} \equiv \phi_{M1,Al_2O_3} z_{Al_2O_3} + \phi_{M1,Fe_2O_3} z_{Fe_2O_3} + \phi_{M1,TiO_2} z_{TiO_2} + \phi_{M1,Cr_2O_3} z_{Cr_2O_3} + \phi_{M1,ZrO_2} z_{ZrO_2} + \phi_{M1,NiO} z_{NiO} + \phi_{M1,MgO} z_{MgO} + \phi_{M1,MnO} z_{MnO}$$

$$\Sigma_{MT} \equiv \phi_{T,SiO_2} z_{SiO_2} + \phi_{T,Al_2O_3} z_{Al_2O_3} + \phi_{T,Fe_2O_3} z_{Fe_2O_3}$$

$$\Sigma_{N1} \equiv \phi_{N1,K_2O} z_{K_2O} + \phi_{N1,Li_2O} z_{Li_2O} + \phi_{N1,Na_2O} z_{Na_2O}$$

$$\Sigma_{T1} \equiv \phi_{T1,SiO_2} z_{SiO_2} + \phi_{T1,Al_2O_3} z_{Al_2O_3} + \phi_{T1,Fe_2O_3} z_{Fe_2O_3} + \phi_{T1,TiO_2} z_{TiO_2}$$

The variance associated with composition measurement can be propagated through the liquidus temperature prediction using Equation 22:

$$V\left(\frac{1}{T_L}\right) \approx \sum_i \sum_j \left\{\left[\frac{\partial}{\partial[i]}\left(\frac{1}{T_L}\right)_{pred}\right](r_i[i])\left[\frac{\partial}{\partial[j]}\left(\frac{1}{T_L}\right)_{pred}\right](r_j[j])\rho_{i,j}\right\}$$

Then the partial derivatives of the expression can be computed and used to estimate the effect of measurement error on the liquidus temperature prediction. This will be demonstrated in the pages to follow. This information was developed using MathCad® 2000.

$$rTL_{pred}(z) = \ln\left[(M2(z))^{a}\cdot(M1(z))^{b}\cdot(MT(z))^{c}\right] + d$$

$$\Sigma M2(z) = A\cdot NiO + B\cdot MgO + C\cdot MnO + D\cdot CaO + E\cdot K2O + F\cdot Li2O + G\cdot Na2O$$

$$\Sigma M1(z) = H\cdot Al2O3 + I\cdot Fe2O3 + J\cdot TiO2 + K\cdot Cr2O3 + L\cdot ZrO2 + M\cdot NiO + N\cdot MgO + O\cdot MnO$$

$$\Sigma MT(z) = P\cdot SiO2 + Q\cdot Al2O3 + R\cdot Fe2O3$$

$$\Sigma N1(z) = S\cdot K2O + T\cdot Li2O + U\cdot Na2O$$

$$\Sigma T1(z) = V\cdot SiO2 + W\cdot Al2O3 + X\cdot Fe2O3 + Y\cdot TiO2$$

$$\Sigma(z) = \Sigma M2(z) + \Sigma M1(z) + \Sigma MT(z) + \Sigma T1(z) + \Sigma N1(z)$$

$$M2(z) = \frac{\Sigma M2(z)}{\Sigma(z)} \qquad M1(z) = \frac{\Sigma M1(z)}{\Sigma(z)} \qquad T(z) = \frac{\Sigma MT(z)}{\Sigma(z)}$$

$$\begin{aligned}\Sigma = {} & (A\cdot NiO + B\cdot MgO + C\cdot MnO + D\cdot CaO + E\cdot K2O + F\cdot Li2O + G\cdot Na2O) \ldots \\ & + (H\cdot Al2O3 + I\cdot Fe2O3 + J\cdot TiO2 + K\cdot Cr2O3 + L\cdot ZrO2 + M\cdot NiO + N\cdot MgO + O\cdot MnO) \ldots \\ & + (P\cdot SiO2 + Q\cdot Al2O3 + R\cdot Fe2O3) + (S\cdot K2O + T\cdot Li2O + U\cdot Na2O) \ldots \\ & + (V\cdot SiO2 + W\cdot Al2O3 + X\cdot Fe2O3 + Y\cdot TiO2)\end{aligned}$$

$$\begin{aligned}\Sigma = {} & (W + H + Q)\cdot Al2O3 + D\cdot CaO + K\cdot Cr2O3 + (X + I + R)\cdot Fe2O3 + (S + E)\cdot K2O + (F + T)\cdot Li2O \ldots \\ & + (N + B)\cdot MgO + (C + O)\cdot MnO + (U + G)\cdot Na2O + (A + M)\cdot NiO + (P + V)\cdot SiO2 \ldots \\ & + (Y + J)\cdot TiO2 + L\cdot ZrO2\end{aligned}$$

$$\begin{aligned}\Sigma = {} & AA\cdot Al2O3 + D\cdot CaO + K\cdot Cr2O3 + BB\cdot Fe2O3 + CC\cdot K2O + DD\cdot Li2O + EE\cdot MgO + FF\cdot MnO \ldots \\ & + GG\cdot Na2O + HH\cdot NiO + II\cdot SiO2 + JJ\cdot TiO2 + L\cdot ZrO2\end{aligned}$$

$$M2 = \frac{A\cdot NiO + B\cdot MgO + C\cdot MnO + D\cdot CaO + E\cdot K2O + F\cdot Li2O + G\cdot Na2O}{\begin{aligned}& AA\cdot Al2O3 + D\cdot CaO + K\cdot Cr2O3 + BB\cdot Fe2O3 + CC\cdot K2O + DD\cdot Li2O + EE\cdot MgO + FF\cdot MnO \ldots \\ & + GG\cdot Na2O + HH\cdot NiO + II\cdot SiO2 + JJ\cdot TiO2 + L\cdot ZrO2\end{aligned}}$$

$$M1 = \frac{H\cdot Al2O3 + I\cdot Fe2O3 + J\cdot TiO2 + K\cdot Cr2O3 + L\cdot ZrO2 + M\cdot NiO + N\cdot MgO + O\cdot MnO}{\begin{aligned}& AA\cdot Al2O3 + D\cdot CaO + K\cdot Cr2O3 + BB\cdot Fe2O3 + CC\cdot K2O + DD\cdot Li2O + EE\cdot MgO + FF\cdot MnO \ldots \\ & + GG\cdot Na2O + HH\cdot NiO + II\cdot SiO2 + JJ\cdot TiO2 + L\cdot ZrO2\end{aligned}}$$

$$MT = \frac{P\cdot SiO2 + Q\cdot Al2O3 + R\cdot Fe2O3}{\begin{aligned}& AA\cdot Al2O3 + D\cdot CaO + K\cdot Cr2O3 + BB\cdot Fe2O3 + CC\cdot K2O + DD\cdot Li2O + EE\cdot MgO + FF\cdot MnO \ldots \\ & + GG\cdot Na2O + HH\cdot NiO + II\cdot SiO2 + JJ\cdot TiO2 + L\cdot ZrO2\end{aligned}}$$

Separate the expression for T_L into linear terms:

$$rTL_{pred}(z) = \ln\left[(M2(z))^{a}\cdot(M1(z))^{b}\cdot(MT(z))^{c}\right] + d = a\cdot\ln(M2) + b\cdot\ln(M1) + c\cdot\ln(MT) + d$$

and take the partial derivatives on each term.

$$\frac{d}{dAl2O3}\left(a\cdot\ln\left(\frac{A\cdot NiO + B\cdot MgO + C\cdot MnO + D\cdot CaO + E\cdot K2O + F\cdot Li2O + G\cdot Na2O}{\begin{array}{l}AA\cdot Al2O3 + D\cdot CaO + K\cdot Cr2O3 + BB\cdot Fe2O3 + CC\cdot K2O + DD\cdot Li2O + EE\cdot MgO\ \ldots\\ +\ FF\cdot MnO + GG\cdot Na2O + HH\cdot NiO + II\cdot SiO2 + JJ\cdot TiO2 + L\cdot ZrO2\end{array}}\right)\right)$$

$$\frac{d}{dAl2O3}(a\cdot\ln(M2)) = \frac{-a}{\Sigma}\cdot AA \qquad \frac{d}{dCaO}(a\cdot\ln(M2)) = a\cdot D\cdot\left(\frac{1}{\Sigma M2} - \frac{1}{\Sigma}\right)$$

$$\frac{d}{dCr2O3}(a\cdot\ln(M2)) = -\left(\frac{a}{\Sigma}\right)\cdot K \qquad \frac{d}{dFe2O3}(a\cdot\ln(M2)) = -\left(\frac{a}{\Sigma}\right)\cdot BB$$

$$\frac{d}{dK2O}(a\cdot\ln(M2)) = a\cdot\left(\frac{E}{\Sigma M2} - \frac{CC}{\Sigma}\right) \qquad \frac{d}{dLi2O}(a\cdot\ln(M2)) = a\cdot\left(\frac{F}{\Sigma M2} - \frac{DD}{\Sigma}\right)$$

$$\frac{d}{dMgO}(a\cdot\ln(M2)) = a\cdot\left(\frac{B}{\Sigma M2} - \frac{EE}{\Sigma}\right) \qquad \frac{d}{dMnO}(a\cdot\ln(M2)) = a\cdot\left(\frac{C}{\Sigma M2} - \frac{FF}{\Sigma}\right)$$

$$\frac{d}{dNa2O}(a\cdot\ln(M2)) = a\cdot\left(\frac{G}{\Sigma M2} - \frac{GG}{\Sigma}\right) \qquad \frac{d}{dNiO}(a\cdot\ln(M2)) = a\cdot\left(\frac{A}{\Sigma M2} - \frac{HH}{\Sigma}\right)$$

$$\frac{d}{dSiO2}(a\cdot\ln(M2)) = -\left(\frac{a}{\Sigma}\right)\cdot II \qquad \frac{d}{dTiO2}(a\cdot\ln(M2)) = -\left(\frac{a}{\Sigma}\right)\cdot JJ$$

$$\frac{d}{dZrO2}(a\cdot\ln(M2)) = -\left(\frac{a}{\Sigma}\right)\cdot L$$

$$\frac{d}{dAl2O3}\left(b\cdot\ln\left(\frac{H\cdot Al2O3 + I\cdot Fe2O3 + J\cdot TiO2 + K\cdot Cr2O3 + L\cdot ZrO2 + M\cdot NiO + N\cdot MgO + O\cdot MnO}{\begin{array}{l}AA\cdot Al2O3 + D\cdot CaO + K\cdot Cr2O3 + BB\cdot Fe2O3 + CC\cdot K2O + DD\cdot Li2O + EE\cdot MgO\ \ldots\\ +\ FF\cdot MnO + GG\cdot Na2O + HH\cdot NiO + II\cdot SiO2 + JJ\cdot TiO2 + L\cdot ZrO2\end{array}}\right)\right)$$

$$\frac{d}{dAl2O3}(b\cdot\ln(M1)) = b\cdot\left(\frac{H}{\Sigma M1} - \frac{AA}{\Sigma}\right) \qquad \frac{d}{dCaO}(b\cdot\ln(M1)) = -\left(\frac{b}{\Sigma}\right)\cdot D$$

$$\frac{d}{dCr2O3}(b\cdot\ln(M1)) = b\cdot\left(\frac{K}{\Sigma M1} - \frac{K}{\Sigma}\right) \qquad \frac{d}{dFe2O3}(b\cdot\ln(M1)) = b\cdot\left(\frac{I}{\Sigma M1} - \frac{BB}{\Sigma}\right)$$

$$\frac{d}{dK2O}(b\cdot\ln(M1)) = -\left(\frac{b}{\Sigma}\right)\cdot CC \qquad \frac{d}{dLi2O}(b\cdot\ln(M1)) = -\left(\frac{b}{\Sigma}\right)\cdot DD$$

$$\frac{d}{dMgO}(b\cdot\ln(M1)) = b\cdot\left(\frac{N}{\Sigma M1} - \frac{EE}{\Sigma}\right) \qquad \frac{d}{dMnO}(b\cdot\ln(M1)) = b\cdot\left(\frac{O}{\Sigma M1} - \frac{FF}{\Sigma}\right)$$

$$\frac{d}{dNa2O}(b\cdot\ln(M1)) = -\left(\frac{b}{\Sigma}\right)\cdot GG \qquad \frac{d}{dNiO}(b\cdot\ln(M1)) = b\cdot\left(\frac{M}{\Sigma M1} - \frac{HH}{\Sigma}\right)$$

$$\frac{d}{dSiO2}(b\cdot\ln(M1)) = -\left(\frac{b}{\Sigma}\right)\cdot II \qquad \frac{d}{dTiO2}(b\cdot\ln(M1)) = b\cdot\left(\frac{J}{\Sigma M1} - \frac{JJ}{\Sigma}\right)$$

$$\frac{d}{dZrO2}(b\cdot\ln(M1)) = b\cdot\left(\frac{L}{\Sigma M1} - \frac{L}{\Sigma}\right)$$

$$\frac{d}{dAl2O3}\left(c\cdot\ln\left(\frac{P\cdot SiO2+Q\cdot Al2O3+R\cdot Fe2O3}{\begin{array}{l}AA\cdot Al2O3+D\cdot CaO+K\cdot Cr2O3+BB\cdot Fe2O3+CC\cdot K2O+DD\cdot Li2O+EE\cdot MgO\ \ldots\\ +FF\cdot MnO+GG\cdot Na2O+HH\cdot NiO+II\cdot SiO2+JJ\cdot TiO2+L\cdot ZrO2\end{array}}\right)\right)$$

$$\frac{d}{dAl2O3}(c\cdot\ln(MT))=c\cdot\left(\frac{Q}{\Sigma MT}-\frac{AA}{\Sigma}\right) \qquad \frac{d}{dCaO}(c\cdot\ln(MT))=-\left(\frac{c}{\Sigma}\right)\cdot D$$

$$\frac{d}{dCr2O3}(c\cdot\ln(MT))=-\left(\frac{c}{\Sigma}\right)\cdot K \qquad \frac{d}{dFe2O3}(c\cdot\ln(MT))=c\cdot\left(\frac{R}{\Sigma MT}-\frac{BB}{\Sigma}\right)$$

$$\frac{d}{dK2O}(c\cdot\ln(MT))=-\left(\frac{c}{\Sigma}\right)\cdot CC \qquad \frac{d}{dLi2O}(c\cdot\ln(MT))=-\left(\frac{c}{\Sigma}\right)\cdot DD$$

$$\frac{d}{dMgO}(c\cdot\ln(MT))=-\left(\frac{c}{\Sigma}\right)\cdot EE \qquad \frac{d}{dMnO}(c\cdot\ln(MT))=-\left(\frac{c}{\Sigma}\right)\cdot FF$$

$$\frac{d}{dNa2O}(c\cdot\ln(MT))=-\left(\frac{c}{\Sigma}\right)\cdot GG \qquad \frac{d}{dNiO}(c\cdot\ln(MT))=-\left(\frac{c}{\Sigma}\right)\cdot HH$$

$$\frac{d}{dSiO2}(c\cdot\ln(MT))=c\cdot\left(\frac{P}{\Sigma MT}-\frac{II}{\Sigma}\right) \qquad \frac{d}{dTiO2}(c\cdot\ln(MT))=-\left(\frac{c}{\Sigma}\right)\cdot JJ$$

$$\frac{d}{dZrO2}(c\cdot\ln(MT))=-\left(\frac{c}{\Sigma}\right)\cdot L$$

Also define the following for each:

$\Sigma Al2O3 = W + H + Q = AA$ $\quad \Sigma CaO = D$

$\Sigma Cr2O3 = K$ $\quad \Sigma Fe2O3 = X + I + R = BB$ $\quad \Sigma K2O = S + E = CC$

$\Sigma Li2O = F + T = DD$ $\quad \Sigma MgO = N + B = EE$ $\quad \Sigma MnO = C + O = FF$

$\Sigma Na2O = U + G = GG$ $\quad \Sigma NiO = A + M = HH$ $\quad \Sigma SiO2 = P + V = II$

$\Sigma TiO2 = Y + J = JJ$ $\quad \Sigma ZrO2 = L$

which can easily be implemented in code. The following partial derivatives follow from above:

$$\frac{d}{dAl2O3}\left(rTL_{pred}\right)=\frac{-a}{\Sigma}\cdot AA+b\cdot\left(\frac{H}{\Sigma M1}-\frac{AA}{\Sigma}\right)+c\cdot\left(\frac{Q}{\Sigma MT}-\frac{AA}{\Sigma}\right)$$

$$\frac{d}{dAl2O3}\left(rTL_{pred}\right)=\frac{-(a+b+c)}{\Sigma}\cdot\Sigma Al2O3+\left(H\cdot\frac{b}{\Sigma M1}+Q\cdot\frac{c}{\Sigma MT}\right)$$

$$\frac{d}{dCaO}\left(rTL_{pred}\right)=a\cdot D\cdot\left(\frac{1}{\Sigma M2}-\frac{1}{\Sigma}\right)+-\left(\frac{b}{\Sigma}\right)\cdot D+-\left(\frac{c}{\Sigma}\right)\cdot D=\frac{-(a+b+c)}{\Sigma}\cdot\Sigma CaO+\left(D\cdot\frac{a}{\Sigma M2}\right)$$

$$\frac{d}{dCr2O3}\left(rTL_{pred}\right)=-\left(\frac{a}{\Sigma}\right)\cdot K+b\cdot\left(\frac{K}{\Sigma M1}-\frac{K}{\Sigma}\right)+-\left(\frac{c}{\Sigma}\right)\cdot K=\frac{-(a+b+c)}{\Sigma}\cdot\Sigma Cr2O3+\left(K\cdot\frac{b}{\Sigma M1}\right)$$

$$\frac{d}{dFe2O3}rTL_{pred}=\frac{-(a+b+c)}{\Sigma}\cdot\Sigma Fe2O3+\left(I\cdot\frac{b}{\Sigma M1}+R\cdot\frac{c}{\Sigma MT}\right)$$

$$\frac{d}{dK2O}\left(rTL_{pred}\right)=a\cdot\left(\frac{E}{\Sigma M2}-\frac{CC}{\Sigma}\right)+-\left(\frac{b}{\Sigma}\right)\cdot CC+-\left(\frac{c}{\Sigma}\right)\cdot CC=\frac{-(a+b+c)}{\Sigma}\cdot\Sigma K2O+\left(E\cdot\frac{a}{\Sigma M2}\right)$$

$$\frac{d}{dLi2O}\left(rTL_{pred}\right) = a\cdot\left(\frac{F}{\Sigma M2} - \frac{DD}{\Sigma}\right) + -\left(\frac{b}{\Sigma}\right)\cdot DD + -\left(\frac{c}{\Sigma}\right)\cdot DD = \frac{-(a+b+c)}{\Sigma}\cdot \Sigma Li2O + \left(F\cdot\frac{a}{\Sigma M2}\right)$$

$$\frac{d}{dMgO}\left(rTL_{pred}\right) = \frac{-(a+b+c)}{\Sigma}\cdot \Sigma MgO + \left(B\cdot\frac{a}{\Sigma M2} + N\cdot\frac{b}{\Sigma M1}\right)$$

$$\frac{d}{dMnO}\left(rTL_{pred}\right) = \frac{-(a+b+c)}{\Sigma}\cdot \Sigma MnO + \left(C\cdot\frac{a}{\Sigma M2} + O\cdot\frac{b}{\Sigma M1}\right)$$

$$\frac{d}{dNa2O}\left(rTL_{pred}\right) = a\cdot\left(\frac{G}{\Sigma M2} - \frac{GG}{\Sigma}\right) + -\left(\frac{b}{\Sigma}\right)\cdot GG + -\left(\frac{c}{\Sigma}\right)\cdot GG = \frac{-(a+b+c)}{\Sigma}\cdot \Sigma Na2O + \left(G\cdot\frac{a}{\Sigma M2}\right)$$

$$\frac{d}{dNiO}\left(rTL_{pred}\right) = \frac{-(a+b+c)}{\Sigma}\cdot \Sigma NiO + \left(A\cdot\frac{a}{\Sigma M2} + M\cdot\frac{b}{\Sigma M1}\right)$$

$$\frac{d}{dSiO2}\left(rTL_{pred}\right) = -\left(\frac{a}{\Sigma}\right)\cdot II + -\left(\frac{b}{\Sigma}\right)\cdot II + c\cdot\left(\frac{P}{\Sigma MT} - \frac{II}{\Sigma}\right) = \frac{-(a+b+c)}{\Sigma}\cdot \Sigma SiO2 + \left(P\cdot\frac{c}{\Sigma MT}\right)$$

$$\frac{d}{dTiO2}\left(rTL_{pred}\right) = -\left(\frac{a}{\Sigma}\right)\cdot JJ + b\cdot\left(\frac{J}{\Sigma M1} - \frac{JJ}{\Sigma}\right) + -\left(\frac{c}{\Sigma}\right)\cdot JJ = \frac{-(a+b+c)}{\Sigma}\cdot \Sigma TiO2 + \left(J\cdot\frac{b}{\Sigma M1}\right)$$

$$\frac{d}{dZrO2}\left(rTL_{pred}\right) = -\left(\frac{a}{\Sigma}\right)\cdot L + b\cdot\left(\frac{L}{\Sigma M1} - \frac{L}{\Sigma}\right) + -\left(\frac{c}{\Sigma}\right)\cdot L = \frac{-(a+b+c)}{\Sigma}\cdot \Sigma ZrO2 + \left(L\cdot\frac{b}{\Sigma M1}\right)$$

$Al2O3 := 0$ $B2O3 := Al2O3 + 1$ $CaO := B2O3 + 1$ $Cr2O3 := CaO + 1$ $Fe2O3 := Cr2O3 + 1$

$K2O := Fe2O3 + 1$ $Li2O := K2O + 1$ $MgO := Li2O + 1$ $MnO := MgO + 1$ $Na2O := MnO + 1$

$NiO := Na2O + 1$ $SiO2 := NiO + 1$ $TiO2 := SiO2 + 1$ $U3O8 := TiO2 + 1$ $ZrO2 := U3O8 + 1$

Now define: $m2 := 0$ $m1 := m2 + 1$ $mt := m1 + 1$ $n1 := mt + 1$ $t1 := n1 + 1$

$Sp := READPRN("speciation.txt")$ containing the constituent distributions.

$a := -0.000259708121$ $b := -0.000566155555$ $c := -0.000152501087$ $d := -0.001442206573$

$$\Sigma M2(z) := Sp_{NiO,\,m2}\cdot z_{NiO} + Sp_{MgO,\,m2}\cdot z_{MgO} + Sp_{MnO,\,m2}\cdot z_{MnO} + Sp_{CaO,\,m2}\cdot z_{CaO} \cdots + Sp_{K2O,\,m2}\cdot z_{K2O} + Sp_{Li2O,\,m2}\cdot z_{Li2O} + Sp_{Na2O,\,m2}\cdot z_{Na2O}$$

$$\Sigma M1(z) := Sp_{Al2O3,\,m1}\cdot z_{Al2O3} + Sp_{Fe2O3,\,m1}\cdot z_{Fe2O3} + Sp_{TiO2,\,m1}\cdot z_{TiO2} + Sp_{Cr2O3,\,m1}\cdot z_{Cr2O3} \cdots + Sp_{ZrO2,\,m1}\cdot z_{ZrO2} + Sp_{NiO,\,m1}\cdot z_{NiO} + Sp_{MgO,\,m1}\cdot z_{MgO} + Sp_{MnO,\,m1}\cdot z_{MnO}$$

$$\Sigma MT(z) := Sp_{SiO2,\,mt}\cdot z_{SiO2} + Sp_{Al2O3,\,mt}\cdot z_{Al2O3} + Sp_{Fe2O3,\,mt}\cdot z_{Fe2O3}$$

$$\Sigma N1(z) := Sp_{K2O,\,n1}\cdot z_{K2O} + Sp_{Li2O,\,n1}\cdot z_{Li2O} + Sp_{Na2O,\,n1}\cdot z_{Na2O}$$

$$\Sigma T1(z) := Sp_{SiO2,\,t1}\cdot z_{SiO2} + Sp_{Al2O3,\,t1}\cdot z_{Al2O3} + Sp_{Fe2O3,\,t1}\cdot z_{Fe2O3} + Sp_{TiO2,\,t1}\cdot z_{TiO2}$$

$$\Sigma(z) := \Sigma M2(z) + \Sigma M1(z) + \Sigma MT(z) + \Sigma N1(z) + \Sigma T1(z)$$

$$M2(z) := \frac{\Sigma M2(z)}{\Sigma(z)} \qquad M1(z) := \frac{\Sigma M1(z)}{\Sigma(z)} \qquad MT(z) := \frac{\Sigma MT(z)}{\Sigma(z)}$$

$$rpred(z) := \ln\left[(M2(z))^{a} \cdot (M1(z))^{b} \cdot (MT(z))^{c} \right] + d$$

$$\Phi(z) := -\left(\frac{a + b + c}{\Sigma(z)} \right) \qquad \Phi a(z) := \frac{a}{\Sigma M2(z)} \qquad \Phi b(z) := \frac{b}{\Sigma M1(z)} \qquad \Phi c(z) := \frac{c}{\Sigma MT(z)}$$

Now the derivatives can be computed for a given molar composition:

$$\Pi_{Al2O3}(z) := \Phi(z) \cdot Sp_{Al2O3-1,\,t1+1} + \left(Sp_{Al2O3-1,\,m1} \cdot \Phi b(z) + Sp_{Al2O3-1,\,mt} \cdot \Phi c(z) \right)$$

$$\Pi_{CaO}(z) := \Phi(z) \cdot Sp_{CaO-1,\,t1+1} + \left(Sp_{CaO-1,\,m2} \cdot \Phi a(z) \right)$$

$$\Pi_{Cr2O3}(z) := \Phi(z) \cdot Sp_{Cr2O3-1,\,t1+1} + \left(Sp_{Cr2O3-1,\,m1} \cdot \Phi b(z) \right)$$

$$\Pi_{Fe2O3}(z) := \Phi(z) \cdot Sp_{Fe2O3-1,\,t1+1} + \left(Sp_{Fe2O3-1,\,m1} \cdot \Phi b(z) + Sp_{Fe2O3-1,\,mt} \cdot \Phi c(z) \right)$$

$$\Pi_{K2O}(z) := \Phi(z) \cdot Sp_{K2O-1,\,t1+1} + \left(Sp_{K2O-1,\,m2} \cdot \Phi a(z) \right)$$

$$\Pi_{Li2O}(z) := \Phi(z) \cdot Sp_{Li2O-1,\,t1+1} + \left(Sp_{Li2O-1,\,m2} \cdot \Phi a(z) \right)$$

$$\Pi_{MgO}(z) := \Phi(z) \cdot Sp_{MgO-1,\,t1+1} + \left(Sp_{MgO-1,\,m2} \cdot \Phi a(z) + Sp_{MgO-1,\,m1} \cdot \Phi b(z) \right)$$

$$\Pi_{MnO}(z) := \Phi(z) \cdot Sp_{MnO-1,\,t1+1} + \left(Sp_{MnO-1,\,m2} \cdot \Phi a(z) + Sp_{MnO-1,\,m1} \cdot \Phi b(z) \right)$$

$$\Pi_{Na2O}(z) := \Phi(z) \cdot Sp_{Na2O-1,\,t1+1} + \left(Sp_{Na2O-1,\,m2} \cdot \Phi a(z) \right)$$

$$\Pi_{NiO}(z) := \Phi(z) \cdot Sp_{NiO-1,\,t1+1} + \left(Sp_{NiO-1,\,m2} \cdot \Phi a(z) + Sp_{NiO-1,\,m1} \cdot \Phi b(z) \right)$$

$$\Pi_{SiO2}(z) := \Phi(z) \cdot Sp_{SiO2-1,\,t1+1} + \left(Sp_{SiO2-1,\,mt} \cdot \Phi c(z) \right)$$

$$\Pi_{TiO2}(z) := \Phi(z) \cdot Sp_{TiO2-1,\,t1+1} + \left(Sp_{TiO2-1,\,m1} \cdot \Phi b(z) \right)$$

$$\Pi_{ZrO2}(z) := \Phi(z) \cdot Sp_{ZrO2-1,\,t1+1} + \left(Sp_{ZrO2-1,\,m1} \cdot \Phi b(z) \right)$$

Error Information: $r := READPRN("rsdm15.prn")$ $Cm := READPRN("Cm15.txt")$

Compositions: $z := READPRN("tldata6.txt")^T$ $rows(z) = 15$ $cols(z) = 105$

$\Pi_{all}(z) :=$
$\Pi a_{Al2O3} \leftarrow \Pi_{Al2O3}(z)$
$\Pi a_{CaO} \leftarrow \Pi_{CaO}(z)$
$\Pi a_{Cr2O3} \leftarrow \Pi_{Cr2O3}(z)$
$\Pi a_{Fe2O3} \leftarrow \Pi_{Fe2O3}(z)$
$\Pi a_{K2O} \leftarrow \Pi_{K2O}(z)$
$\Pi a_{Li2O} \leftarrow \Pi_{Li2O}(z)$
$\Pi a_{MgO} \leftarrow \Pi_{MgO}(z)$
$\Pi a_{MnO} \leftarrow \Pi_{MnO}(z)$
$\Pi a_{Na2O} \leftarrow \Pi_{Na2O}(z)$
$\Pi a_{NiO} \leftarrow \Pi_{NiO}(z)$
$\Pi a_{SiO2} \leftarrow \Pi_{SiO2}(z)$
$\Pi a_{TiO2} \leftarrow \Pi_{TiO2}(z)$
$\Pi a_{ZrO2} \leftarrow \Pi_{ZrO2}(z)$
Πa

$Var(Sp, z, r, C) :=$
$\Pi \leftarrow \Pi_{all}(z)$
$V \leftarrow 0.0$
for $i \in Al2O3..ZrO2$
for $j \in Al2O3..ZrO2$
$V \leftarrow V + (\Pi_i \cdot r_i \cdot z_i) \cdot (\Pi_j \cdot r_j \cdot z_j) \cdot C_{i,j}$
V

$Var(Sp, z^{\langle 0 \rangle}, r, Cm) = 2.477 \times 10^{-10}$

$\sqrt{Var(Sp, z^{\langle 0 \rangle}, r, Cm)} = 1.574 \times 10^{-5}$

$ki := 0..cols(z) - 1$ $v_{ki} := Var(Sp, z^{\langle ki \rangle}, r, Cm)$ $min(v) = 4.8 \times 10^{-11}$ $\sqrt{min(v)} = 6.93 \times 10^{-6}$

$max(v) = 1.62 \times 10^{-9}$ $\sqrt{max(v)} = 4.02 \times 10^{-5}$

$\frac{1}{rpred(z^{\langle 0 \rangle})} - 273 = 1105.832$ $\frac{1}{z_{0,0}} - 273 = -227.683$

$rv_{ki} := 100 \cdot \left(\frac{\sqrt{v_{ki}}}{rpred(z^{\langle ki \rangle})} \right)$ $min(rv) = 0.813$

$max(rv) = 5.419$

$\alpha := READ("alpha.txt")$ $u_{ki} := qt(1 - \alpha, 22 - 1) \cdot \sqrt{\frac{v_{ki}}{4}}$ $results_{ki,0} := rpred(z^{\langle ki \rangle})$

$ru_{ki} := 100 \cdot \left(\frac{u_{ki}}{rpred(z^{\langle ki \rangle})} \right)$ $min(ru) = 0.2791$ $results_{ki,1} := u_{ki}$

$max(ru) = 1.86$

17. APPENDIX: VISUAL BASIC (VB) CODE FOR IMPLEMENTATION OF PROPOSED LIQUIDUS TEMPERATURE MODEL

The portion of interest in the DWPF SME Acceptability spreadsheet (which was entitled "**Batch 1B SME xx Acceptability.xls**" where xx is the DWPF SME batch number) is illustrated in Figure 17-1 where the SME composition corresponds to SB2-Frit 200 at a waste loading of 31% (as provided in Table XXVIII). For each property, the linear constraint array defined for PCCS [1] (or "The Value of the Alpha's For Each Constraint" as indicated in the worksheet) is provided. For example, this array for the current liquidus temperature model is provided in cells **F97** through **F129** in the **Acceptability** worksheet. (All subsequent references will be made to this worksheet.) As illustrated in Equation 24, the linear combination of this vector and the vector containing the molar oxide concentrations (which is provided in cells **B97** through **B129** and has been named **SMEcomp** in the spreadsheet) provides the **Derived Value** (or cell **F135** for liquidus temperature). This linear combination corresponds to a prediction accounting for prediction error [1], which was constant in the original PCCS. As indicated in Equation 21, the prediction error for the new model is a function of the SME composition (as defined in **SMEcomp**), and the new derived value (i.e., 1009ºC) is computed using the VB code provided in Listing 17-1 using the call:

```
=computePAR(XTX,Std_Err,Alpha,ROWS(SMEcomp),SMEcomp,Sp,COLUMNS(Sp),COLUMNS(XTX)-1)
```

where `XTX` is the product moment matrix (defined in cells **N147** to **Q150**), `Std_Err` is the root mean square error (defined in cell **N151**), `Alpha` is the significance level (defined in cell **N152**), and `Sp` is the distribution matrix (defined in cells **CA97** to **CF130**). Figure 17-2 and Figure 17-3 provide the pertinent values for the various named items used in the above function call. (Note that the function Listing 17-1 calls the function in Listing 17-2 needed to computed the liquidus temperature at a given composition.) In the original PCCS, this derived liquidus temperature value would be compared to a PAR limit of 0.0 (in cell **F130**); for the new model, the derived value can be compared to the PAR limit of 1050ºC (now in cell **F130**).

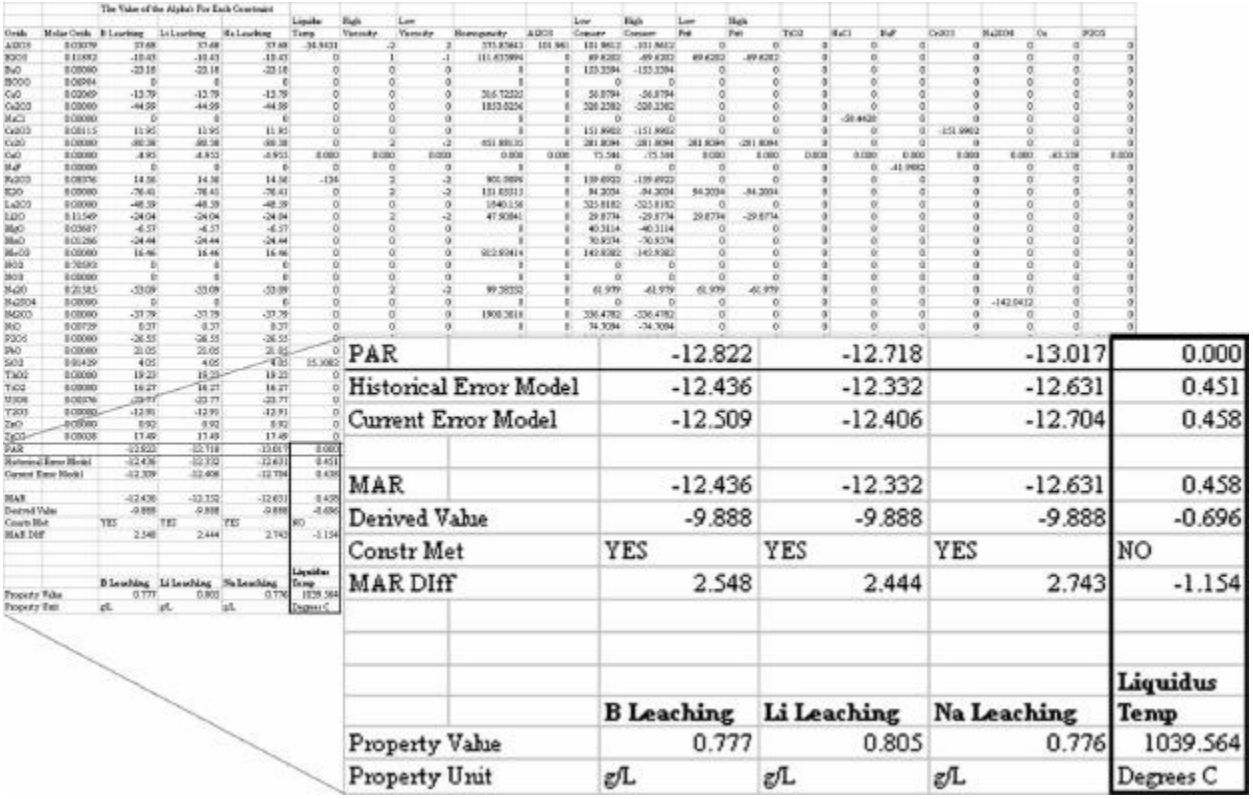

PAR	-12.822	-12.718	-13.017	0.000
Historical Error Model	-12.436	-12.332	-12.631	0.451
Current Error Model	-12.509	-12.406	-12.704	0.458
MAR	-12.436	-12.332	-12.631	0.458
Derived Value	-9.888	-9.888	-9.888	-0.696
Constr Met	YES	YES	YES	NO
MAR Diff	2.548	2.444	2.743	-1.154
				Liquidus
	B Leaching	Li Leaching	Na Leaching	Temp
Property Value	0.777	0.805	0.776	1039.564
Property Unit	g/L	g/L	g/L	Degrees C

Figure 17-1. Pertinent Information on the DWPF SME Acceptability EXCEL® Spreadsheet. The above information is found in the worksheet entitled "Acceptability."

Table XXVIII. SME Composition used in Implementation Example

Cation	Wt(%)	Oxide	Moles/100g glass
Aluminum	2.741 wt%	Al_2O_3	0.05078829
Boron	2.571 wt%	B_2O_3	0.11892361
Calcium	0.829 wt%	CaO	0.02069066
Chromium	0.119 wt%	Cr_2O_3	0.00114869
Copper	0.000 wt%	CuO	0
Iron	9.356 wt%	Fe_2O_3	0.08376049
Potassium	0.000 wt%	K_2O	0
Lithium	1.603 wt%	Li_2O	0.11549335
Magnesium	0.877 wt%	MgO	0.03606595
Manganese	0.662 wt%	MnO	0.01205647
Sodium	9.888 wt%	Na_2O	0.21505254
Nickel	0.446 wt%	NiO	0.00759474
Silicon	22.870 wt%	SiO_2	0.81429063
Titanium	0.000 wt%	TiO_2	0
Uranium	2.689 wt%	U_3O_8	0.00376493
Zirconium	0.026 wt%	ZrO_2	0.00028338

XTX	Const.	M2	M1	MT
Const.	105	-126.56	-309.14	-162.47
M2	-126.56	154.22	371.50	194.98
M1	-309.14	371.50	913.84	473.73
MT	-162.47	194.98	473.73	265.64
Std Err	2.2775E-05			
TL Alpha	0.05			
Conf. Level	95%			

Figure 17-2. Pertinent Information on the DWPF SME Acceptability EXCEL® Spreadsheet showing cells **M146** through **Q153** where `XTX`, `Std_Err`, and `Alpha` are defined.

The relevant measurement uncertainty is propagated through the new model (as indicated in Equation 22) based upon both the historic (i.e., the result in cell **F131**) and current measured (i.e., the result in cell **F132**) SME composition and then subtracted from the PAR limit. The VB function needed to provide the new MAR based limit (i.e., the minimum of the two as provided in cell **F134**) is provided in Listing 17-3 using either the function call:

```
=computeMAR(F130,rsd,Corr,Alpha,ROWS(HISTcomp),HISTcomp,Sp,COLUMNS(Sp),COLUMNS(XTX)-1)
```

or

```
=computeMAR(F130,rsd,Corr,Alpha,ROWS(SMEcomp),SMEcomp,Sp,COLUMNS(Sp),COLUMNS(XTX)-1)
```

for the historic and current measured SME compositions, respectively, where a total of four samples is assumed, cell **F130** contains the liquidus temperature limit (i.e., 1050°C), `rsd` is the array (in cells **U148** through **U180**) of relative standard deviations, `Corr` is the matrix (in cells **W148** through **BC180**) containing the relevant pair-wise correlations, and `HISTcomp` is the array of historic molar oxide concentrations which has been added to the spreadsheet in cells **S148** through **S180** which are computed in the same manner as the concentrations in SMEcomp. Thus if the derived value (in cell **F135**) is less than the MAR value (in cell **F134**), the test result (in cell **F136**) will indicate a positive (or "YES") result; otherwise, the results will be negative (or "NO"). To round out the liquidus temperature information, the prediction is computed in cell **F142** using:

```
=computeTL(ROWS(SMEcomp),SMEcomp,Sp,COLUMNS(Sp),COLUMNS(XTX)-1)
```

and the difference between the MAR and derived values is computed in cell **F137**. The pertinent results for the new model are provided in Figure 17-4. Note that the new model indicates that the predicted liquidus temperature for the composition in Table XXVIII is acceptable whereas the old model indicated that the liquidus temperature would be unacceptable.

Speciation (Sp)	M2	M1	MT	N1	T1	SUM
Al2O3	0	0.0607	0.9393	0	0	1
B2O3	0	0	0	0	0	0
BaO						
HCOO						
CaO	0.029	0	0	0	0	0.029
Ce2O3						
NaCl						
Cr2O3	0	0.9202	0	0	0	0.9202
Cs2O						
CuO						
NaF						
Fe2O3	0	0.1079	0.0193	0	0.6094	0.7366
K2O	0.3041	0	0	0.1049	0	0.409
La2O3						
Li2O	0.1745	0	0	0.1068	0	0.2813
MgO	0.0167	0.0223	0	0	0	0.039
MnO	0.994	0.00603	0	0	0	1
MoO3						
NO2						
NO3						
Na2O	0.1671	0	0	0.2518	0	0.4189
Na2SO4						
Nd2O3						
NiO	0	0.1079	0	0	0	0.1079
P2O5						
PbO						
SiO2	0	0	0.0193	0	0.0133	0.0326
ThO2						
TiO2	0	0.0568	0	0	0.5667	0.6235
U3O8	0	0	0	0	0	0
Y2O3						
ZnO						
ZrO2	0	0.0458	0	0	0	0.0458
coeff	-0.0002597	-0.0005662	-0.0001525			-0.0014422

Figure 17-3. Pertinent Information on the DWPF SME Acceptability EXCEL® Spreadsheet showing cells **BY96** through **CF130** where Sp is defined.

PAR	-12.8215	-12.7178	-13.0167	1050
Historical Error Model	-12.436	-12.332	-12.631	1022.864
Current Error Model	-12.509	-12.406	-12.704	1022.828
MAR	-12.4357	-12.3320	-12.6309	1023
Derived Value	-9.8878	-9.8878	-9.8878	1004
Constr Met	YES	YES	YES	YES
MAR Diff	2.5479	2.4442	2.7431	19
				Liquidus
	B Leaching	**Li Leaching**	**Na Leaching**	**Temp**
Property Value	0.777	0.805	0.776	984
Property Unit	g/L	g/L	g/L	Degrees C

Figure 17-4. Pertinent Information on the DWPF SME Acceptability EXCEL® Spreadsheet showing cells **A130** through **F143** where the new liquidus temperature results are displayed.

Listing 17-1. The `computePAR` function returns a double precision value representing the upper 100(1–α)% prediction interval associated with the liquidus temperature prediction where the parameters passed to the function are defined in the function call.

```
Public Function computePAR(XTX, sr As Double, alpha As Double, q As Integer, z, Sp, qs As Integer, qt As Integer) As Double
    ' This function computes the one-sided bound on predicted TL
    ' XTX = product moment matrix, sr = root mean square error, alpha = significance level, q = number of components
    ' z = qx1 array of molar oxide concentrations, Sp = distribution matrix, qs = number of pyroxene-like clusters
    ' qt = number of model terms (excluding intercept)
    Dim i, j As Integer
    Dim msum(10) As Double
    Dim cterm(10) As Double
    Dim sum, TL As Double
    Dim XTXinv As Variant
    ' Compute the predicted TL
    TL = computeTL(q, z, Sp, qs, qt)
    ' Need the inverse of the product moment matrix
    XTXinv = Application.WorksheetFunction.MInverse(XTX)
    ' Now construct terms for prediction error determination
    For i = 1 To qs - 1
    ' Compute the sum for each pyroxene-like complex
        For j = 1 To q
            msum(i) = msum(i) + Sp(j, i) * z(j)
        Next j
        sum = sum + msum(i) ' compute denominator
    Next i
    cterm(1) = 1#
    For i = 1 To qt ' number of model terms
        cterm(i + 1) = Log(msum(i) / sum)
    Next i
    ' Compute the value corresponding to the prediction
    sum = cterm(qt + 1) * cterm(qt + 1) * XTXinv(qt + 1, qt + 1)
    For i = 1 To qt
        sum = sum + cterm(i) * cterm(i) * XTXinv(i, i)
        For j = i + 1 To qt + 1
            sum = sum + 2# * cterm(i) * cterm(j) * XTXinv(i, j)
        Next j
    Next i
    ' The prediction uncertainty will be place in sum
    sum = sr * Sqr((qt + 1#) * Application.WorksheetFunction.FInv(2 * alpha, qt + 1#, XTX(1, 1) - qt - 1#)) * Sqr(sum)
    ' The prediction uncertainty is related to reciprocal K
    computePAR = 1# / ((1# / (TL + 273#)) - sum) - 273#
End Function
```

Listing 17-2. The `computeTL` function returns a double precision value representing the liquidus temperature prediction where the parameters passed to the function are defined in the function call.

```
Public Function computeTL(q As Integer, z, Sp, qs As Integer, qt As Integer) As Double
    ' q = number of components, z = qx1 array of molar oxide concentrations, Sp = distribution matrix,
    ' qs = number of pyroxene-like clusters, qt = number of model terms (excluding intercept)    Dim i, j As Integer
    Dim msum(10) As Double
    Dim sum As Double
    computeTL = 0#
    For i = 1 To qs - 1
    ' Compute the sum for each complex
        For j = 1 To q
            msum(i) = msum(i) + Sp(j, i) * z(j)
        Next j
        sum = sum + msum(i) ' compute denominator
    Next i
    ' Specific model information follows
    For i = 1 To qt ' number of model terms
        computeTL = computeTL + Sp(q + 1, i) * Log(msum(i) / sum) ' 1/TL(K)
    Next i
    computeTL = (1# / (computeTL + Sp(q + 1, qs))) - 273#
End Function
```

Listing 17-3. The `computeMAR` function returns a double precision value representing measurement uncertainty subtracted from the liquidus temperature limit where the parameters passed to the function are defined in the function call.

```
Public Function computeMAR(EPAR, r, C, alpha As Double, q As Integer, z, Sp, qs As Integer, qt As Integer) As Double
    ' EPAR = upper limit on TL, r = array of relative standard deviations, C = correlation matrix,
    ' alpha = significance level, q = number of components, z = qx1 array of molar oxide concentrations,
    ' Sp = distribution matix, qs = number of pyroxene-like clusters, qt = number of model terms (excluding intercept)
    Dim i, j, m2, m1, mt, n1, t1 As Integer
    Dim msum(10) As Double
    Dim P(50) As Double
    Dim sum, Sz, Saz, Sbz, Scz As Double
    ' The indices that follow are specific for the documented case
    m2 = 1
    m1 = m2 + 1
    mt = m1 + 1
    n1 = mt + 1
    t1 = n1 + 1
```

Listing 17-3. Continued

```
For i = 1 To qs - 1
    ' Compute the sum for each complex
        For j = 1 To q
            msum(i) = msum(i) + Sp(j, i) * z(j)
        Next j
        sum = sum + msum(i) ' compute denominator
    Next i
    ' More definitions
    Sz = -(Sp(q + 1, m2) + Sp(q + 1, m1) + Sp(q + 1, mt)) / sum
    Saz = Sp(q + 1, m2) / msum(m2)
    Sbz = Sp(q + 1, m1) / msum(m1)
    Scz = Sp(q + 1, mt) / msum(mt)
    ' Now compute the partial derivatives -- this cannot be generalized at this time
    ' The following assumes the oxides are in the following positions: Al2O3 1, CaO 5,
    '   Cr2O3 8, Fe2O3 12, K2O 13, Li2O 15, MgO 16, MnO 17, Na2O 21, NiO 24, SiO2 27,
    '   TiO2 29, ZrO2 33
    P(1) = Sz * Sp(1, t1 + 1) + (Sp(1, m1) * Sbz + Sp(1, mt) * Scz)
    P(5) = Sz * Sp(5, t1 + 1) + (Sp(5, m2) * Saz)
    P(8) = Sz * Sp(8, t1 + 1) + (Sp(8, m1) * Sbz)
    P(12) = Sz * Sp(12, t1 + 1) + (Sp(12, m1) * Sbz + Sp(12, mt) * Scz)
    P(13) = Sz * Sp(13, t1 + 1) + (Sp(13, m2) * Saz)
    P(15) = Sz * Sp(15, t1 + 1) + (Sp(15, m2) * Saz)
    P(16) = Sz * Sp(16, t1 + 1) + (Sp(16, m2) * Saz + Sp(16, m1) * Sbz)
    P(17) = Sz * Sp(17, t1 + 1) + (Sp(17, m2) * Saz + Sp(17, m1) * Sbz)
    P(21) = Sz * Sp(21, t1 + 1) + (Sp(21, m2) * Saz)
    P(24) = Sz * Sp(24, t1 + 1) + (Sp(24, m2) * Saz + Sp(24, m1) * Sbz)
    P(27) = Sz * Sp(27, t1 + 1) + (Sp(27, mt) * Scz)
    P(29) = Sz * Sp(29, t1 + 1) + (Sp(29, m1) * Sbz)
    P(33) = Sz * Sp(33, t1 + 1) + (Sp(33, m1) * Sbz)
    ' Now compute the measurement variance
    sum = 0#
    For i = 1 To q
        For j = 1 To q
            sum = sum + (P(i) * r(i) * z(i)) * (P(j) * r(j) * z(j)) * C(i, j)
        Next j
    Next i
    computeMAR = 1# / ((1# / (EPAR + 273#)) + Application.WorksheetFunction.TInv(2# * alpha, 22# - 1#) * Sqr(0.25 * sum)) -
273#
End Function
```

18. APPENDIX: LIQUIDUS TEMPERATURE PREDICTIONS FOR THE MODEL DATA

Table XXIX. Measured versus Predicted Liquidus Temperatures (°C) for the DWPF Model Data

Glass ID	Melted	T_L(°C) Meas.	T_L(°C) New	T_L(°C) Old	Glass ID	Melted	T_L(°C) Meas.	T_L(°C) New	T_L(°C) Old
AH-131Fe-AB-PNNL	1992	1108	1106	1063	SG50	1996	1285	1263	1045
AH-165Fe-AB-PNNL	1992	1099.5	1105	1046	SG51	1996	1033	1045	1092
AH-168Av-AB-PNNL	1992	969	970	1001	AH 131AL-1992#	1992	835	863	927
AH-200Fe-AB-PNNL	1992	1087.5	1095	1064	AH 131AL-1985	1988	863	849	923
AH-202Fe-AB-PNNL	1992	1122.5	1116	1035	AH 131AV-1985 - No La	1985	990	970	1047
SG01	1996	1124	1110	1069	AH 131AV-1992 - No La#	1992	995	967	982
SG03	1996	1164	1134	1014	AH 131 FE -RED-1992-No La#	1992	1075	1106	1063
SG04	1996	1261	1265	1072	AH 165AL-1985	1985	863	863	893
SG05	1996	1084	1075	980	AH 165AL-1992#	1992	840	890	904
SG05b	1996	1082	1072	979	AH 165AV -1985	1985	917	980	998
SG06	1996	921	977	1087	AH 165AV-REVISED LIQ - 1988	1988	1006	962	994
SG07	1996	950	984	905	AH 165AV - 1992#	1992	1000	950	981
SG08	1996	1114	1068	994	AH165FE-RED-1985	1985	1102	1091	1046
SG09	1996	1173	1123	1138	AH 165FE-RED -1992#	1992	1085	1105	1046
SG10	1996	1098	1067	929	AH165FE-OX-1996# (not ox)	1996	1135	1060	1060
SG11	1996	895	883	928	AH 168AL-1988#	1988	846	867	894
SG12	1996	1030	1012	1009	AH 168AV-1985	1985	1014	970	1001
SG13	1996	1063	1075	921	AH 168AV-1988	1988	925	970	1001
SG14	1996	951	950	1084	AH 168AV-1992	1992	990	973	990
SG16	1996	995	949	956	AH 168AV-1992(peeler)	1992	980	973	990
SG17	1996	1075	1019	1030	AH 168FE-RED-1988	1988	1022	1038	992
SG18	1996	859	884	1048	AH 168FE-RED (?)-1992	1992	1085	1127	1060
SG18	1996	883	884	1048	AH 168 FE-OX-1996#	1996	1130	1084	1141
SG18	1996	886.5	884	1048	AH 200AL - 1988#	1988	929	901	905
SG18b	1996	869	895	1049	AH 200AL -1992#	1992	845	913	913
SG18b	1996	883	895	1049	AH200AV(AH-8)-1988#	1988	996	1005	1012
SG18b	1996	886.5	895	1049	AH 200AV - 1988#	1988	997	988	1001
SG19	1996	929	992	925	AH 200AV - 1992#	1992	985	1007	1010
SG20	1996	799	850	916	AH 200FE-RED-1988	1988	1126	1072	1062
SG21	1996	987	1041	925	AH 200FE-RED-1992#	1992	1065	1095	1064
SG22	1996	1145	1123	1036	AH 200FE-1992(peeler)#	1992	1070	1095	1064
SG23	1996	1069	1059	927	AH 202AL - 1988 (AH131Fe/Av?)	1988	959	922	889
SG25	1996	1309.5	1322	1097	AH 202AL (Pt not good) - 1992#	1992	965	942	900
SG26	1996	1071	1011	1002	AH202AV (AH-10) - 1985#	1985	965	1011	980
SG27	1996	1086	1106	1021	AH 202AV - 1988#	1988	967	1023	990
SG29	1996	811	762	911	AH 202AV - 1992#	1992	1010	1036	989
SG30	1996	1030	1000	935	AH 202FE-RED - 1988#	1988	1123	1135	1055
SG31	1996	1081	1132	1157	AH 202FE-RED-1992#	1992	1110	1116	1035
SG32	1996	1132	1108	1149	AH 202FE-1992(peeler)#	1992	1160	1116	1035
SG33	1996	943	1008	930	AH 202FE-OX - 1996#	1996	1100	1081	1045
SG34	1996	1282	1265	1155	AH-5-1985#	1985	991	960	988
SG35	1996	1231	1189	1136	AH-9-1985#	1985	1000	989	1004
SG37	1996	944.5	905	882	AH-13 -1985#	1985	1096	1055	1054
SG38	1996	897	945	1077	AH-16-1985#	1985	1073	1123	1042
SG39	1996	1164	1111	1021	DWPF STARTUP FRIT (10/26/87)	1987	1066	1015	1052
SG40	1996	1173	1172	927	DWPF STARTUP FRIT (10/28/87)	1987	1062	1014	1058
SG41	1996	1304	1310	1145	DWPF STARTUP FRIT (10/27/87)	1987	1012	1017	1056
SG42	1996	990	1009	1030	DWPF STARTUP FRIT (10/27/87)	1987	997	1017	1056
SG43	1996	924	933	944	Carters 165 Black Frit	1988	909	906	982
SG44	1996	1244	1218	1031	AH 131 FE-1992 (peeler)-No La#	1992	1035	1106	1063
SG45	1996	936	956	886	AH 165AL-1988#	1988	946	863	893
SG46	1996	1247	1242	1043	AH 165 FE-1992 (peeler)#	1992	1015	1105	1046
SG47	1996	1144	1124	1067					

This page intentionally left blank.